Nagra
Nationale
Genossenschaft
für die Lagerung
radioaktiver Abfälle

Cédra
Société coopérative
nationale
pour l'entreposage
de déchets radioactifs

Cisra
Società cooperativa
nazionale
per l'immagazzinamento
di scorie radioattive

TECHNICAL REPORT 86-21

Modelling Interaction of Deep Groundwaters with Bentonite and Radionuclide Speciation

Hans Wanner

April 1986

Swiss Federal Institute for Reactor Research, Würenlingen

Parkstrasse 23 5401 Baden/Schweiz Telephon 056/20 55 11

Nagra
Nationale
Genossenschaft
für die Lagerung
radioaktiver Abfälle

Cédra
Société coopérative
nationale
pour l'entreposage
de déchets radioactifs

Cisra
Società cooperativa
nazionale
per l'immagazzinamento
di scorie radioattive

TECHNICAL REPORT 86-21

Modelling Interaction of Deep Groundwaters with Bentonite and Radionuclide Speciation

Hans Wanner

April 1986

Swiss Federal Institute for Reactor Research, Würenlingen

Parkstrasse 23 5401 Baden/Schweiz Telephon 056/20 55 11

Der vorliegende Bericht wurde im Auftrag der Nagra erstellt. Die Autoren haben ihre eigenen Ansichten und Schlussfolgerungen dargestellt. Diese müssen nicht unbedingt mit denjenigen der Nagra übereinstimmen.

Le présent rapport a été préparé sur demande de la Cédra. Les opinions et conclusions présentées sont celles des auteurs et ne correspondent pas nécessairement à celles de la Cédra.

This report was prepared as an account of work sponsored by Nagra. The viewpoints presented and conclusions reached are those of the author(s) and do not necessarily represent those of Nagra.

Summary

In the safety analysis recently reported for a potential Swiss high-level waste repository, radionuclide speciation and solubility limits are calculated for expected granitic groundwater conditions. With the objective of deriving a more realistic description of radionuclide release from the near-field, an investigation has been initiated to quantitatively specify the chemistry of the near-field. In the Swiss case, the main components of the near-field are the glass waste-matrix, a thick steel canister horizontally emplaced in a drift, and a backfill of highly compacted sodium bentonite.

This report describes a thermodynamic model which is used to estimate the chemical composition of the pore water in compacted sodium bentonite. Solubility limits and speciation of important actinides and the fission product technetium in the bentonite pore water are then calculated.

The model is based on available experimental data on the interaction of sodium bentonite and groundwater and represents means of extrapolation from laboratory data to repository conditions. The basic reactions between sodium bentonite and groundwater are described by an ion-exchange model for sodium, potassium, magnesium, and calcium. The model assumes equilibrium with calcite as long as sufficient carbonates remain in the bentonite, as well as quartz saturation. It is calculated that the pore water of compacted sodium bentonite saturated with Swiss Reference Groundwater will have a pH value of 9.7 and a free carbonate activity of $8 \cdot 10^{-4}$ M. The long-term situation is modelled by the assumption that the near-field of a deep repository behaves like a mixing tank. In this way, an attempt is made to account for the continuous water exchange between the near-field and the host rock. It is found that sodium bentonite will be slowly converted to calcium bentonite. This conversion is roughly estimated to be completed after 2 million years. Illitisation of sodium bentonite is not taken into account.

The modelled composition of the pore water of compacted sodium bentonite, as well as the various compositions resulting from the long-term extrapolation, are used to estimate radionuclide solubilities in the near-field of a deep repository. The elements considered are: uranium, neptunium, plutonium, thorium, americium, and technetium. The redox potential in the near-field is assumed to be controlled by the corrosion products of the iron canister. Except for uranium and neptunium, radionuclide solubilities turn out to be lower under the modelled near-field conditions than in the groundwater of the surrounding granitic host rock. Uranium and neptunium solubility might be higher by orders of magnitude in the near-field than in the far-field. This could lead to a comparatively strong downhill concentration gradient at the near-to-far-field boundary or within the buffer material. The possible extent of uranium and neptunium colloid formation in this area, and release into the far-field, is not discussed in detail but will strongly depend on the stability and mobility of such colloids.

From the chemical point of view, calcium bentonite seems to be more stable than sodium bentonite in the presence of Swiss Reference Groundwater. Since the effect of calcium bentonite on the groundwater chemical composition will be considerably less marked than that of sodium bentonite, especially with respect to key parameters for the nuclide speciation like carbonate concentration and pH, the use of calcium bentonite instead of sodium bentonite will improve the reliability in the prediction of source terms for radionuclide transport in the geosphere.

Zusammenfassung

In der kürzlich veröffentlichen Sicherheitsanalyse für ein mögliches Endlager für hochradioaktive Abfälle in der Schweiz wurde der Quellterm für die Nuklidmigration in der Geosphäre unter anderem aufgrund der oberen Löslichkeitsgrenzen der Nuklide im tiefen granitischen Grundwasser abgeschätzt. Um eine realistischere Beschreibung der Freisetzung von radioaktiven Abfallstoffen aus dem Endlager zu ermöglichen, muss die Nahfeldchemie eines Endlagers für stark radioaktive Abfälle quantitativ spezifiziert werden. Die Hauptbestandteile des Nahfeldes sind im schweizerischen Fall die verglaste Abfallmatrix, welche von einem massiven Stahlbehälter umgeben und horizontal in einem mit Natriumbentonit verfüllten Stollen gelagert sein wird.

In dieser Arbeit wird ein Modell vorgestellt, welches die Berechnung der zeitabhängigen chemischen Zusammensetzung des Porenwassers in hochverdichtetem Natriumbentonit erlaubt. Für dieses Porenwasser werden anschliessend Löslichkeitslimiten und Speziation wichtiger Aktiniden und des Spaltproduktes Technetium berechnet.

Das Modell basiert auf Messungen der Einwirkung von Natriumbentonit auf Grundwasser und extrapoliert die Labordaten auf Endlagerbedingungen. Die Wechselwirkung zwischen Natriumbentonit und Grundwasser wird mit einem Ionenaustauschmodell beschrieben, welches Natrium, Kalium, Magnesium und Calcium als austauschbare Kationen berücksichtigt. Es wird angenommen, dass das Porenwasser des verdichteten Bentonits mit Calcit gesättigt ist, solange der Bentonit über genügend Karbonate verfügt, um dieses Gleichgewicht aufrechtzuerhalten. Als weitere Randbedingung wird Quarzsättigung angenommen. Für das Porenwasser des verdichteten Natriumbentonits, welcher mit schweizerischem Referenzgrundwasser gesättigt ist, sagt das Modell einen pH-Wert von 9.7 und eine Karbonataktivität von $8 \cdot 10^{-4}$ M voraus. Um Aussagen über das Langzeitverhalten des Bentonits machen zu können, wurde ein einfaches Modell entworfen, welches das Nahfeld als Mischtank betrachtet. Damit

wird versucht, den kontinuierlichen Austausch von Grundwasser zwischen Nahfeld und Wirtgestein zu modellieren. Die Rechnung zeigt, dass sich der Natriumbentonit dabei langsam in Calciumbentonit umwandelt. Diese Umwandlung wird, grob geschätzt, nach etwa zwei Millionen Jahren beendet sein. Die Illitisierung von Natriumbentonit wird nicht berücksichtigt.

Die so modellierten chemischen Zusammensetzungen des Nahfeldwassers dienen als Grundlage für die Berechnung der Löslichkeitslimiten und der Speziation der folgenden Elemente: Uran, Neptunium, Plutonium, Thorium, Americium und Technetium. Es wird angenommen, dass das Redoxpotential im Nahfeld durch die Korrosionsprodukte des Stahlbehälters bestimmt wird. Mit Ausnahme von Uran und Neptunium sind die Löslichkeitslimiten im Porenwasser des Nahfeldes kleiner, als im Wasser des ungestörten granitischen Gesteins. Die Löslichkeiten von Uran und Neptunium können im Nahfeld um Grössenordnungen höher sein als im Fernfeld, was zu einem verhältnismässig steilen Konzentrationsgefälle an der Nah-Fernfeldgrenze oder innerhalb des Verfüllmaterials führen kann. Die Bildung von Uran- und Neptunium-Kolloiden in diesem Bereich kann nicht mit Sicherheit ausgeschlossen werden. Eine Freisetzung solcher Kolloide in die Geosphäre wäre allerdings stark von deren Stabilität und Mobilität abhängig.

Aus chemischer Sicht scheint Calciumbentonit stabiler als Natriumbentonit zu sein. Schlüsselparameter für die Nuklidspeziation, wie pH und Karbonatkonzentration, werden von Calciumbentonit bedeutend weniger stark beeinflusst, als von Natriumbentonit. Aus diesen Gründen wäre die Calciumform der Natriumform als Verfüllmaterial vorzuziehen, auch weil dabei eine zuverlässigere Voraussage der Quellterme für den Radionuklidtransport in der Geosphäre möglich würde.

Résumé

Une analyse de sécurité concernant la possibilité d'un stockage définitif de déchets hautement radioactifs en Suisse a été récemment publiée. Dans cette dernière, le terme source pour la migration des nucléides dans la géosphère a été éstimé sur la base des limites de solubilité maximales des nucléides dans les eaux granitiques profondes. Pour permettre une description plus réaliste de la libération de déchets hautement radioactifs, stockés définitivement, il faut spécifier quantativement, pour le dépôt considéré, la chimie du champ proche. La matrice de déchets vitrifiés, contenue dans un conteneur massif en acier, lui-même déposé horizontalement dans une galerie calmatée de bentonite de sodium constitue le champ proche tel qu'il est envisagé dans le concept suisse.

Ce travail présente d'une part un modèle qui permet de calculer, en fonction du temps, la composition chimique de l'eau interstitielle de la bentonite de sodium fortement compactée. D'autre part, les limites de solubilité et la spéciation sont calculés pour quelques actinides importants et pour le produit de fission technetium.

Le modèle se base sur la mesure de l'action de la bentonite de sodium sur une eau profonde et extrapole des données de laboratoire aux conditions de stockage. L'interaction entre la bentonite de sodium et l'eau profonde est décrite par une modèle d'échange ionique qui considère les cations échangeables suivants: sodium, potassium, magnesium et calcium. Deux hypothèses sont faites, à savoir que l'eau interstitielle de la bentonite compactée est saturée en calcite, aussi longtemps que la bentoniteee contient suffisemment de carbonates pour maintenir cet équilibre et d'autre part qu'il y a saturation en quartz. Le modèle prédit un pH de 9.7 et une activité de carbonate de $8 \cdot 10^{-4}$ M pour l'eau interstitielle de la bentonite compactée, saturée en eau profonde de référence suisse. Pour prédire le comportement à long terme de la bentonite un modèle simple a été ébauché qui considère le champ proche comme un réservoir mélangeur. Ainsi on essaye de modeler

l'échange continu de l'eau profonde entre le champ proche et la roche d'acceuil. Le calcul montre que la bentonite de sodium se transforme lentement en bentonite de calcium. Cette transformation durera, grossièrement estimé, environ deux millions d'années. L'altération en illite de la bentonite de sodium n'est pas considérée.

Les compositions chimiques du champ proche ainsi modelée sont à la base du calcul des limites de solubilité et de la spéciation des éléments suivant: uranium, neptunium, plutonium, thorium, américium et technetium. Il est supposé que le potential d'oxydoréduction du champ proche est déterminé par les produit de corrosion des conteneurs en acier. Sauf pour l'uranium et le neptunium, les limites de solubilité dans l'eau interstitielle du champ proche sont inférieures à celle des eaux granitiques non perturbées. Les solubilités de l'uranium et du neptunium dans le champ proche peuvent dépasser de plusieurs ordres de grandeur celles du champ éloigné, ce qui peut provoquer une brusque diminution de la concentration à la limite des champs ou à l'intérieur du matériaux de colmatage. La formation de colloïdes d'uranium et de neptunium dans cette zone ne peut pas être exclue avec certitude. La libération de tels colloïdes dans la géosphère dépendrait fortement de leur stabilité et de leur migration.

Chimiquement, la bentonite de calcium semble être plus stable que la bentonite de sodium. L'influence des paramètres clés sur la spéciation des nucléides tels que le pH et la concentration en carbonates est nettement plus faible en milieu bentonite de calcium qu'en milieu bentonite de sodium. C'est pourquoi, l'utilisation de la bentonite de calcium devrait être préférée à celle de sodium, d'autant plus que la prédiction du terme source pour le transport des radionucléides dans la géosphère serait plus sûre.

Table of Contents

1. Introduction 9

2. The Bentonite Model 13

2.1. The Effect of Sodium Bentonite on Groundwater: Available Experimental Data 13

2.2. Development of the Bentonite Model 21
2.2.1. General Remarks 21
2.2.2. Model Assumptions 22
2.2.3. Estimation of the Ion-Exchange Constants 26

2.3. Testing the Bentonite Model 33

2.4. Prediction of the Pore Water Chemical Composition in Compacted Sodium Bentonite: The Extrapolation Model 35

2.5. Long-Time Extrapolations: The Mixing Tank Model 39

2.6. A Natural Analogue to the Bentonite Model 46

3. Actinide and Technetium Speciation and Solubility Limits in the Bentonite Model Water 48

3.1. General Procedure 48

3.2. Uranium 51

3.3. Neptunium 55

3.4. Plutonium 60

3.5. Thorium 64

3.6. Americium 68

3.7. Technetium 73

4. Conclusions 77

Acknowledgements 79

References 80

Tables: Table 1..... 14
Table 2..... 16
Table 3..... 18
Table 4..... 31
Table 5..... 32
Table 6..... 34
Table 7..... 36
Table 8..... 42
Table 9..... 43
Tables B-1 to B-8.....from 88

Figures: Figure 1..... 9
Figure 2..... 11
Figure 3..... 23
Figure 4..... 38
Figure 5..... 44
Figure 6..... 44
Figure 7..... 45
Figure 8..... 50
Figures 9 to 26.....from 52
Figure A-1..... 86

Appendix A: The Speciation Model..... 84

Appendix B: Thermodynamic Data..... 87

1. Introduction

The near-field of a potential Swiss high-level waste (HLW) repository is envisaged to consist of a glass waste matrix, a thick steel canister horizontally emplaced in a tunnel, and a backfill of compacted bentonite, as shown in Figure 1 below (Nagra concept, 1985 [1]). In this report, the near-field boundary is assumed to be the tunnel walls. The unit cell, which is used as the reference area for the model, contains one waste container and is limited by the tunnel walls and the horizontal pitch of 5 meters (see Figure 1). It is called the Representative Elementary Volume (REV). The repository will be situated around 1200 meters below the surface in the granitic bedrock and, for the Project Gewaehr analysis [1], was considered to contain 5895 canisters of waste.

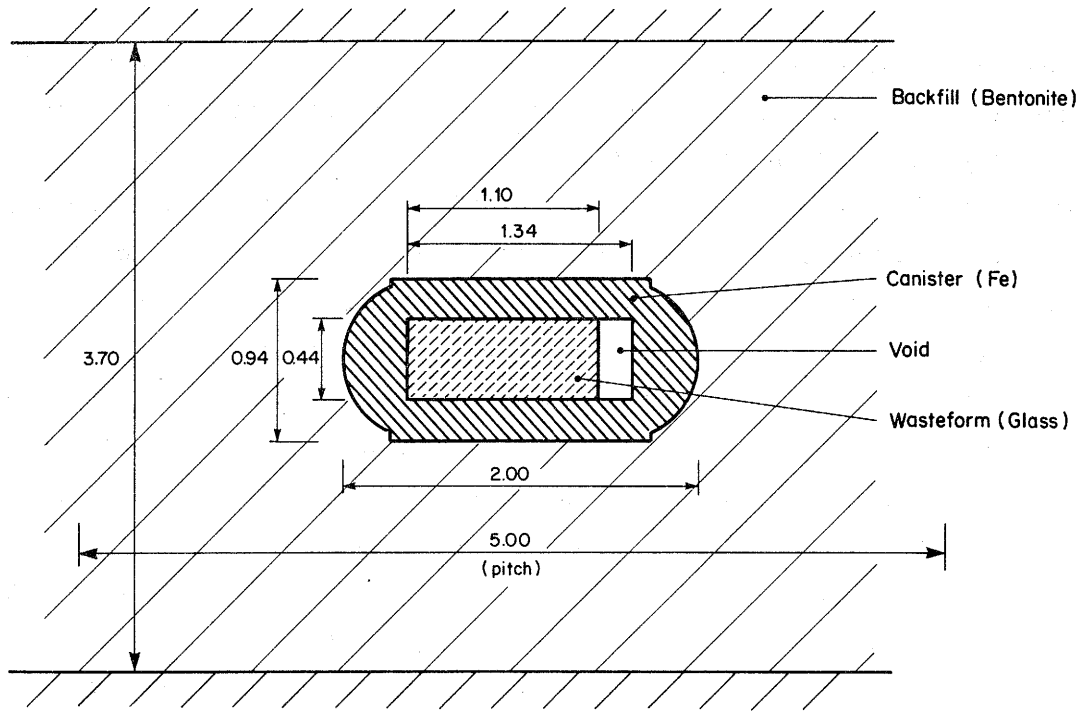

Figure 1: Waste emplacement geometry for a potential Swiss repository (dimensions given in meters). The figure shows a cross-section of the Representative Elementary Volume (REV).

The safety analysis of a final repository for radioactive waste involves a chain of models for the various processes, as shown in Figure 2. The compacted sodium bentonite in the near-field is an important barrier for the release of radionuclides into the geosphere. The geochemistry of the near-field has, to date, only been analysed at a rather general level [2]. In order to determine the source term (the release rate of radionuclides into the far-field), it is important to have some idea about the solubilities of essential radionuclides in the near-field water. Such an estimation requires information on the chemical composition of the pore water in compacted sodium bentonite. Although some experimental data exist on the influence of sodium bentonite on the chemical composition of groundwater, these experiments cannot reflect reality in a final repository. In the laboratory, small amounts of bentonite are brought into contact with large volumes of water, while the near-field of a final waste repository contains large amounts of sodium bentonite and a comparatively small volume of water. To date, extrapolation of chemical data from laboratory experiments to repository conditions has not been justified in the literature.

Based on available experimental data, this report presents a thermodynamic model which allows estimation of the pore water chemistry in compacted sodium bentonite. It should be emphasised that simplifications have to be made to describe the reactions between sodium bentonite and water quantitatively, in order to allow extrapolation to repository conditions. These simplifications aim at reducing the chemical complexity of the bentonite/water interaction by limiting the treatment to those processes which are considered the most relevant. The assumptions made herein are discussed in section 2.2.2. The model takes the tunnel walls to be the boundary between near- and far-field and is applicable to any type of groundwater infiltrating the near-field. A reaction path model, which considers the near-field as a mixing tank, has also been developed. It is dimensioned for the Swiss HLW near-field described above and used as a rough approximation to account for continuous water exchange between the near- and the far-field. The various chemical compositions of the bentonite pore water modelled in this way are used to estimate radionuclide solubilities in the near-field. The elements considered are: uranium, neptunium, plutonium, thorium, americium, and technetium.

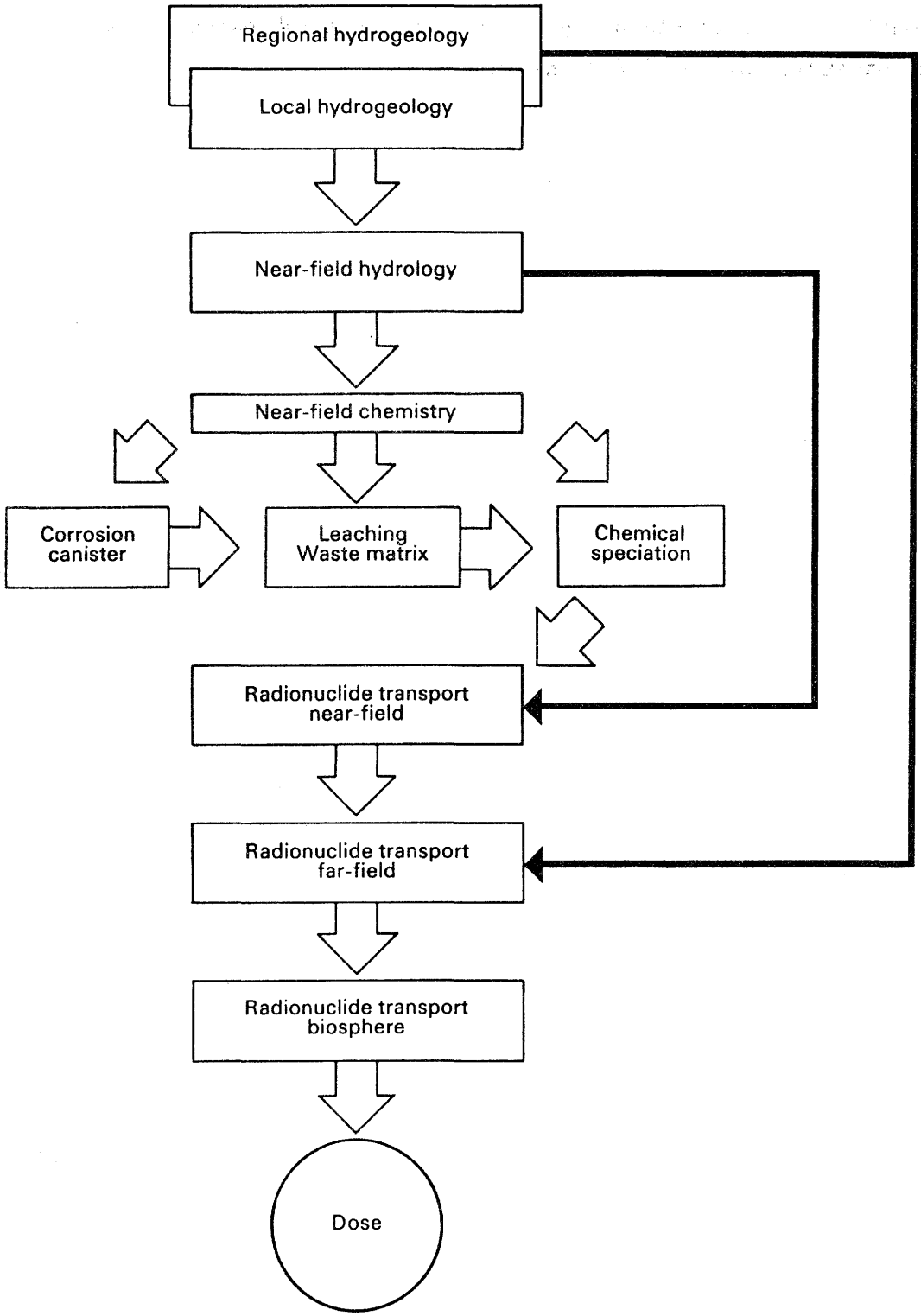

Figure 2: Model chain for the safety analysis.

The computer code used is an extended version of MINEQL/EIR [3,4,5]. More detailed information (e.g., the estimation of activity coefficients and the temperature dependence of equilibrium constants) is given in Appendix A. Appendix B presents a comprehensive list of the thermodynamic data used for the calculations.

2. The Bentonite Model

2.1. The Effect of Sodium Bentonite on Groundwater: Available Experimental Data

Among the very few experiments performed to date to study the consequences of bentonite reaction with groundwater, only one deals with the gradual change of the chemical composition of groundwater when brought into contact with bentonite [6]. In this experiment, samples of sodium bentonite powder MX-80 (40 cm^3) packed in filters were brought into contact with 1700 cm^3 of synthetic groundwater (Standard Swedish Groundwater). The samples were placed on a plastic net in a polyethylene can which was filled with water. Before placing the cans in an anaerobic box (at 25°C), the water was degassed with nitrogen. After certain time intervals, water samples were taken for analysis. The removed water was replaced by the same volume of water from parallel samples in an attempt to maintaining undisturbed consitions. Later, these experiments were repeated to allow improvement in experimental technique, but now using 40 g of bentonite and 1500 cm^3 of synthetic groundwater. These more recent data are listed in Table 1, but have not yet been published [7]. They show

- no evidence that an equilibrium state is reached between the groundwater and the bentonite after 90 days.

- an increase of the sodium concentration in the liquid phase, accompanied by a decrease of the concentrations of calcium, magnesium, and potassium.

- a marked increase of the alkalinity (which is defined as "the acid-neutralizing capacity of a solution when the end point of the titration is the CO_2 equivalence point" [8]).

- a significant rise in pH during the first 7 days followed by a surprising decrease during the subsequent time period, perhaps due to inadequate sampling (see below).

Table 1: The interaction between 1500 cm^3 of synthetic Standard Swedish Groundwater and 40 g of sodium bentonite MX-80 (measurements performed at 25°C by Snellman [7]).

Component (charges omitted)	Initial concentration [mol/l]	Concentration [mol/l] after contact with bentonite		
		7 days	30 days	90 days
Al	-	-	-	4.5 E-6
Na	2.26 E-3	5.35 E-3	8.52 E-3	1.01 E-2
K	1.0 E-4	7.7 E-5	5.6 E-5	4.6 E-5
Mg	1.9 E-4	1.2 E-4	1.4 E-5	1.9 E-5
Ca	4.64 E-4	2.84 E-4	3.17 E-5	4.57 E-5
Fe	-	-	-	4. E-7
NH_3	3. E-7	2.9 E-5	6. E-7	-
SiO_2	1.39 E-4	* 2.01 E-4	1.6 E-4	1.80 E-4
Cl	1.48 E-3	1.62 E-3	1.8 E-3	1.88 E-3
F	-	1.4 E-5	2.2 E-5	3.0 E-5
NO_3	3. E-7	2. E-7	1.8 E-6	-
NO_2 **	7. E-8	2. E-7	1.5 E-6	1. E-7
PO_4	2.1 E-6	-	1.5 E-6	8.3 E-6
HCO_3	1.80 E-3	1.63 E-3	3.31 E-3	6.78 E-3
CO_3	-	7.90 E-4	7.50 E-4	5.67 E-4
SO_4	1.0 E-4	5.99 E-4	6.09 E-4	1.52 E-4
pH	8.12	9.58	* 9.26	9.09
Alkalinity [eq/l]	1.94 E-3	3.24 E-3	5.20 E-3	7.93 E-3
Eh [mV]	-	-	-	-200 to -300

* Large differences in replicate samples
** Nitrite is not taken into consideration in the bentonite model.

- the concentration of silicic acid remaining more or less unchanged.

- the Eh measurements performed for the 90-days sample indicating reducing conditions, although such measurements have to be regarded with great care [9].

- the concentration of bicarbonate in the initial groundwater being suspicious, since, at this pH value, it would be expected to be virtually equal to the alkalinity.

Assuming ion-diffusion reactions between the liquid in the packed bentonite powder and the bulk solution to be the rate determining processes (neglecting the possible occurrence of mineral transformation) and therefore the species in the analysed samples to be in thermodynamic equilibrium with each other, allows the use of the code MINEQL/EIR [3,4,5] (the speciation model applied is described in Appendix A, the thermodynamic database used for all calculations is listed in Appendix B.) to check the consistency of the experimental results. Given the alkalinities and the total concentrations of the components from the corresponding analytical data (see Table 1), the charge balance for the dissolved species, the pH, and the saturation index for calcite can be calculated. Table 2a shows that the charge balance is not satisfactory for the 7-days and especially the 30-days analysis, which indicates some experimental inadequacy. Further, the bentonite solutions are found to be oversaturated with respect to calcite. Since the turbid samples had not been filtered before analysis [7], it is possible that part of the turbidity consisted of precipitated calcium carbonate. Therefore, the speciation calculations are repeated, allowing calcium carbonate to precipitate as calcite. In this way, the total concentration of calcium, which is an important parameter for the development of the bentonite model discussed below, can be corrected for the amount of calcite precipitate. The results of these evaluations are listed in Table 2b. It can be seen that, beside quartz saturation, oversaturation with dolomite is calculated for all the solutions in contact with sodium bentonite. There are, however, good reasons to believe that, contrary to calcite, dolomite did not precipitate in the laboratory experiment. Stumm and Morgan [10] point out that dolomite

Table 2: Specification of the water analyses listed in Table 1 by means of the code MINEQL/EIR, assuming thermodynamic equilibrium between the dissolved species (Temperature = 25 °C).

	Initial	7 days	30 days	90 days
a) No precipitation assumed:				
Charge balance (%) *	+2.0	+3.7	+9.6	+1.4
pH calculated	8.15	9.66	9.45	9.02
log $p(CO_2)$	-3.09	-4.63	-4.14	-3.41
log SI ** of calcite	-0.03	1.06	0.14	0.20
log SI ** of dolomite	-0.17	2.09	0.26	0.34
log SI ** of quartz	0.10	0.03	0.01	0.15
Ionic strength [mol/l]	0.0044	0.0073	0.0094	0.0108
b) Calcite Precipitation:				
Charge balance (%) *	2.0	3.9	9.6	1.4
pH calculated	8.15	9.53	9.44	9.01
log $p(CO_2)$	-3.09	-4.51	-4.14	-3.40
$CaCO_3$ precipitated [mol/l]	-	2.53 E-4	8.41 E-6	1.60 E-5
Calc. calcium conc. [mol/l]	4.64 E-4	3.09 E-5	2.33 E-5	2.97 E-5
log SI ** of dolomite	-0.17	0.92	0.12	0.14
log SI ** of quartz	0.10	0.09	0.01	0.16
Ionic strength [mol/l]	0.0044	0.0066	0.0094	0.0108

* Percentage difference between the total positive and the total negative charge, referred to the total positive charge.

** SI = saturation index. SI is defined as the quotient of the ion activity product of the potentially dissolved free components of the solid, and the solubility product, Kso, of the solid. SI > 1 (log SI > 0) represents oversaturation.

$$SI(Calcite) = \frac{\{Ca^{2+}\} \cdot \{CO_3^{2-}\}}{Kso(CaCO_3)}$$

generally will not precipitate from oversaturated solutions, and hence such precipitation appears unimportant as a controlling factor in carbonate equilibria in most natural waters.

From these experimental results, the main reactions between sodium bentonite and groundwater can be described in the following way: Sodium ions in the bentonite exchange for calcium ions from the groundwater. This leads to a considerable decrease of the calcium concentration in the aqueous solution. Sodium bentonite contains carbonates (see Table 3), which can dissolve if the water is undersaturated with respect to carbonate bearing minerals, such as calcite. This case exists as soon as calcite saturated groundwater comes in contact with sodium bentonite and calcium is removed from the solution to a certain extent. The subsequent dissolution of carbonate from the sodium bentonite (limited by the solubility product of calcite) is the reason for the increase of the alkalinity (see Table 1) and of pH:

$$2\ Na(ex) + CaCO_3\ (s) + H_2O \rightleftharpoons Ca(ex) + 2\ Na^+ + HCO_3^- + OH^-$$

This process has been observed in nature (and is discussed in section 2.6.) and is therefore a realistic explanation of the experimental data. The fact that, after a considerable initial increase in pH, the pH was measured to decrease again after a certain time, could be due to experimental limitations (see discussion in section 2.3.). Although the experiments are reported to be carried out under anaerobic conditions, the content of carbon dioxide in the nitrogen atmosphere was not measured. It is not reported if the anaerobic box was checked to be completely impermeable for carbon dioxide. Further, commercial nitrogen gas may contain small amounts of carbon dioxide, and should therefore be passed through hydroxide solution before use. Since alkalinic solutions absorb carbon dioxide strongly, uptake of carbon dioxide by the groundwater in contact with sodium bentonite can therefore not be excluded. This could explain the lower pH in the 30- and 90-days samples compared to the 7-days sample provided that carbon dioxide could slowly diffuse through the walls of the anaerobic box, or that CO_2 got into the solution during the sampling procedures after 7 and 30 days. It is shown in section 2.3. that the bentonite model, as described in section 2.2., predicts the same pH value and alkalinity as was measured

Table 3: Sodium bentonite MX-80: Data required to develop the bentonite model.

Cation-exchange capacity *:		76.4 meq/100 g		[11]
Exchangeable cations *:	Na	62.4 meq/100 g	(85.5 %)	[11]
	K	0.2 meq/100 g	(0.3 %)	[11]
	Mg	3.0 meq/100 g	(4.1 %)	[11]
	Ca **	7.4 meq/100 g	(10.1 %)	[11]
	sum	73.0 meq/100 g	(100.0 %)	[11]
Total content of carbonates (calculated as $CaCO_3$):		1.4 %		[11]
Dry density of highly compacted bentonite:		1.70 g/cm^3		[12]
Density of water-saturated, highly compacted bentonite:		2.07 g/cm^3		[12]
Volume of bentonite per waste canister (REV ***) in a Swiss high-level repository:		52.8 m^3		[2]
Approximate volume of pore water per REV *** in the saturated mass of bentonite (108.5 tonnes):		20.1 m^3		[2]

* These numbers refer to 100 g of oven-dried material.

** The method used to determine exchangeable calcium could be subject to a systematic error because it allows calcite from the bentonite to dissolve [13].

*** REV = Representative Elementary Volume (cf. Fig. 1).

for the 90-days sample, if the solution is assumed to be in contact with air (log $p(CO_2)$ = -3.5).

There are other experiments reported in the open literature which also consider the interaction between groundwater and sodium bentonite. However, most of these experiments had been designed to get information which is different from that required for the prediction of the pore water chemical composition in compacted sodium bentonite. Among these are: the leachability of bentonite, mineral alteration and swelling properties of clays, the influence of bentonite on canister corrosion, sorption of nuclides on clay minerals, and solute-diffusion through compacted bentonite. In most of these cases, the pH value is the only experimental parameter analysed which gives some information on the chemical status of the water that had been brought into contact with the bentonite. For example, in KBS-3 [14] it is assumed that the pH value of bentonite pore water lies in the range of 8 to 9. Simpson [15] stated that "Bentonite ..... is expected to buffer the pH in the range of 7 to 9 and possesses ion exchange properties". Grauer [16] noted that the pH value in bentonite suspensions is between 8.5 and 10. On the other hand, it should be mentioned that there are some experiments in which a decrease of pH has been observed when groundwater was brought into contact with sodium bentonite at elevated temperatures. For instance, Johnston and Miller [17] reported that the pH of sodium montmorillonite suspensions is measured to be 9.5 at 25°C, but decreases to pH = 3 to 6 after hydrothermal treatment at temperatures between 150°C and 300°C for up to 30 days. This behaviour could be due to a mineral transformation which might also occur at low temperatures but is accelerated at elevated temperatures, and which converts the clay layer surfaces into proton-rich surfaces that are likely to release hydrogen ions even in neutral or slightly acidic solutions. On the other hand, such transformations could be so strongly hindered that they do not occur at low temperatures, even on geological timescales. As alternative explanation, the acidification might be due to a charge increase of the montmorillonite layers, as recently pointed out by Grauer [18, p.21] with the additional note that this process is so slow under repository conditions that the bentonite itself possesses enough buffering capabilities to outweigh the mentioned effect before the water is transported away. The two latter interpretations are supported by

observations in nature, where aquifers in clay-rich formations are found to have unusually high pH values and bicarbonate concentrations (see section 2.6.). A decrease in the pH of groundwater in contact with sodium bentonite thus seems very improbable under repository conditions, even if there are mechanisms which imply a release of protons from the bentonite, because such reactions appear to be veiled by faster pH buffering processes.

In this context, a paper recently presented by Grambow et al. [19] needs to be discussed. In that work, an equilibrium model for the bentonite/water system is presented. It is used to reproduce the analytical results of 3 equilibration experiments of sodium bentonite and water. Part of the experiments, on which this model in based, are taken from the same source [7] as those described in section 2.1. of the present report. Other data were obtained by leaching bentonite at 45°C for one day or for eight hours, without specifying the initial composition of the water used. In total, the chemical analyses of eight experimental solutions are reported with a clay/water ratio in the range of 0.03 to 0.23. The final pH was found to be around 9 for all solutions. Since a constant partial pressure of CO_2, according to equilibrium with air, is assumed as a boundary condition, the model cannot be used to predict the chemical composition of bentonite pore water under deep repository conditions. The chemical interaction of sodium bentonite and water is interpreted in terms of an ion-exchange reaction involving Na^+ and H^+ as the only exchangeable cations, whereas the bentonite model developed in the present report considers Na^+, K^+, Mg^{2+}, and Ca^{2+} as the exchangeable cations (see paragraph ii. of section 2.2.2.). Grambow et al. state that the active component of the bentonite is montmorillonite, and that the influence of minor constituents such as quartz, felspar, calcite, and siderite can be neglected. In fact, calcite dissolution and precipitation equilibrium (which is affected by ion-exchange of Ca^{2+}) is of critical importance as it influences key parameters for actinide speciation like pH and carbonate activity. The bentonite model described in section 2. considers calcite and quartz saturation rather than a bulk solubility of montmorillonite as the model of Grambow et al. does.

2.2. The Development of the Bentonite Model

2.2.1. General Remarks

A model of the chemical composition of pore water in compacted bentonite involves more than interpretation of laboratory data, followed by qualitative extrapolation to the possible situation in a deep repository. Such extrapolations are very difficult, especially if the dominating processes are ion-exchange reactions which affect key parameters. For example, the implication of calcium in ion-exchange processes between sodium bentonite and groundwater is of significance, because the calcium concentration controls the carbonate activity through the saturation equilibrium with calcite. Consequently, calcium indirectly also influences the bicarbonate activity and pH. The whole system of equilibria is thus very sensitive to the proportion of calcium which reacts with the bentonite and, since ion-exchange reactions are concerned, is also very sensitive to the clay/water ratio. In the experiments performed to date, the clay/water ratio lies between 0.02 and 0.2, whereas in compacted and water-saturated bentonite the ratio is around 5, i.e. one to two orders of magnitude higher. That is why the chemical composition of the water in compacted sodium bentonite could considerable deviate from that measured in the laboratory. In addition, a high degree of compaction may lead to an increased surface effect (e.g., change in the pK of water, surface charge effects, steric effects), parameters which are not taken into account in the bentonite model.

2.2.2. Model Assumptions

The model developed here, which can be applied to predict the pore water chemical composition in compacted sodium bentonite, involves to a number of assumptions.

i. It is assumed that thermodynamic models can be applied to describe the chemical processes occurring in the near-field. This assumption implies that there are interconnected pores in compacted sodium bentonite, which contain water (so-called pore water), so that the proportion of water molecules firmly bound to the surface of the montmorillonite is low, which means that the liquid phase in saturated compacted sodium bentonite can be considered as an aqueous solution. Since the purpose of this model is to describe the characteristics of the near-field aqueous phase which is capable of enabling the transport of waste nuclides, the microscopic state of the water in the interlamellar space (i.e. the 1 to 2 nm wide space between the double layers [20]) is not of importance to the bentonite model.

ii. Sodium, potassium, magnesium, and calcium are assumed to be the only ions participating in ion-exchange reactions between sodium montmorillonite and the aqueous phase (see footnote). A possible implication of H^+ in the ion-exchange processes is discounted, because such a reaction is not found to be of major importance regarding the analytical data in Table 1. Moreover, the sodium bentonite pore water is assumed to be saturated with a powerful pH

Strontium could also conceivably take part in such ion-exchange reactions, but it has not been analysed in the experiments considered here. However, strontium can be neglected anyway in the Swiss case because its concentration in the Swiss deep-crystalline reference groundwater (see Table 7) is two orders of magnitude below that of the similarly reacting calcium.

buffer: calcite (see paragraph iii.). Equilibrium with this mineral will most probably dominate over a possible H^+-exchange reaction anyway. The ion-exchange processes modelled are based on complex formation equilibria involving ion-exchange sites (represented as Z^-) of the montmorillonite and the cations mentioned, as shown in Figure 3 below. The ion-exchange sites are theoretically treated as simple ligands dissolved in the pore water. All sites are considered equivalent, carrying one negative charge and being capable of coordinating sodium, potassium, magnesium, and calcium only. The assumption of dynamic equilibrium between the solid and the liquid phase implies that each of the four reactions can be described by an equilibrium relation. These relations are assumed to be constant over the ion concentrations modelled and can thus be described by equilibrium constants. The equilibrium constants are derived from the corrected analytical data of groundwater having been in contact with sodium bentonite for 90 days at a temperature of 25°C. The corresponding data are listed in Table 1 and Table 2.

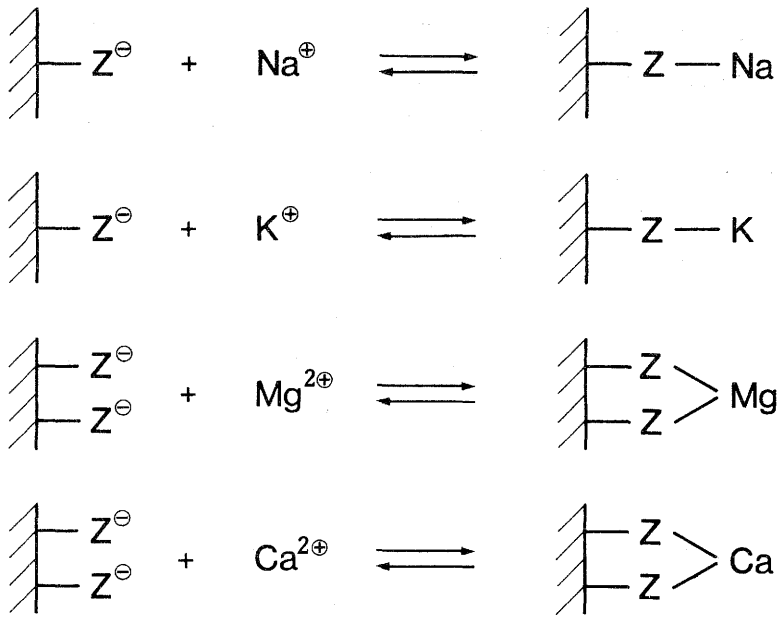

Figure 3: Complexation reactions of sodium, potassium, magnesium, and calcium with the negatively charged ion-exchange sites (described by the symbol Z) on the surface of the montmorillonite layers. These equilibria are taken as a basis for the ion-exchange reactions between bentonite and groundwater.

Data on the exchangeable cations, Na^+, K^+, Mg^{2+}, and Ca^{2+}, of sodium bentonite MX-80 (see Table 3) are also needed for the calculation of the constants, and it is assumed that the entire ion-exchange capacity is available for the pore water. No correction is made for possible inter-ionic repulsions between the cations sorbed on the montmorillonite layers, because only the proportions of the absorbed ions change during the modelled reaction pathway, not the total sum of positive charges. Because of the lack of corresponding data, no temperature correction of the ion-exchange constants is made between 25°C (experimental procedure) and 55°C (ambient temperature at a potential deep crystalline repository site). It should be noted that the ion-exchange constants derived in this way are possibly subject to a certain error, because it is not sure whether the analysis of the 90-days sample represents an equilibrium state or how far away from equilibrium the analysed solution is. Nevertheless, the derived constants can be considered as best estimates which may be used to show the directions and the relative extents of the relevant ion-exchange reactions between sodium bentonite and groundwater. It is important to mention that a possible disequilibrium in the 90-days sample does not invalidate the mechanisms involved in the equilibrium model, because the possible disequilibrium is confined to ion-diffusion processes between the liquid in the packed bentonite powder and the bulk solution. The relevant reactions in the liquid phase, as well as the precipitation and dissolution of calcite, are fast processes where the equilibrium state is acknowledged to be established in a short time. The only consequence of lack of equilibrium would be that the ion-exchange constants would change. A few test calculations (which are not presented in this report) have shown that such changes would be small, and that the ion-exchange constants would vary proportionally, thus not exhibiting a principal impact on the results of the model.

iii. The pore water in compacted bentonite is assumed to be saturated with respect to calcite and quartz. This assumption is not unreasonable as long as enough carbonates are available in the bentonite, since most groundwaters are found to be in equilibrium

with these two minerals. Oversaturation of calcite or quartz is generally not observed in natural groundwaters, except for a number of cases where amorphous silica is present which has a slightly higher solubility than quartz (cf. Table B-3, Appendix B). The assumption of quartz saturation rather than saturation with amorphous silica is nevertheless justified because the silica in the bentonite is found to be present in the form of quartz [11]. For the model calculations, the carbonate reservoir of sodium bentonite is known initially (see Table 3) and checked during the calculations. Although the model calculations predict oversaturation with respect to dolomite, this mineral is not assumed to be formed, since it is observed that dolomite does not form by precipitation [10].

iv. For long-time extrapolations, the near-field is considered as a box or mixing tank. That is, the groundwater which flows past the repository is modelled to mix with the near-field water and to leave the repository area with an altered composition resulting from the equilibration with sodium bentonite. In this way, account is taken for the leaching of the bentonite. Reaction ends when groundwater diffusing into the near-field is no longer altered because the ion-exchange capacity of sodium bentonite is exhausted relative to the groundwater chemical composition.

2.2.3. Estimation of the Ion-Exchange Constants

There are 6 conceivable ion-exchange reactions among the four cations considered. Each of these reactions is characterised by an equilibrium constant, K(i):

$$(1) \quad ZNa + K^{+} \rightleftharpoons ZK + Na^{+} \quad ; \quad K(1)$$

$$(2) \quad 2\,ZNa + Mg^{2+} \rightleftharpoons Z_2Mg + 2\,Na^{+} \quad ; \quad K(2)$$

$$(3) \quad 2\,ZNa + Ca^{2+} \rightleftharpoons Z_2Ca + 2\,Na^{+} \quad ; \quad K(3)$$

$$(4) \quad 2\,ZK + Mg^{2+} \rightleftharpoons Z_2Mg + 2\,K^{+} \quad ; \quad K(4)$$

$$(5) \quad 2\,ZK + Ca^{2+} \rightleftharpoons Z_2Ca + 2\,K^{+} \quad ; \quad K(5)$$

$$(6) \quad Z_2Mg + Ca^{2+} \rightleftharpoons Z_2Ca + Mg^{2+} \quad ; \quad K(6)$$

Since the 6 equilibrium reactions are mutually dependent, it is expedient to separate them into their four fundamental equilibria which, in fact, are analogous to complexation reactions:

$$(7) \quad Z^{-} + Na^{+} \rightleftharpoons ZNa \quad ; \quad K(7)$$

$$(8) \quad Z^{-} + K^{+} \rightleftharpoons ZK \quad ; \quad K(8)$$

$$(9) \quad 2\,Z^{-} + Mg^{2+} \rightleftharpoons Z_2Mg \quad ; \quad K(9)$$

$$(10) \quad 2\,Z^{-} + Ca^{+} \rightleftharpoons Z_2Ca \quad ; \quad K(10)$$

All the species involved in reactions (7) to (10) are theoretically considered to be dissolved in the aqueous phase. It is not possible to extract the absolute values of constants K(7) through K(10) from analytical data, but the experiments give information about the relations between the four constants. The problem can be solved with the assumption that virtually all exchange sites Z^- are occupied. This is done by arbitrarily setting the logarithm of K(7) equal to 20.0, which is so high that the activity of uncoordinated Z^- is practically equal to zero. The constants are defined as follows (brackets, { }, indicate activities):

(11) $\log K(7) = 20.0 = \log\{ZNa\} - \log\{Z^-\} - \log\{Na^+\}$

(12) $\log K(8) = \log\{ZK\} - \log\{Z^-\} - \log\{K^+\}$

(13) $\log K(9) = \log\{Z_2Mg\} - 2\log\{Z^-\} - \log\{Mg^{2+}\}$

(14) $\log K(10) = \log\{Z_2Ca\} - 2\log\{Z^-\} - \log\{Ca^{2+}\}$

The MINEQL/EIR database (see Appendix B) comprises activity constants, which refer to zero ionic strength [3]. Since the analytical data are concentration values, not activities, the constants derived from these data have to be corrected for corresponding activity coefficients:

(15) $\log\{i\} = \log[i] + \log f(i)$

The equation system (11),(12),(13),(14) can now be written as follows:

(16) $\log K(7) = 20.0 = \log[ZNa] - \log[Z^-] - \log[Na^+] + \log f(ZNa) - \log f(Z^-) - \log f(Na^+)$

(17) $\log K(8) = \log[ZK] - \log[Z^-] - \log[K^+] + \log f(ZK) - \log f(Z^-) - \log f(K^+)$

(18) $\log K(9) = \log[Z_2Mg] - 2 \log[Z^-] - \log[Mg^{2+}] + \log f(Z_2Mg) - 2 \log f(Z^-) - \log f(Mg^{2+})$

(19) $\log K(10) = \log[Z_2Ca] - 2 \log[Z^-] - \log[Ca^{2+}] + \log f(Z_2Ca) - 2 \log f(Z^-) - \log f(Ca^{2+})$

The equilibrium constants log K(8), log K(9), and log K(10) of equilibrium system (16),(17),(18),(19) can now be expressed in relation to log K(7) by eliminating $[Z^-]$ and $f(Z^-)$:

(20) $\log K(7) = 20.0$ (by definition)

(21) $\log K(8) = \log K(1) + \log[Na^+] - \log[ZNa] - \log[K^+] + \log[ZK] + \log f(Na^+) - \log f(ZNa) - \log f(K^+) + \log f(ZK)$

(22) $\log K(9) = 2 \log K(1) + 2 \log[Na^+] - 2 \log[ZNa] - \log[Mg^{2+}] + \log[Z_2Mg] + 2 \log f(Na^+) - 2 \log f(ZNa) - \log f(Mg^{2+}) + \log f(Z_2Mg)$

(23) $\log K(10) = 2 \log K(1) + 2 \log[Na^+] - 2 \log[ZNa] - \log[Ca^{2+}] + \log[Z_2Ca] + 2 \log f(Na^+) - 2 \log f(ZNa) - \log f(Ca^{2+}) + \log f(Z_2Ca)$

The concentrations $[Na^+]$, $[K^+]$, $[Mg^{2+}]$, and $[Ca^{2+}]$ are taken from the 90-days analysis (listed in Table 1 for Na^+, K^+, and Mg^{2+}, and in Table 2 for Ca^{2+}) for which the ionic strength is calculated to be I = 0.0108 mol/l (298 K). The activity coefficients for each species are estimated using Davie's approximation (see Appendix A):

(24) $\log f(ZNa) = \log f(ZK) = \log f(Z_2Mg) = \log f(Z_2Ca) = 0$

(25) $\log f(Na^+) = \log f(K^+) = \log f(Z^-) = -0.046$

(26) $\log f(Mg^{2+}) = \log f(Ca^{2+}) = -0.184$

Combining equations (20), (24), (25), and (26) with equations (21), (22), and (23) gives

(27) $\log K(8) = 20.0 + \log[Na^+] - \log[ZNa] - \log[K^+] + \log[ZK]$

(28) $\log K(9) = 40.0 + 2\log[Na^+] - 2\log[ZNa] - \log[Mg^{2+}] + \log[Z_2Mg] + 0.092$

(29) $\log K(10) = 40.0 + 2\log[Na^+] - 2\log[ZNa] - \log[Ca^{2+}] + \log[Z_2Ca] + 0.092$

The concentrations values [ZNa], [ZK], [Z_2Mg], and [Z_2Ca] are considered to correspond to the initial exchangeable cations of the bentonite, corrected for the amount of the exchanged cations after 90 days (added or subtracted). They are calculated as follows:

The exchangeable cations of sodium bentonite are given in meq per 100 g of bentonite. In order to be applicable to the model used here, they have to be converted into concentration values, expressed as mmols per litre of water. In the reference experiment, 40 g of sodium bentonite were contacted with 1500 cm^3 of synthetic groundwater, which corresponds to a proportional mass of 26.7 g of bentonite available for 1000 cm^3 of water. Consequently, the exchangeable cations (meq/100 g) listed in Table 3 have to be multiplied by 0.267 to get the initial concentrations of ZNa, ZK, Z_2Mg, and Z_2Ca in meq per litre of water, listed in the first line of the Table 4 below.

The amount of exchanged cations per litre of water is simply calculated by deducting the concentration measured in the 90-days sample from the initial concentration (Table 1). The resulting values are listed in the second line of Table 4 below. The value of magnesium was multiplied by 2 to convert from mmol to meq. The calculation mentioned above cannot

be done for calcium, because the assumption of calcite saturation introduces another calcium source to the system. Assuming the ion-exchange capacity of bentonite to be constant, allows the calculation of the equilibrium content of calcium (9.45 meq). The resulting values (below the dotted line in Table 4) correspond to the concentrations [ZNa], [ZK], [Z_2Mg], and [Z_2Ca] in meq/l. After conversion to molar units (implying division by the index of Z), they can be input (as logarithms) in equations (27), (28), and (29) to calculate the equilibrium constants log K(8), log K(9), and log K(10). The values for [Na^+], [K^+], and [Mg^{2+}] are taken from the 90-days analysis (see Table 1). For [Ca^{2+}], the corrected value from Table 2b is used. The resulting constants are listed in Table 5 below. These values are used to model the effect of bentonite on groundwater, assuming equilibrium with calcite and quartz. The extrapolation to repository conditions is made by increasing the total concentration of Z^- to a value corresponding to the availability of ion-exchange sites per litre of pore water in compacted sodium bentonite, as described in section 2.4.

Table 4: The change in the single ion-exchange capacities of sodium bentonite MX-80 during the reaction with Standard Swedish Groundwater, calculated from the experimental data in Table 1 and Table 3, referred to 26.7 g of bentonite and 1000 cm^3 of water).

	Na^+	K^+	Mg^{2+}	Ca^{2+}
Initial content in bentonite (meq)	16.7	0.05	0.8	2.0
Exchanged after 90 days (meq)	- 7.8	+ 0.05	+ 0.3	
Equilibrium content in bentonite (meq)	8.9	0.1	1.1	9.45

Table 5: Equilibrium constants caluclated for the 4 fundamental reactions involved in the ion-exchange processes considered: (7), (8), (9), and (10), and those derived for the ion-exchange reactions: (1), (2), (3), (4), (5), and (6).

(7)	Z^-	+ Na^+	$\rightleftharpoons$	ZNa	;	log K(7)	= 20.0 (by def.)
(8)	Z^-	+ K^+	$\rightleftharpoons$	ZK	;	log K(8)	= 20.4
(9)	2 Z^-	+ Mg^{2+}	$\rightleftharpoons$	Z_2Mg	;	log K(9)	= 41.7
(10)	2 Z^-	+ Ca^{2+}	$\rightleftharpoons$	Z_2Ca	;	log K(10)	= 42.4

(1)	ZNa	+ K^+	$\rightleftharpoons$	ZK	+ Na^+	;	log K(1)	=	0.4
(2)	2 ZNa	+ Mg^{2+}	$\rightleftharpoons$	Z_2Mg	+ 2 Na^+	;	log K(2)	=	1.7
(3)	2 ZNa	+ Ca^{2+}	$\rightleftharpoons$	Z_2Ca	+ 2 Na^+	;	log K(3)	=	2.4
(4)	2 ZK	+ Mg^{2+}	$\rightleftharpoons$	Z_2Mg	+ 2 K^+	;	log K(4)	=	0.9
(5)	2 ZK	+ Ca^{2+}	$\rightleftharpoons$	Z_2Ca	+ 2 K^+	;	log K(5)	=	1.6
(6)	Z_2Mg	+ Ca^{2+}	$\rightleftharpoons$	Z_2Ca	+ Mg^{2+}	;	log K(6)	=	0.7

2.3. Testing the Bentonite Model

The bentonite model developed in section 2.2. can be tested by applying it to the groundwater used for the experiments in the following way: To the initial chemical composition of Standard Swedish Groundwater, sodium bentonite is theoretically added in the form of [Z]tot = 19.5 meq/l, which corresponds to the ion-exchange capacity of the sodium bentonite mass (26.7 g per litre of water) used in the experiment. The ion-exchange sites are considered to be initially bound to sodium, potassium, magnesium, and calcium according to the proportional distribution of the exchangeable ions in sodium bentonite as given in Table 3.

The presumable composition of the equilibrated bentonite water is calculated using the speciation code MINEQL/EIR [3,4,5] (The speciation model applied is described in Appendix A, the thermodynamic database used for all calculations is listed in Appendix B.). The resulting values of those parameters, which allow a comparison with the experimental ones, are listed in the third column of Table 6 below and refer to completely anaerobic conditions. It is not surprising that the model predicts a pH value which is considerably higher than that measured after 90 days, since there are reasons to suspect that the experiments were not carried out under strictly anaerobic conditions. However, with the assumption that the partial pressure of CO_2 equals that of the air (log $p(CO_2)$ = -3.5), the calculated parameters match the measured ones very well, as can be seen from the last column of Table 6 below. The reason for this is the dissolution of carbon dioxide gas, which is an especially favoured process at high pH values. The subsequent deprotonation of carbonic acid:

$$CO_2 + H_2O \rightleftharpoons HCO_3^- + H^+$$

does not only result in a decrease of pH, but also in an increase of the alkalinity, because the addition of acid leads to an enhanced dissolution of calcite.

Table 6: Comparison of experimental and modelled composition of Standard Swedish Groundwater after contact with sodium bentonite, in terms of a test application of the bentonite model. The first column contains values of the original groundwater, the second gives the analytical results from Table 1 and Table 2 (Ca^{2+}). The model was applied to the initial groundwater composition for 25°C, assuming the added bentonite to be represented by [Z]tot = 19.5 meq/l (all ion-exchange sites Z^- being coordinated with the corresponding proportions of the exchangeable cations, Na^+, K^+, Mg^{2+}, and Ca^{2+}) according to the bentonite/water ratio used in the experiment. The results are shown in the third column, whereas those presented in the last column are calculated with the additional assumption of a constant partial pressure of CO_2, equivalent to equilibrium with air: log $p(CO_2)$ = -3.5.

	Initial composition	Experimental after 90 days	Modelled anaerobic	Modelled aerobic
pH	8.12	9.09	10.0	9.1
Alkalinity	1.94 E-3	7.93 E-3	5.7 E-3	7.7 E-3
log $p(CO_2)$	-3.09	-3.40	-4.9	-3.5 (set)
[Na]tot (mol/l)	2.26 E-3	1.01 E-2	7.3 E-3	9.3 E-3
[K]tot (mol/l)	1.0 E-4	4.6 E-5	3.2 E-5	4.5 E-5
[Mg]tot (mol/l)	1.9 E-4	1.9 E-5	8.9 E-6	1.6 E-5
[Ca]tot (mol/l)	4.64 E-4	2.97 E-5	1.3 E-5	2.7 E-5

2.4. Prediction of the Pore Water Chemical Composition in Compacted Sodium Bentonite: The Extrapolation Model

The prediction of the chemical composition of the pore water in the near-field of a high-level waste repository requires an extrapolation of the experimental data to conditions, which correspond to compacted sodium bentonite saturated with groundwater. From the data listed in Table 3, it can be calculated that 100 g of dry sodium bentonite will take up 21.8 g of water to become saturated, which means that 21.8 ml of pore water will be in contact with 73 meq of ion-exchange sites Z^- (taking 1.00 g/ml as the density of water). Accordingly, the availability of ion-exchange sites per litre of pore water will amount to [Z]tot = 3.35 eq/l in compacted sodium bentonite.

Two different types of groundwater are used for the application of the model. The reference water for this report is the same as that used for the safety analysis recently reported by Nagra [1]. It is a deep-crystalline groundwater sampled in the granitic basement of northern Switzerland, at a depth of 1326 m below the surface. The water is characterised by a relatively high degree of mineralisation. Its composition is listed in Table 7. For comparative reasons, the model calculations are also carried out for a granitic groundwater of low ionic strength, represented by Standard Swedish Groundwater. The composition of this type of groundwater is given in the first column of Table 1.

The extrapolation process is represented as a titration experiment, where the water is titrated with bentonite (represented by Z): The alteration of the groundwater composition is first calculated for the case that [Z]tot = 10^{-4} mol/l, using the ion-exchange constants listed in Table 5. Subsequently, [Z]tot is increased step by step, up to [Z]tot = 10 mol/l. As counter-ions to Z^-, the cations Na^+, K^+, Mg^{2+}, and Ca^{2+} are introduced to the system, according to their proportional contribution to the ion-exchange capacity of sodium bentonite (see Table 3). The changes of some chemical parameters during this extrapolation process are presented in Figure 4 for both types of groundwater. In both cases, the calculations are carried out for a

Table 7: Chemical composition of the deep-crystalline Swiss Reference Groundwater (Boettstein water) used for the safety analysis in project Gewaehr 1985.
Source: Refs. [21,22].

Component	Concentration
Na	1.756 E-1 mol/l
K	1.15 E-3 mol/l
Mg	1.07 E-4 mol/l
Ca	2.17 E-2 mol/l
Sr	2.40 E-4 mol/l
Fe	8.06 E-6 mol/l
Mn	5.64 E-5 mol/l
NH_3	1.1 E-5 mol/l
SiO_2	2.83 E-4 mol/l
Cl	1.867 E-1 mol/l
F	1.90 E-4 mol/l
SO_4	1.62 E-2 mol/l
PO_4	1.9 E-6 mol/l
Alkalinity	1.58 E-3 eq/l
Temperature	55 °C
Ionic strength	0.24 mol/l
pH	6.78
CO_3 (total)	1.91 E-3 mol/l
Eh [mV]	-230 to -60

temperature of 55°C, which is the reference temperature for a deep Swiss repository envisaged in Project Gewaehr 1985 [1] (Temperature profile calculations show that the main thermal peak will decay away within some tens of years after the canister emplacement [23].). The dotted vertical intersection at [Z]tot = 3.35 mol/l in Figure 4 gives the chemical composition of the pore water in compacted sodium bentonite. Although the pore water compositions predicted by the bentonite model are similar for both types of groundwater, the buffering effect of the highly mineralised Swiss Reference Groundwater is obvious. Contrary to the Swedish type of groundwater, no major changes in the water composition would be expected if the experiments by Snellman [6,7] (where [Z]tot = $1.95 \cdot 10^{-2}$ mol/l) were carried out with Swiss Reference Groundwater. For the Swiss case, the pH value is predicted to be 9.7 in the near-field pore water. The assumption of calcite and quartz saturation leads to a total dissolution of $7.5 \cdot 10^{-3}$ mol $CaCO_3$ and $9.3 \cdot 10^{-4}$ mol SiO_2 per litre of Swiss Reference Groundwater, or $3.5 \cdot 10^{-2}$ mol $CaCO_3$ and $6.9 \cdot 10^{-3}$ mol SiO_2 per litre of Standard Swedish Groundwater, during the saturation process of compacted sodium bentonite with water.

Some other chemical effects should be noted, although they are of marginal significance to the consequences of the bentonite model:

- The high carbonate activity in the bentonite water will limit both Sr^{2+} and Mn^{2+} concentration due to the formation of $SrCO_3$ (s) and $MnCO_3$ (s). For [Z]tot = 3.35 mol/l, the solubility limit of strontium is calculated to be $6 \cdot 10^{-6}$ M, that of manganese(II) is $2 \cdot 10^{-7}$ M.

- The maximum concentration of Fe^{2+} will be controlled by either carbonate or silicate activity according to the formation of $FeCO_3$ (s) or Fe_2SiO_4 (s). In the pore water of compacted sodium bentonite, the dissolved silicate keeps the total Fe^{2+} concentration below 10^{-9} mol/l.

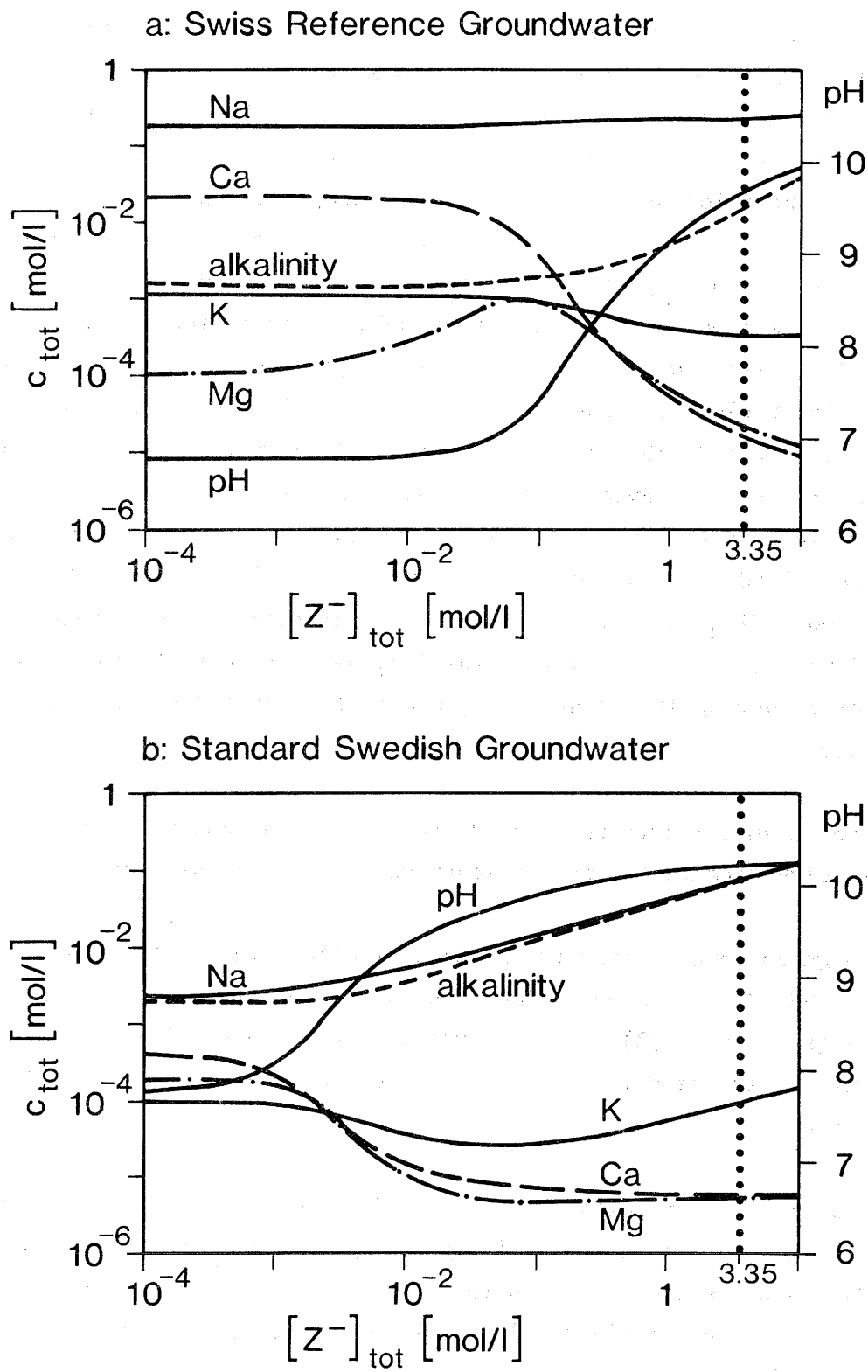

Figure 4: Modelled change in the composition of (a) Swiss Reference Groundwater [22] and (b) Standard Swedish Groundwater [6] when brought into contact with an increasing quantity of sodium bentonite (represented by the total concentration of ion-exchange sites Z^-). Alkalinity is expressed in eq/l. The dotted vertical line represents the predicted conditions in water saturated compacted sodium bentonite.

2.5. Long-Time Extrapolations: The Mixing Tank Model

Once the bentonite backfill in a waste repository is saturated and equilibrated with the enclosed water, advection of water through the near-field is negligible [24]. However, slow diffusion of ions from the near-field to the far-field (and vice versa) will take place. Consequently, the composition of the bentonite pore water will not remain constant, but will slowly change with time. This arises because the ion-exchange properties of bentonite alter as the exchange reactions progress, in the main giving an increasing capacity of exchangeable calcium as well as a decreasing proportion of exchangeable sodium. As it would be important to know more about these long-time alterations, a very simple model was applied in order to derive quantitative information on trends of variation in the composition of the bentonite pore-water in the very far future.

As a first approximation, the near-field of a potential Swiss high-level waste repository can be considered as a mixing tank. That is, the volume of water flowing past the repository is assumed to mix with the near-field water and to leave the repository area with an altered composition. Assuming a constant annual water flow of 0.71 l past each canister [25], the time period required to replace the entire volume of the near-field water by fresh groundwater will be 28 thousand years, taking a total pore water volume of 20.1 m^3 per REV (see Table 3). In the following text, this process will be called one water exchange cycle (see footnote). The parameter 'time', however, is not used as an

---

It should be mentioned that 28,000 years per water exchange cycle is a very rough estimation which assumes that also the water in the interlamellar spaces of the montmorillonite is replaced. If only the pore water is going to be replaced, the time period for one water exchange cycle could be considerably shorter.

explicit variable in the model. The water exchange may be imagined to take place by ion-diffusion, exclusively. The ion-exchange capacity of bentonite (73 meq/100 g) is assumed to remain constant over the period modelled. The only variable bentonite parameters are the proportions of the exchangeable cations in the bentonite and, since calcite and quartz are assumed to be in dynamic equilibrium with the available water, the total content of carbonates and silicates in the bentonite. The total amount of carbonate available for 1 litre of pore water is calculated to be 0.64 mol. The amount of silicate dissolving can be neglected. The individual steps of the calculation are as follows:

- The bentonite mass of a repository tunnel becomes saturated with groundwater. By means of the bentonite model, the equilibrium composition of the bentonite water is calculated, assuming [Z]tot = 3.35 mol/l. The new distribution of exchangeable cations on the montmorillonite layers is calculated. It will be different from the original one given in Table 3.

- The total volume of equilibrated bentonite pore water is replaced by fresh groundwater, which then contacts the new distribution of exchangeable ions in the bentonite. Again, the equilibrium state is calculated.

- This water exchange procedure is repeated 100 times.

- Mineral transformation (e.g. montmorillonite to illite) is not considered in this report.

The results of these calculations are listed in Table 8 (Swiss Reference Groundwater) and Table 9 (Standard Swedish Groundwater), and presented in Figures 5 and 6, as well as in Figure 7.

It can be seen from Figure 5 that the available carbonate in bentonite will be consumed after 35 water exchange cycles, if the groundwater in the host rock is as poorly mineralised as Standard Swedish Groundwater. After this time period, which roughly corresponds to at least one million years, the pH of the bentonite pore water will drop to that of the ambient groundwater, but the concentrations of Mg^{2+} and Ca^{2+} in the

pore water will still considerably differ from the groundwater values (see Table 9). In a potential Swiss high-level waste repository, less than one sixth of the carbonate pool will be dissolved by this mechanism and be carried away. The pH of the near-field water will have returned to the value of the host rock water after 60 to 70 water exchange cycles (roughly 2 million years), indicating exhaustion of the ion-exchange capacity relative to the groundwater chemical composition. Figure 6 reveals that the sodium bentonite will have been converted to calcium bentonite at this time, containing 95% exchangeable calcium relative to the sum of exchangeable ions. In the case of a poorly mineralised groundwater with a low calcium concentration, it takes enormous times to convert sodium bentonite to calcium bentonite, because the calcium supply from the bentonite is exhausted after the total dissolution of calcite, and the concentrations of the relevant cations in this type of groundwater are very low. The potential partial pressure of carbon dioxide in the bentonite pore water will return to that of the groundwater after the depletion of calcite. Note that log $p(CO_2)$ listed in Table 9 after N=35 (-2.73) differs from the value of the initial groundwater in Table 2 (-3.09) due to the difference in the temperature.

Obviously, calcium bentonite is thermodynamically more stable in contact with such groundwater than sodium bentonite. This conclusion is also supported by a very recent experiment [26]: 6 g of calcium bentonite (Montigel) with a calcium content equivalent to 61% of the exchangeable cations, was equilibrated with one litre of Swiss Reference Groundwater for two weeks. The calcium content increased to 78%, the magnesium content decreased from 36% to 5%, and the sodium content increased from 3% to 16%. This experiment reveals that the proportion of exchangeable calcium in calcium bentonite still increases in contact with Swiss Reference Groundwater, and that the magnesium content is going to be very low. These observations are in agreement with the predictions of the bentonite model developed in this work.

Finally, it should be mentioned that the mixing tank model is a greatly simplified approximation, because is assumes the composition of the near field water to be homogeneous over the entire near field area.

Table 8: Chemical situations in the near-field after selected numbers of exchange cycles of equilibrated bentonite pore water by Swiss Reference Groundwater (calculated for 55°C and the dimensions of a Swiss case repository).

N : Number of water-exchange cycles
[ ]tot : Total ion concentration (mol/l) in the near-field water (without the absorbed species ZNa, ZK, Z_2Mg, and Z_2Ca)
{ } : Ion activity (mol/l) in the near-field water
$p(CO_2)$: Potential partial pressure of carbon dioxide
Alk : Alkalinity of the near-field water (eq/l)
Calcite: Total supply of carbonates (mol) in the near-field, calculated as calcite and referred to 1 litre of water

N	pH	[Na]tot	[K]tot	[Mg]tot	[Ca]tot	$[CO_3]$tot	$\{CO_3^{2-}\}$	log $p(CO_2)$	Alk	Calcite
0	9.67	2.35 E-1	3.63 E-4	2.55 E-5	1.81 E-5	9.39 E-3	7.92 E-4	-4.24	1.63 E-2	0.633
1	9.62	2.33 E-1	3.93 E-4	2.55 E-5	2.02 E-5	8.33 E-3	6.76 E-4	-4.21	1.42 E-2	0.626
2	9.57	2.31 E-1	4.24 E-4	2.58 E-5	2.24 E-5	7.52 E-3	5.85 E-4	-4.18	1.26 E-2	0.621
5	9.45	2.28 E-1	5.18 E-4	2.73 E-5	2.99 E-5	5.89 E-3	4.04 E-4	-4.10	9.43 E-3	0.607
10	9.27	2.25 E-1	6.75 E-4	3.17 E-5	4.57 E-5	4.45 E-3	2.44 E-4	-3.9	6.61 E-3	0.592
20	8.94	2.22 E-1	9.90 E-4	4.79 E-5	9.97 E-5	3.18 E-3	1.04 E-4	-3.66	4.11 E-3	0.575
30	8.59	2.20 E-1	1.30 E-3	8.28 E-5	2.24 E-4	2.64 E-3	4.47 E-5	-3.34	3.04 E-3	0.565
40	8.19	2.18 E-1	1.60 E-3	1.74 E-4	5.79 E-4	2.37 E-3	1.70 E-5	-2.95	2.51 E-3	0.559
50	7.65	2.14 E-1	1.82 E-3	5.14 E-4	2.08 E-3	2.22 E-3	4.68 E-6	-2.4	2.20 E-3	0.556
60	7.03	1.94 E-1	1.63 E-3	1.93 E-3	1.04 E-2	2.03 E-3	9.28 E-7	-1.91	1.82 E-3	0.554
70	6.83	1.77 E-1	1.21 E-3	2.11 E-3	1.88 E-2	1.94 E-3	5.08 E-7	-1.76	1.64 E-3	0.553
80	6.80	1.76 E-1	1.16 E-3	1.29 E-3	2.04 E-2	1.92 E-3	4.69 E-7	-1.74	1.61 E-3	0.553
90	6.79	1.76 E-1	1.15 E-3	7.59 E-4	2.09 E-2	1.92 E-3	4.56 E-7	-1.73	1.60 E-3	0.553
100	6.79	1.76 E-1	1.15 E-3	4.60 E-4	2.13 E-2	1.92 E-3	4.48 E-7	-1.73	1.60 E-3	0.553

Table 9: Chemical situations in the near-field after selected numbers of exchange cycles of equilibrated bentonite pore water by Standard Swedish Groundwater (calculated for 55°C and the dimensions of a Swiss case repository).

N : Number of water-exchange cycles
[ ]tot : Total ion concentration (mol/l) in the near-field water (without the absorbed species ZNa, ZK, Z_2Mg, and Z_2Ca)
{ } : Ion activity (mol/l) in the near-field water
$p(CO_2)$: Potential partial pressure of carbon dioxide
Alk : Alkalinity of the near-field water (eq/l)
Calcite: Total supply of carbonates (mol) in the near-field, calculated as calcite and referred to 1 litre of water

N	pH	[Na]tot	[K]tot	[Mg]tot	[Ca]tot	$[CO_3]$tot	$\{CO_3^{2-}\}$	log $p(CO_2)$	Alk	Calcite
0	10.23	7.40 E-2	9.46 E-5	5.64 E-6	6.34 E-6	3.71 E-2	7.65 E-3	-4.39	6.92 E-2	0.605
1	10.22	6.84 E-2	9.03 E-5	4.93 E-6	6.38 E-6	3.44 E-2	7.19 E-3	-4.39	6.40 E-2	0.572
2	10.22	6.38 E-2	8.67 E-5	4.40 E-6	6.40 E-6	3.21 E-2	6.87 E-3	-4.40	5.95 E-2	0.542
5	10.20	5.69 E-2	8.16 E-5	3.70 E-6	6.44 E-6	2.72 E-2	6.13 E-3	-4.41	5.29 E-2	0.487
10	10.18	4.62 E-2	7.41 E-5	2.81 E-6	6.51 E-6	2.25 E-2	5.35 E-3	-4.43	4.28 E-2	0.371
20	10.14	3.50 E-2	7.06 E-5	2.11 E-6	6.65 E-6	1.72 E-2	4.35 E-3	-4.44	3.21 E-2	0.193
30	10.10	2.85 E-2	7.04 E-5	1.83 E-6	6.78 E-6	1.41 E-2	3.68 E-3	-4.43	2.59 E-2	0.067
40	8.01	3.66 E-3	1.10 E-5	1.04 E-8	2.32 E-8	1.94 E-3	1.24 E-5	-2.73	1.94 E-3	-
50	8.01	3.65 E-3	1.18 E-5	1.07 E-8	2.37 E-8	1.94 E-3	1.24 E-5	-2.73	1.94 E-3	-
60	8.01	3.64 E-3	1.29 E-5	1.13 E-8	2.42 E-8	1.94 E-3	1.24 E-5	-2.73	1.94 E-3	-
70	8.01	3.64 E-3	1.42 E-5	1.18 E-8	2.48 E-8	1.94 E-3	1.24 E-5	-2.73	1.94 E-3	-
80	8.01	3.64 E-3	1.49 E-5	1.23 E-8	2.54 E-8	1.94 E-3	1.24 E-5	-2.73	1.94 E-3	-
90	8.01	3.63 E-3	1.60 E-5	1.29 E-8	2.60 E-8	1.94 E-3	1.24 E-5	-2.73	1.94 E-3	-
100	8.01	3.63 E-3	1.69 E-5	1.32 E-8	2.64 E-8	1.94 E-3	1.24 E-5	-2.73	1.94 E-3	-

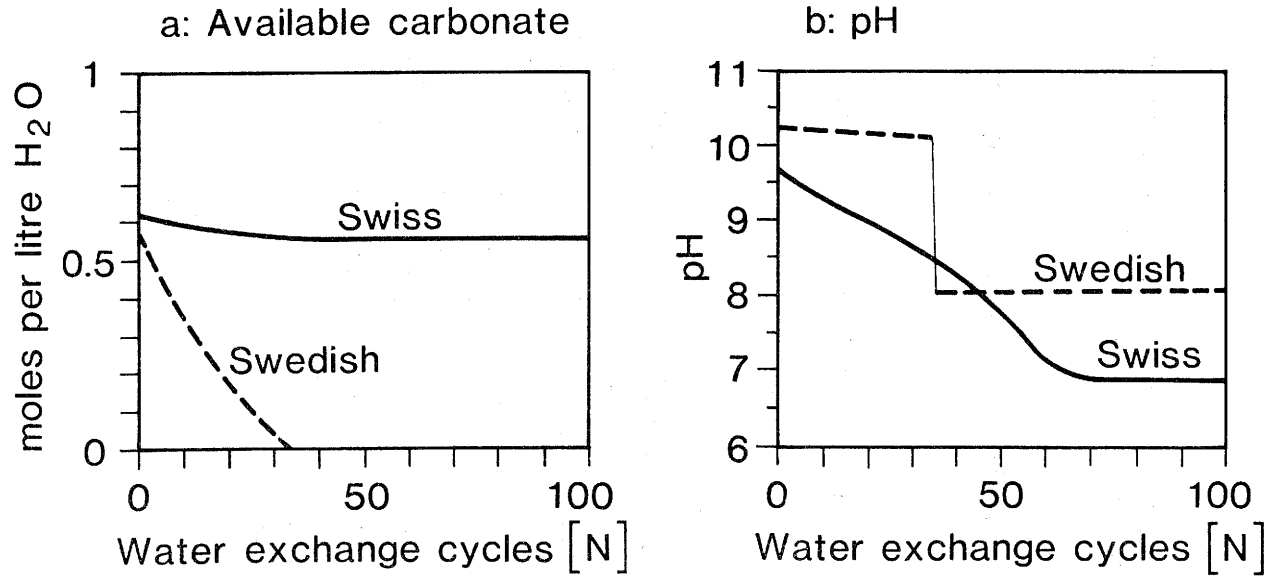

Figure 5: Long-term change in the carbonate reservoir (calculated as calcite available for 1 litre of water) present in sodium bentonite (a), as well as in the pH of the near-field pore water (b), calculated by application of the water exchange model to the Swiss Reference Groundwater and to Standard Swedish Groundwater (dashed).

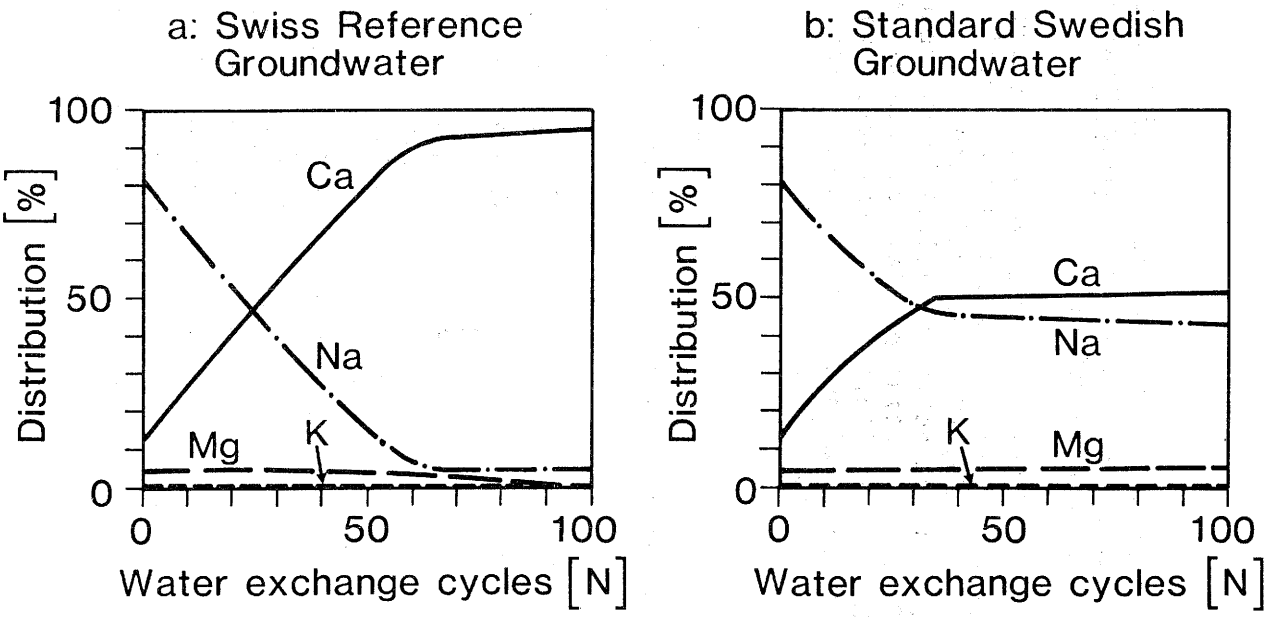

Figure 6: Alteration of the percentage distribution of exchangeable cations in sodium bentonite as a function of exchange cycles by Swiss Reference Groundwater (a) and Standard Swedish Groundwater (b), respectively.

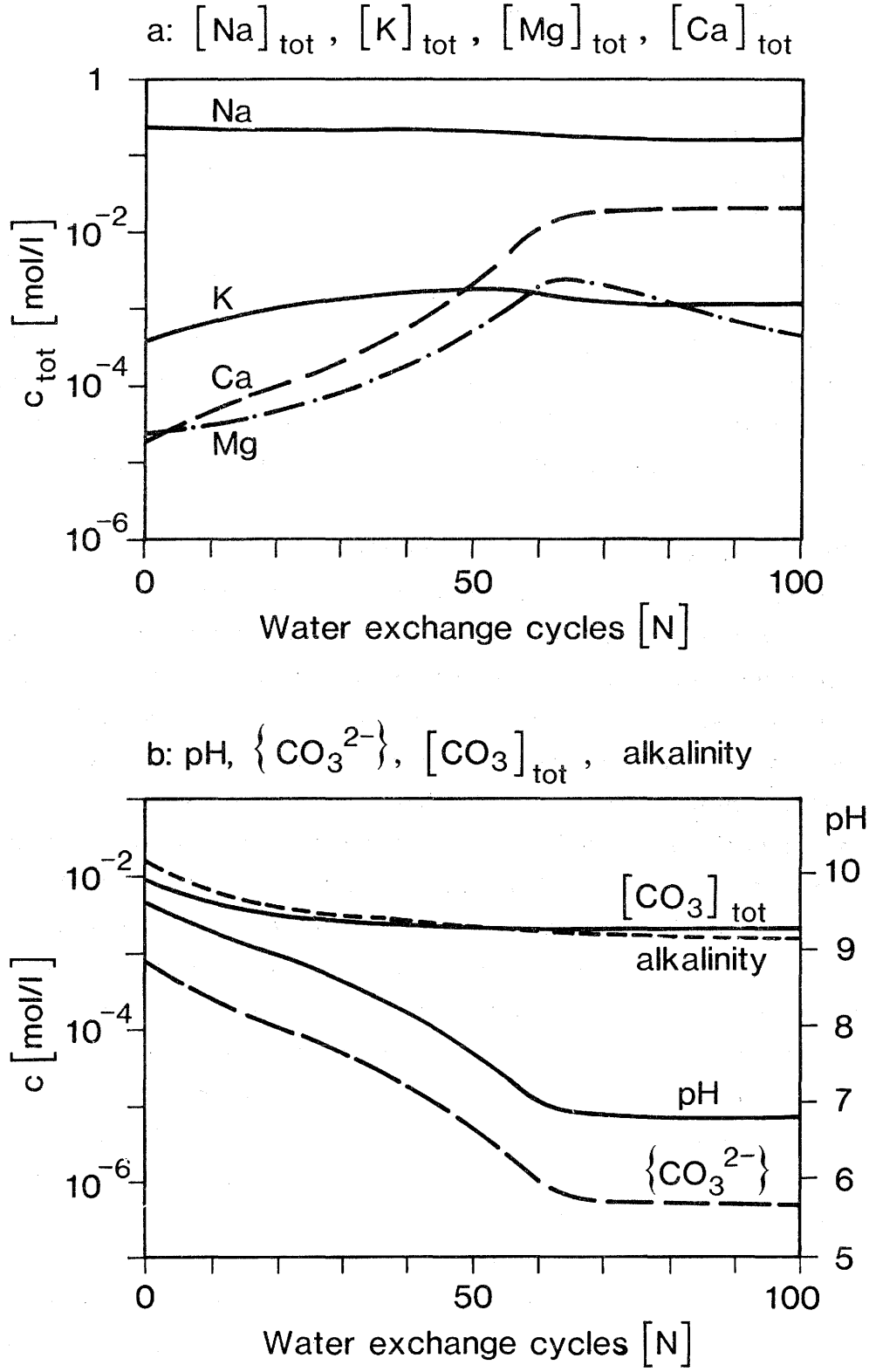

Figure 7: Modelled long-term change in the chemical composition of the pore water in saturated sodium bentonite as a function of hypothetical water exchange cycles N, applying the mixing tank model to Swiss Reference Groundwater. Alkalinity is expressed in eq/l.

2.6. A Natural Analogue to the Bentonite Model

The best validation of a theoretical model like the bentonite model, which is based on laboratory data only, is the appearance of analogous processes in nature. This is due to the fact that extrapolations of short-term knowledge (e.g., from laboratory experiments) to geological time-scales are speculative because of the complexity of geological and geochemical alteration processes [27]. In the context of this report, investigations of groundwaters which had been altered by clay minerals are important to gain assurance about the predicted pore water composition in the near-field of a bentonite-infilled waste repository.

In 1979, Thorstenson et al. [28] published investigations on the geochemistry of an aquifer located at a depth between 300 and 600 meters in North Dakota and South Dakota. The water flowing in this aquifer was found to have a high pH value around 8.5, as well as a very low content of calcium and magnesium. Water was sampled and analysed at four different sites in the recharge area, at two sites in the transition zone, and at three sites in the discharge area. In the discharge area, pH has slightly decreased to 8.3, whereas the alkalinity has increased from 13 to 21 meq/l with a parallel increase in sodium from 18 to 27 mmol/l. The geologic formation is known to contain bentonitic clay minerals. The processes creating these chemical alterations were not interpretable with simple dissolution and saturation reactions of minerals present in the surrounding rock formations. The observations could be explained by accounting for the ion-exchange capability of clay minerals. According to the $\delta\,^{13}C$ values measured, CO_2 derived from lignitic carbon reacts to dissolve carbonate minerals, like calcite, dolomite, and siderite. Since no increase in calcium, magnesium, or ferrous iron, but only an increase in sodium was observed, ion-exchange reactions on clay minerals seem to be the most probable processes. The waters sampled were found to be slightly oversaturated with respect to calcite and distinctly undersaturated with respect to siderite. The authors conclude that the major alkalinity-producing reaction occurring in the recharge area is a combination of ion-exchange on bentonitic clays and calcite dissolution:

$$CaCO_3 + H_2CO_3 + 2\ Na(ex) \rightleftharpoons Ca(ex) + 2\ Na^+ + 2\ HCO_3^+$$

The validity of this natural analogue for the near-field water of a deep repository should be briefly discussed: In the aquifer investigated by Thorstenson et al. [28], the production of CO_2 obviously initiates the ion-exchange processes between the clay minerals and the groundwater by the ability of CO_2 to dissolve calcite. At the depth of a deep repository, however, no lignitic carbon is present to produce CO_2. Nevertheless, the alkalinity-producing process can also be initiated in the absence of CO_2, because it is directly controlled by the concentration of calcium in the aqueous phase. The calcium concentration in the aquifer described is very low, even in the recharge area (0.07 mmol/l), whereas the deep-crystalline Swiss Reference Groundwater has a very high calcium concentration (21.7 mmol/l). It is most probable that the alkalinity-producing process will be initiated by exchange of calcium for sodium on the clay, and a subsequent reestablishment of calcite saturation by dissolution of calcite. The absence of CO_2 at great depths can obviously lead to pH values higher than 8.5, as predicted by the bentonite model (section 2.4.).

Some other observations in the discharge area of the aquifer described [28] will be briefly summarised: Chloride concentration has increased from 0.7 to 5.5 mmol/l, which is interpreted by input of NaCl from other formations. Sulphate concentration has decreased from 2.72 to 0.14 mmol/l. This is attributed to reduction of sulphate to pyrite by lignitic material. There is thus no direct indication for sulphate and chloride dissolution from clay minerals, as suggested by Grambow et al. [19]. In any case, such reactions need not necessarily be accounted for in the bentonite model, because they are not of great importance for the estimation of radionuclide solubilities in the near-field of a potential HWL repository, with the possible exception of Pu(III) and Am(III) which form sulphato complexes.

3. Actinide and Technetium Speciation and Solubility Limits in the Bentonite Model Water

3.1. General Procedure

All the following calculations refer to Swiss Reference Groundwater. Its modelled compositions in the near-field of a deep repository are shown in Figure 4 and Figure 7, and listed in Table 8.

The calculation of actinide and technetium solubilities is subject to a number of premises. The speciation model and the basic assumptions are presented in Appendix A. Nevertheless, one important constraint should be reemphasised: As was the case with the calculations performed in the safety analysis of a potential high-level nuclear waste repository in Switzerland [1,29], the solubility determining solid phases of the actinides and of technetium are assumed to be pure oxides or hydroxides, exclusively. In the case of americium, this constraint was recognised to be very unrealistic, and solid phases associated with carbonate were also allowed to be present.

Each step in both the extrapolation model (discussed in section 2.4.) and the mixing tank model (discussed in section 2.5.) gives as a result the complete speciation of the near-field water. The water compositions of each step can thus be used to calculate the speciation of an actinide or of technetium, as long as its maximum solubility is so low that it does not affect the composition of the water. As a general rule, applicable to the cases where Swiss Reference Groundwater is involved, an actinide concentration below 10^{-4} M does not influence the water chemistry.

A key parameter is the redox potential (Eh value) because many actinides and technetium have different oxidation states which are stable under groundwater conditions. Therefore, the maximum solubilities of these elements are critically dependent on the redox conditions. Experience has shown that groundwaters are normally not, or only poorly, buffered with respect to the redox potential [9] because redox pairs like

SO_4^{2-}/HS^- or NO_3^-/NH_4^+ do not seem to be in equilibrium. This is not surprising since such redox reactions involving an 8-electron transfer are known to be kinetically strongly hindered.

In the case of a potential high-level waste repository, however, a powerful Eh buffer is expected to control Eh conditions in the near-field pore water. Since the waste canister consists of metallic iron which is subject to corrosion in the presence of water, large amounts of corrosion products will be present at the time of canister failure, and the corrosion of the remaining iron will continue for significant periods of time. The near-field area will thus be electrochemically reducing. At each step of the extrapolation model and the mixing tank model, actinide and technetium speciation and solubility limits are calculated for an Eh range varying from -600 mV to 0 mV, with intervals of 50 mV.

The hydrogen gas produced during the corrosion process could control the redox potential if the equilibrium H^+/H_2 (g) is kinetically fast. On the other hand, the hydrogen gas produced will possibly be transported outside the near-field area through channels and pores which need not be the same as those in which the waste nuclides are transported. Consequently, account has to be taken for other possible redox buffers. Although it is not clear which iron oxides or hydroxides will be the most likely corrosion product, it can be presumed that oxidation of iron to a pure Fe(III) mineral is extremely improbable in deep rock formations. In spite of this, the redox pair used in this report to define the upper redox boundary contains the most stable pure Fe(III) mineral: hematite (Fe_2O_3). In this way, account is taken for a possible oxic oxidation of metallic iron to Fe(III) by trapped oxygen gas in the tunnel section [2]. The lower redox boundary is represented by the lower stability limit of water, assuming hydrogen gas to be the only gas present. Since pressure dependence of equilibria is neglected throughout this report, log $p(H_2) = 0$ is taken to calculate the lower redox potential. An increase of the partial pressure of H_2 (g) from 1 atm to 100 or 300 atm would reduce the lower redox boundary by 130 or 160 mV, respectively. The two limiting redox functions depend on pH only. They are plotted in Figure 8 below and relevant thermodynamic data are listed in Table B-4 (Appendix B).

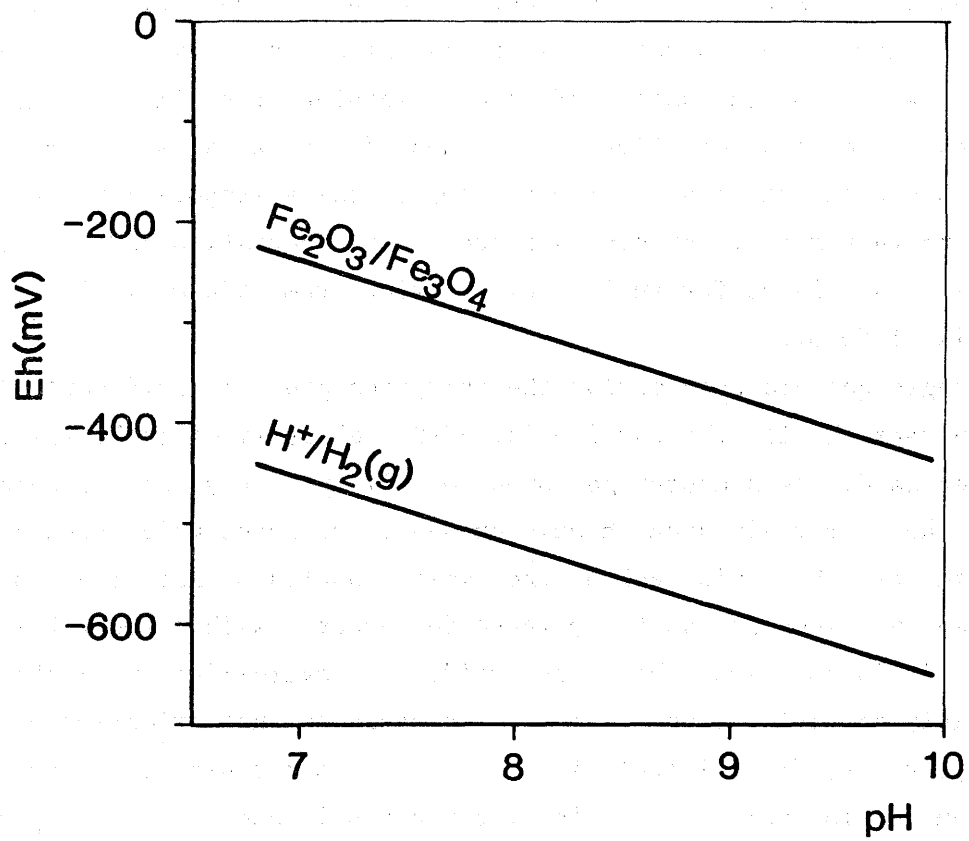

Figure 8: Eh/pH functions of the hematite/magnetite and the H^+/H_2 (g) redox pairs for log $p(H_2)$ = 0. Thermodynamic data are listed in Table B-4 (Appendix B). The redox potential of the near-field water of a nuclear waste repository containing iron canisters is expected to be within these two boundary lines.

3.2. Uranium

Within the expected Eh range, maximum uranium solubility is predicted to be independent of the redox potential. This is indicated by the two limiting lines in Figure 9a and represented by the coinciding cross-sections along these lines, as shown in Figure 9b. The Eh value is thus not a critical parameter for the uranium speciation in the near-field of a deep reporitory containing iron canisters. Figure 9b also shows that the solubility limit of uranium will decrease with time, reaching a constant value of less than 10^{-10} M after about 60 water exchange cycles (corresponding to 1.7 million years).

Figure 9a reveals that maximum uranium solubility would be very high in the unrealistic case of high pH (N=0) and high Eh (Eh=0), simultaneously. In this case, oxidation of U(IV) to U(VI) would be favoured due to the comparatively high carbonate activity (see Table 8), leading to the formation of the complexes $UO_2(CO_3)_2^{2-}$ and $UO_2(CO_3)_3^{4-}$. This behaviour is shown by Figure 10b and Figure 11. Parallel to the oxidation of aqueous uranium species, the solubility limiting solid phase (which is calculated to be UO_2 (s) over the expected Eh/pH range)would be oxidised to U_4O_9 (s) and U_3O_8 (s) under these unrealistic conditions, as can be seen from Figure 10a. The predominant solute species is calculated to be $U(OH)_5^-$ over the entire range of water exchange cycles modelled and redox conditions expected, even at neutral pH values (N > 50, see Table 8). Probably, the stability of $U(OH)_5^-$ (log K = -13.15 for the formation of $U(OH)_5^-$ from U^{4+} and H_2O [30], see Table B-5 in Appendix B) is largely overestimated. The true existence of $U(OH)_5^-$ in aqueous solutions has recently been called into question [31]. If either the complex $U(OH)_5^-$ does not exist, or its stability is considerably lower than assumed, uranium solubility will be lower throughout the expected Eh/pH range, i.e. the entire curve plotted in Figure 9b will be shifted down along the y-axis.

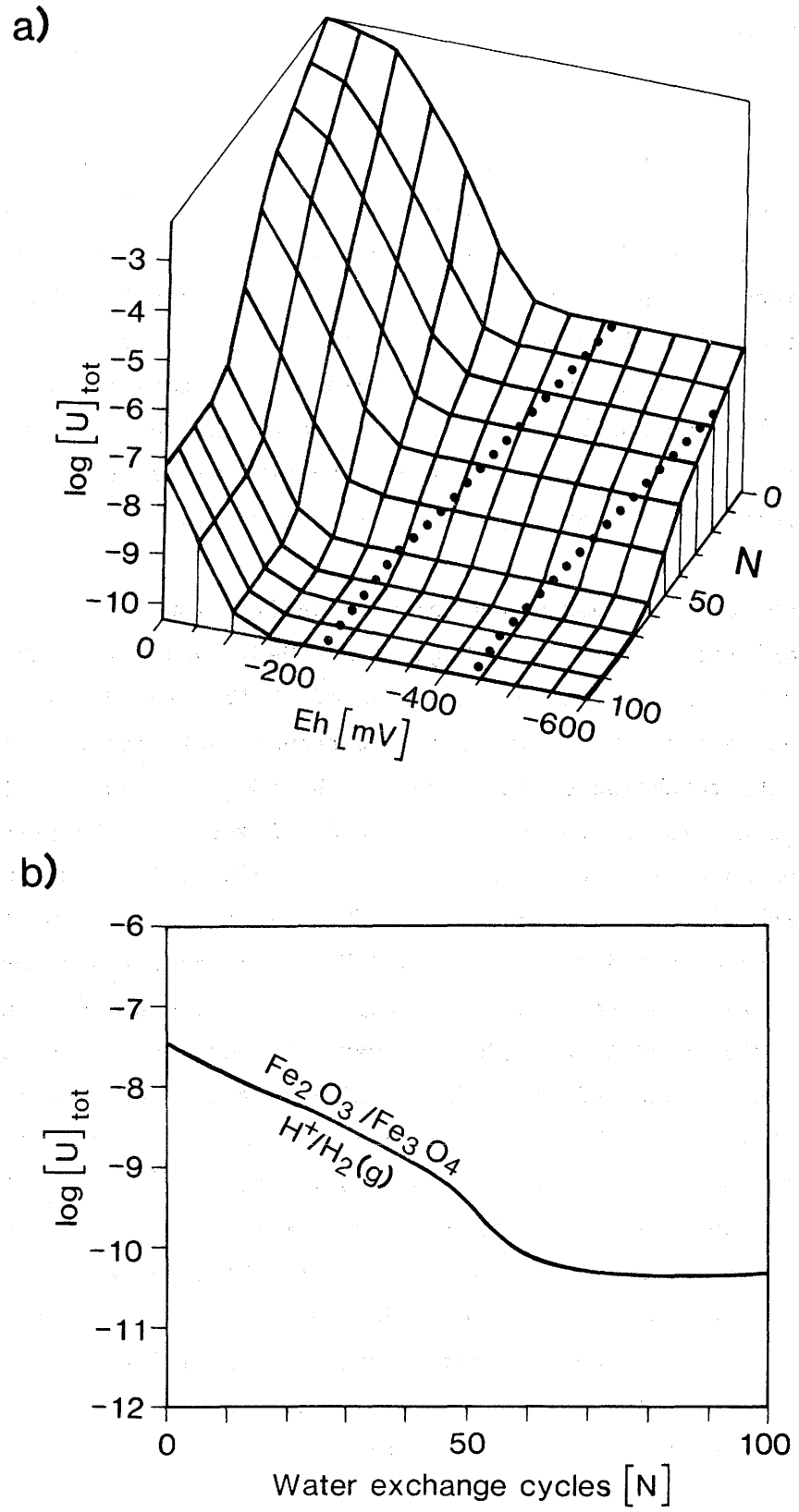

Figure 9: Representation of uranium solubility limits (a) for the entire Eh range considered in the mixing tank model, as well as (b) in the form of cross-sections along the Eh/pH functions (dotted lines in the upper figure) which define the probable Eh range in the near-field.

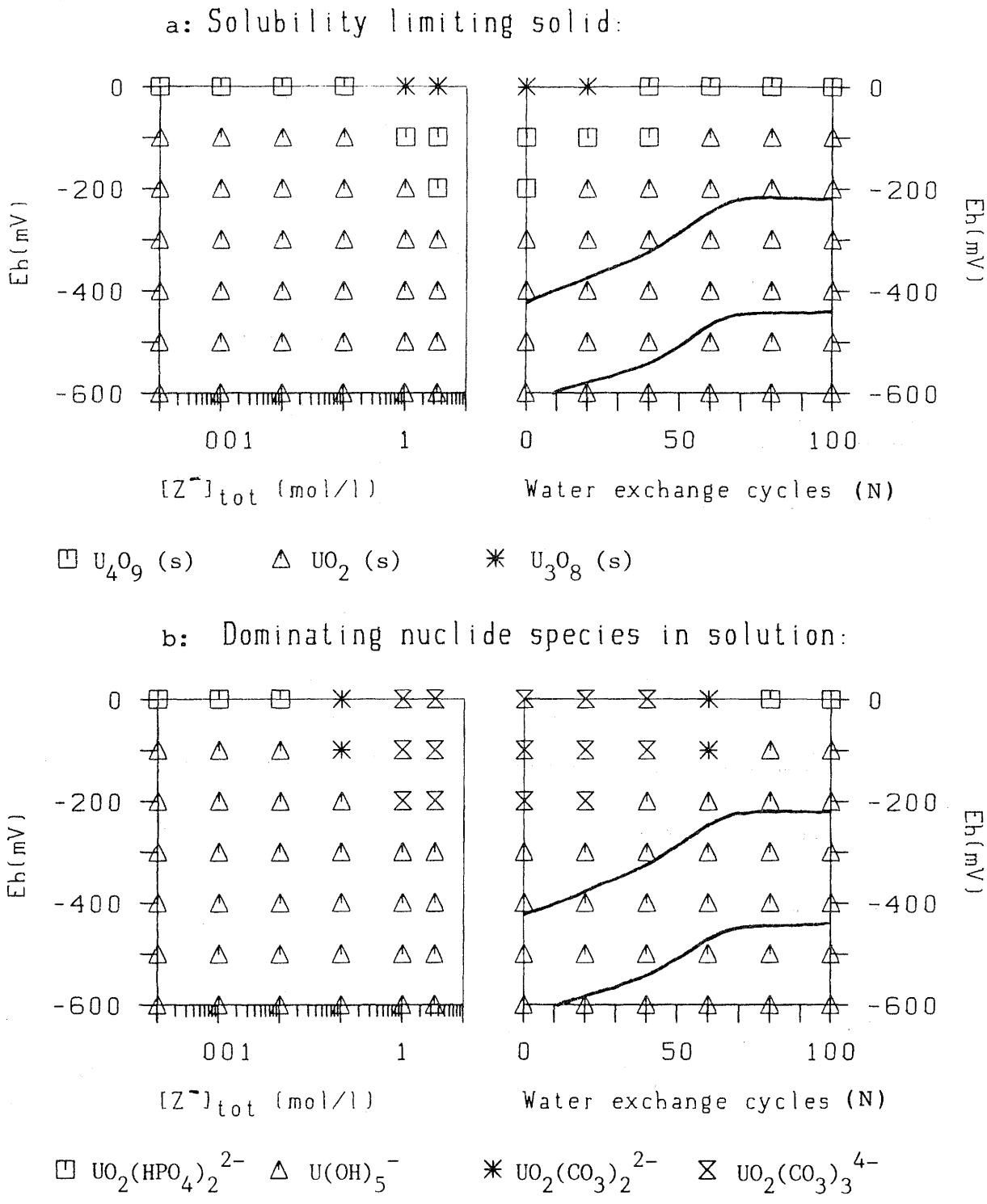

Figure 10: Grid diagram for solubility limiting solids (a) and for the dominant uranium species under the modelled conditions (b). The diagrams on the left hand side refer to the extrapolation model (water speciation depicted in Figure 4) and those on the right hand side to the mixing tank model (water speciation depicted in Figure 7 and listed in Table 8).

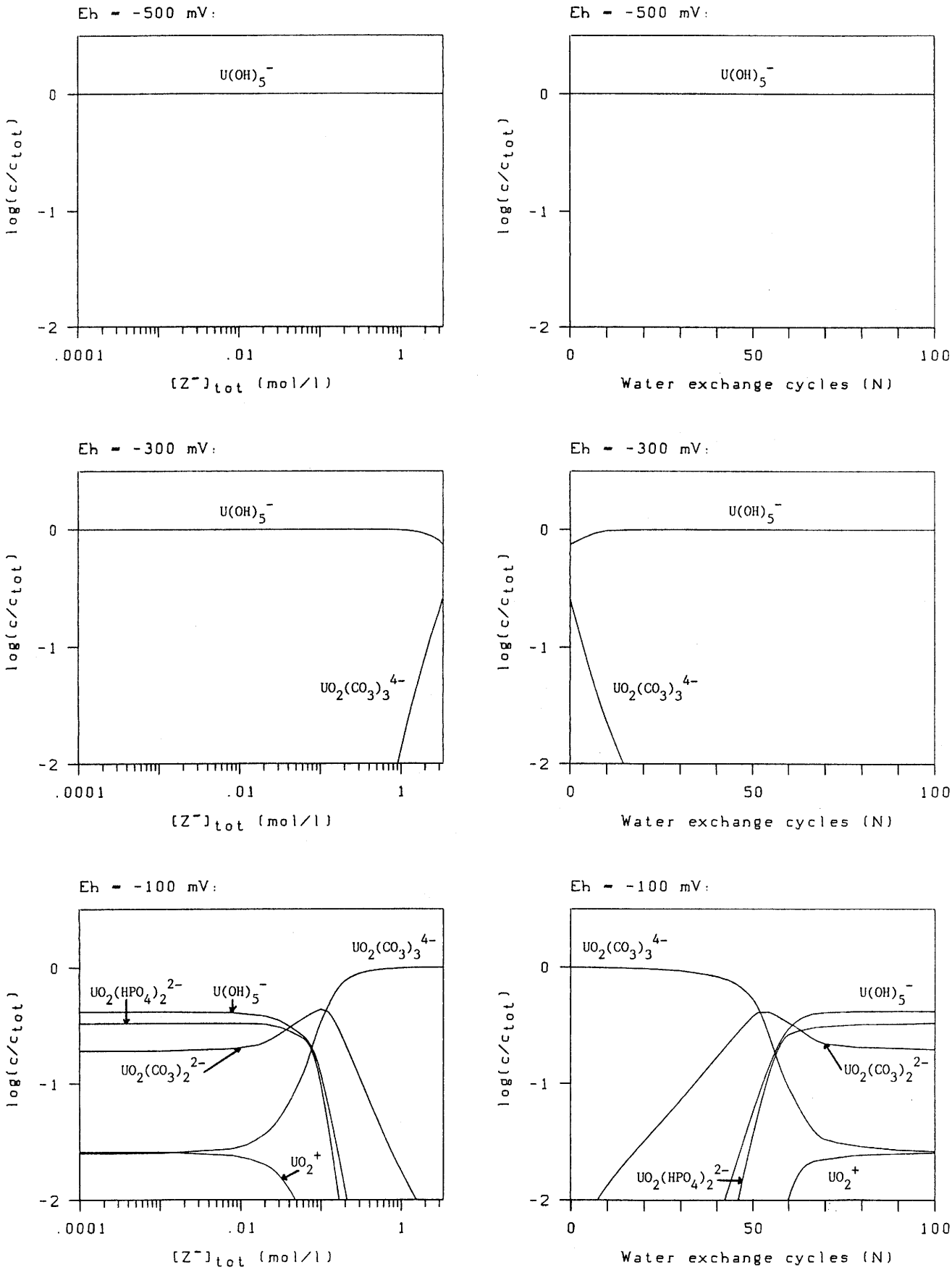

Figure 11: Uranium speciation plots for selected Eh values (stoichiometric species concentrations divided by total uranium concentration).

3.3. Neptunium

The chemical behaviour of neptunium is generally observed to be analogous to that of uranium, so that the results can be expected similar for the two elements. A comparison of Figure 12a (Np) with Figure 9a (U) plainly demonstrates the similarities, but there are nevertheless differences in a few important parameters.

Maximum neptunium solubility is strongly Eh dependent in the bentonite model water at N=0 (high pH, high carbonate activity, see Table 8), as shown by Figure 12a. This leads to a range of three orders of magnitude (see Figure 12b) for the solubility limit of neptunium in the near-field during the first 200,000 to 300,000 years after canister emplacement ($N < 10$). The predicted solubility limits decrease and the range narrows with time until a constant neptunium saturation concentration of $5 \cdot 10^{-10}$ M is reached after 55 water exchange cycles (roughly 1.5 million years), as can be seen from Figure 12b.

The solubility limiting solid will be NpO_2 (s) over the entire Eh/pH range modelled (Figure 13a). However, Np(IV) will not be the dominating aqueous oxidation state of neptunium under all conditions. Oxidation to Np(V) will take place in solutions with high carbonate activity even under reducing conditions (see Figure 13b). In fact, it is the formation of carbonato complexes, such as $NpO_2(CO_3)_2^{3-}$ and $NpO_2(CO_3)_3^{5-}$, which makes the neptunium solubility increase. A comparison of Figure 13b with Figure 12a demonstrates that maximum neptunium solubility will be below 10^{-9} M whenever $Np(OH)_4^0$ is the dominating neptunium species. The predominance of $NpO_2(CO_3)_3^{5-}$ is an indication for high neptunium concentrations. At this point, it should be mentioned that a recent compilation of stability constants for the neptunyl-carbonate system [32] exhibits large divergencies among the values from different sources. The overall complex formation constant of $NpO_2(CO_3)_3^{5-}$ in the MINEQL/EIR database is $\log K = 16.3$ (cf. Table B-5, Appendix B) published by Allard [33]. This value was used for the safety analysis calculations [1] and has been used again for the

calculations presented here. For the same reaction, Maya [34] reported log K = 8.53, and scientists in the CEA laboratories in Fontenay-aux-Roses (F) found log K = 5.86 [32]. The value reported by Nitsche and Edelstein [35] (log K = 17.4) is even slightly higher than the one by Allard [33]. The value used in the MINEQL/EIR database might thus be overestimated by several orders of magnitude. In this case, the stability of the NpO_2^+ carbonato complexes would be considerably lower than assumed here, resulting in an overall predominance of $Np(OH)_4^o$. The maximum solubility of neptunium might then be as low as about 10 M for the entire Eh/pH range considered here. The solubility limits for neptunium presented in this report are therefore very conservative. The fact that, contrary to uranium, the species $Np(OH)_5^-$ never dominates in solution (cf. Figure 14) is due to the different sources of the values. The value for the formation of $Np(OH)_5^-$ is taken from Allard [33] and is certainly more realistic than that for $U(OH)_5^-$ by Langmuir [30] (cf. Table B-5, Appendix B). Rai and Ryan [36] recently found that the stability of $Np(OH)_5^-$ must be very low, and they doubt that this species exists at all.

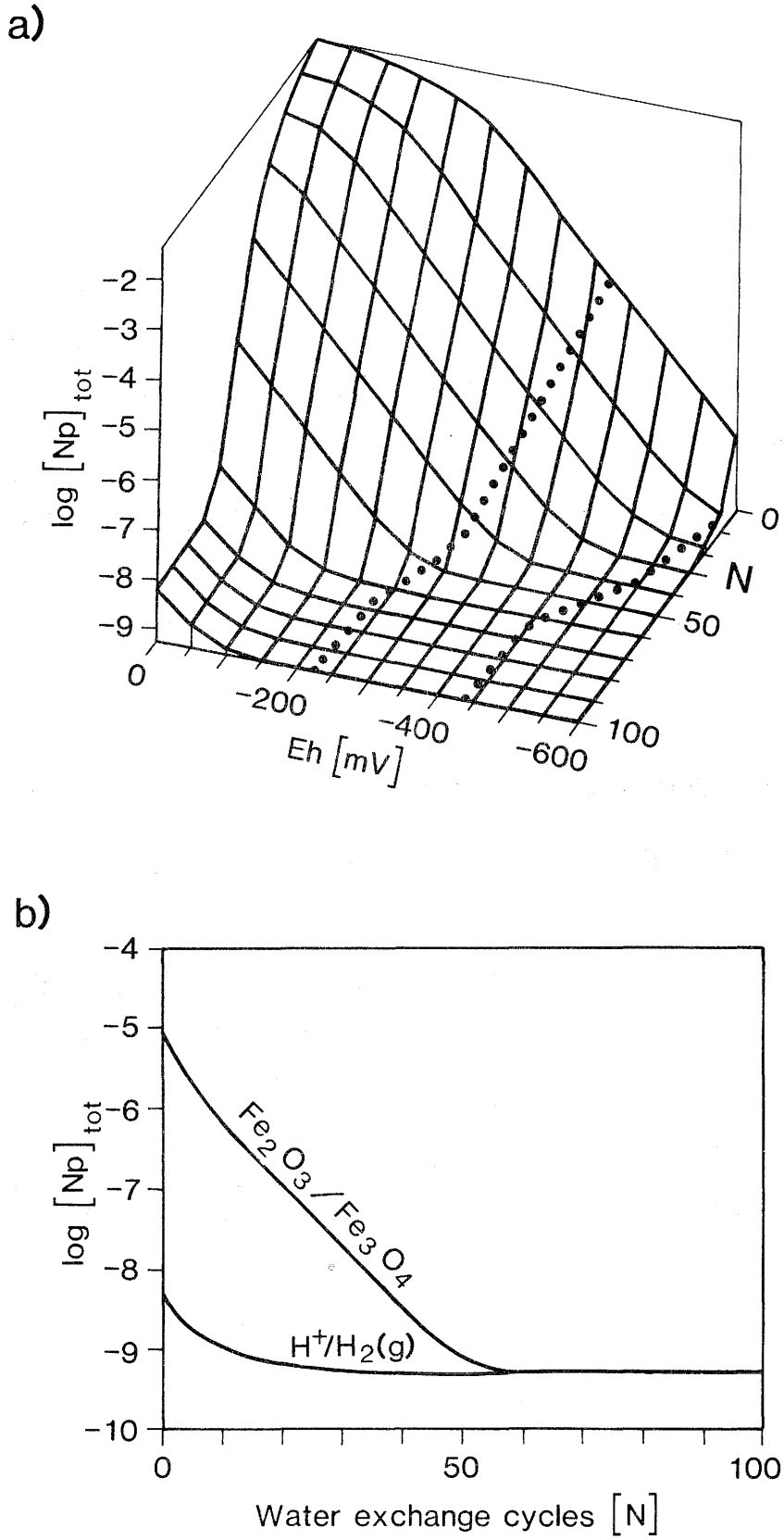

Figure 12: Representation of neptunium solubility limits (a) for the entire Eh range considered in the mixing tank model, as well as (b) in the form of cross-sections along the Eh/pH functions (dotted lines in the upper figure) which define the probable Eh range in the near-field.

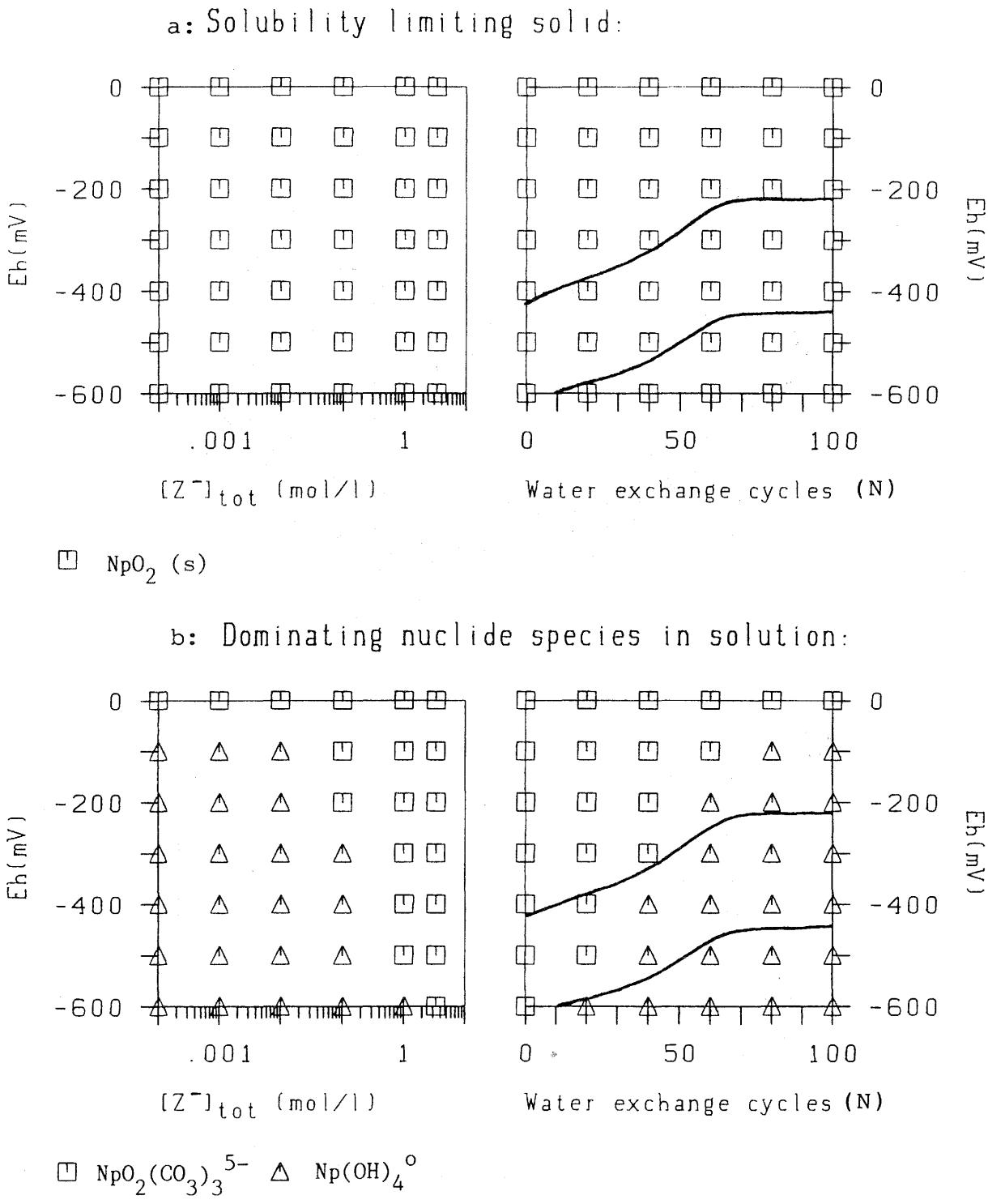

Figure 13: Grid diagram for solubility limiting solids (a) and for the dominant neptunium species under the modelled conditions (b). The diagrams on the left hand side refer to the extrapolation model (water speciation depicted in Figure 4) and those on the right hand side to the mixing tank model (water speciation depicted in Figure 7 and listed in Table 8).

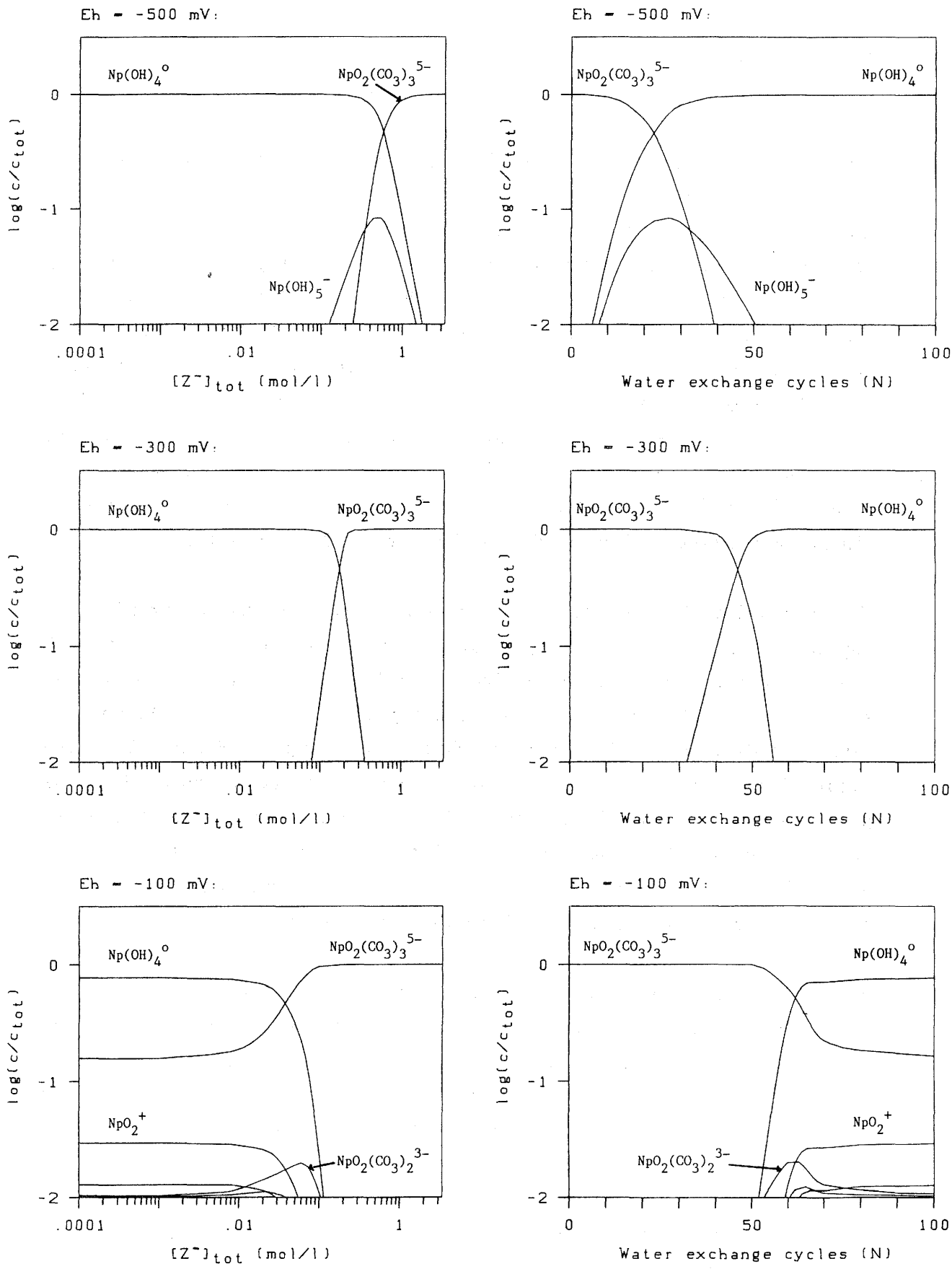

Figure 14: Neptunium speciation plots for selected Eh values (stoichiometric species concentrations divided by total neptunium concentration).

3.4. Plutonium

Although the chemical behaviour of plutonium is, in principal, similar to that of uranium or neptunium, its solubility limits calculated for the various conditions in the bentonite model behave inversely to those of uranium and neptunium. This fact is clearly demonstrated by Figure 15a and Figure 15b (Please note that Figure 15a is rotated around the vertical axis by 180 degrees compared to Figure 9a and Figure 12a.). It can be seen that plutonium solubility is predicted to be initially very low (10^{-9} M) and will remain low for a long period of time. After 1 million years (N=35), the solubility limit of plutonium is calculated to be between $3 \cdot 10^{-10}$M and $5 \cdot 10^{-9}$ M, but the uncertainty interval grows with time. After 2 million years (N > 70) the range of expected plutonium solubility limits will be between $3 \cdot 10^{-8}$ M and $4 \cdot 10^{-5}$ M.

The reason for the inverse behaviour of plutonium to that of uranium and neptunium is the ability of plutonium to form stable soluble Pu(III) species under reducing conditions. Under the chemical conditions specified by the bentonite model, the predominance of Pu(III) species always leads to high plutonium solubilities (compare Figure 15a with Figure 16b), whereas low plutonium solubility is accompanied by the predominance of a Pu(IV) species, $Pu(OH)_4^o$, because its stoichiometric composition is the same as that of the least soluble plutonium solid under the expected conditions: PuO_2 (s) (see Figure 16a). Figure 17 gives an idea of the complexity of plutonium chemistry.

Very few thermodynamic data on Pu(III) species are available from the literature. In order to fill this gap, americium(III) was taken as an analogue for plutonium(III). Almost no data for these calculations are thus based on experiments with plutonium(III), but rather are derived from the available americium(III) data (cf. Table B-5, Table B-6, Appendix B). Such a procedure might be questionable, and thus those model areas in which Pu(III) species dominate in solution, should be regarded with caution, particularly with respect to the solubility limits calculated.

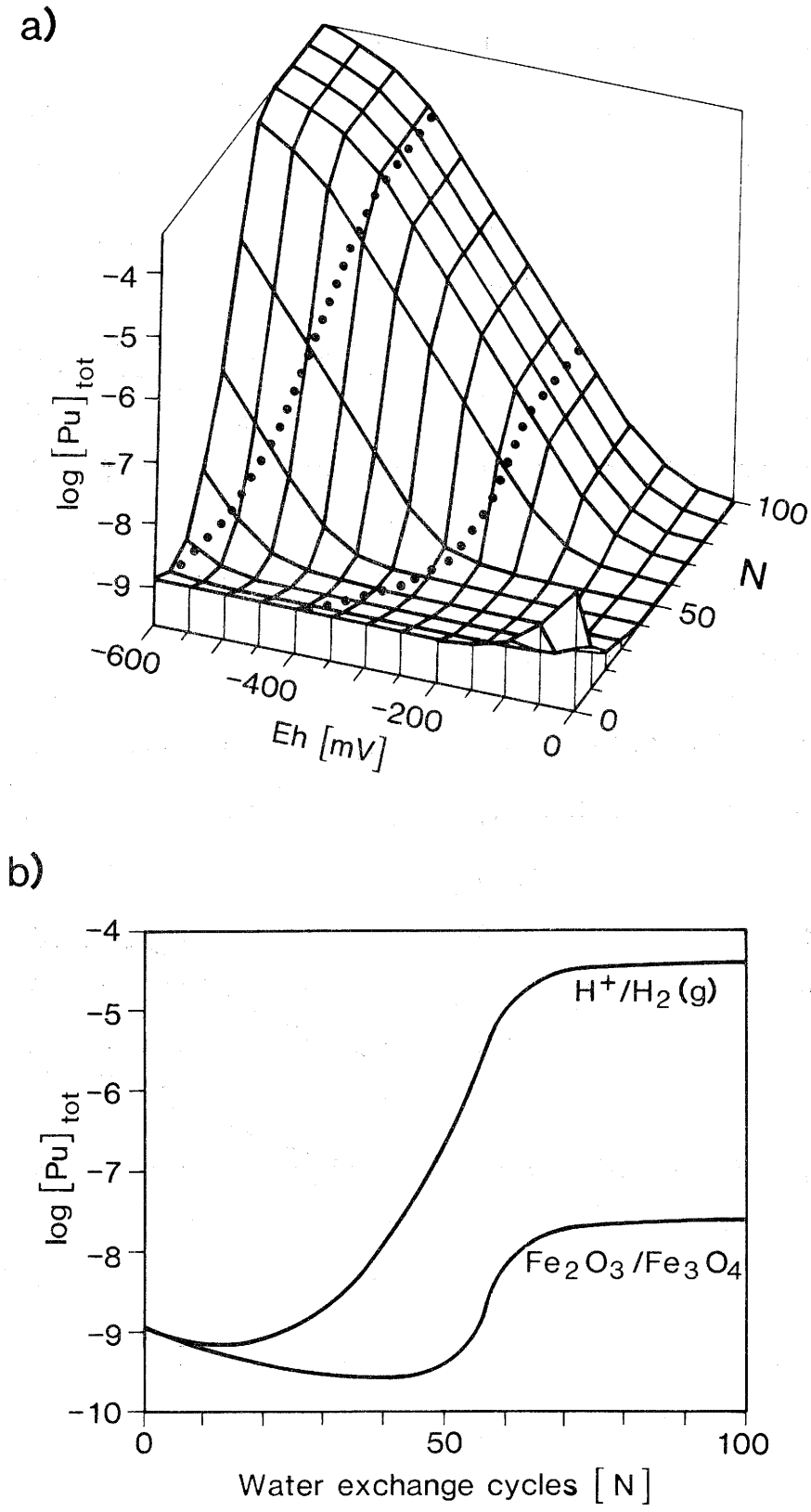

Figure 15: Representation of plutonium solubility limits (a) for the entire Eh range considered in the mixing tank model, as well as (b) in the form of cross-sections along the Eh/pH functions (dotted lines in the upper figure) which define the probable Eh range in the near-field.

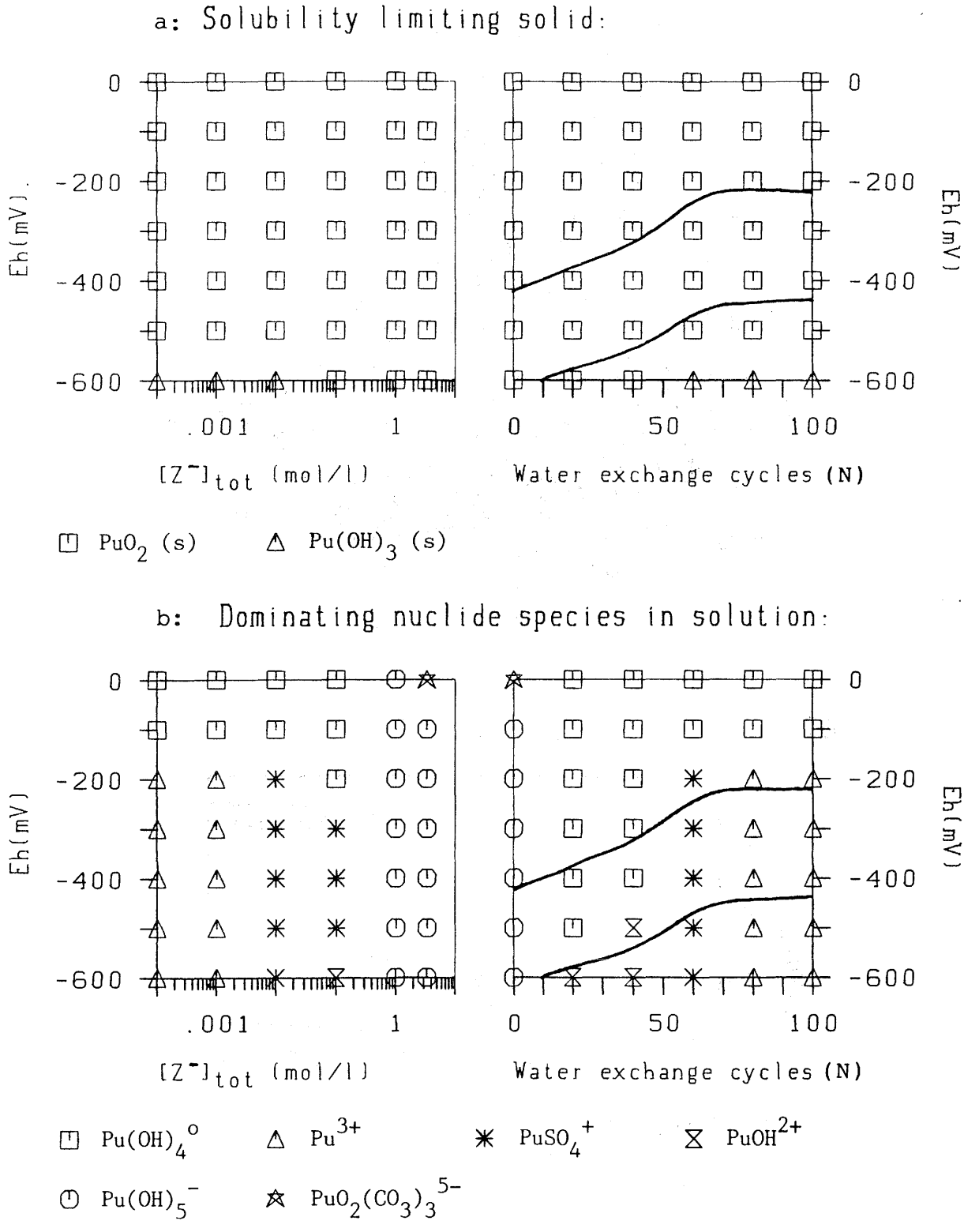

Figure 16: Grid diagram for solubility limiting solids (a) and for the dominant plutonium species under the modelled conditions (b). The diagrams on the left hand side refer to the extrapolation model (water speciation depicted in Figure 4) and those on the right hand side to the mixing tank model (water speciation depicted in Figure 7 and listed in Table 8).

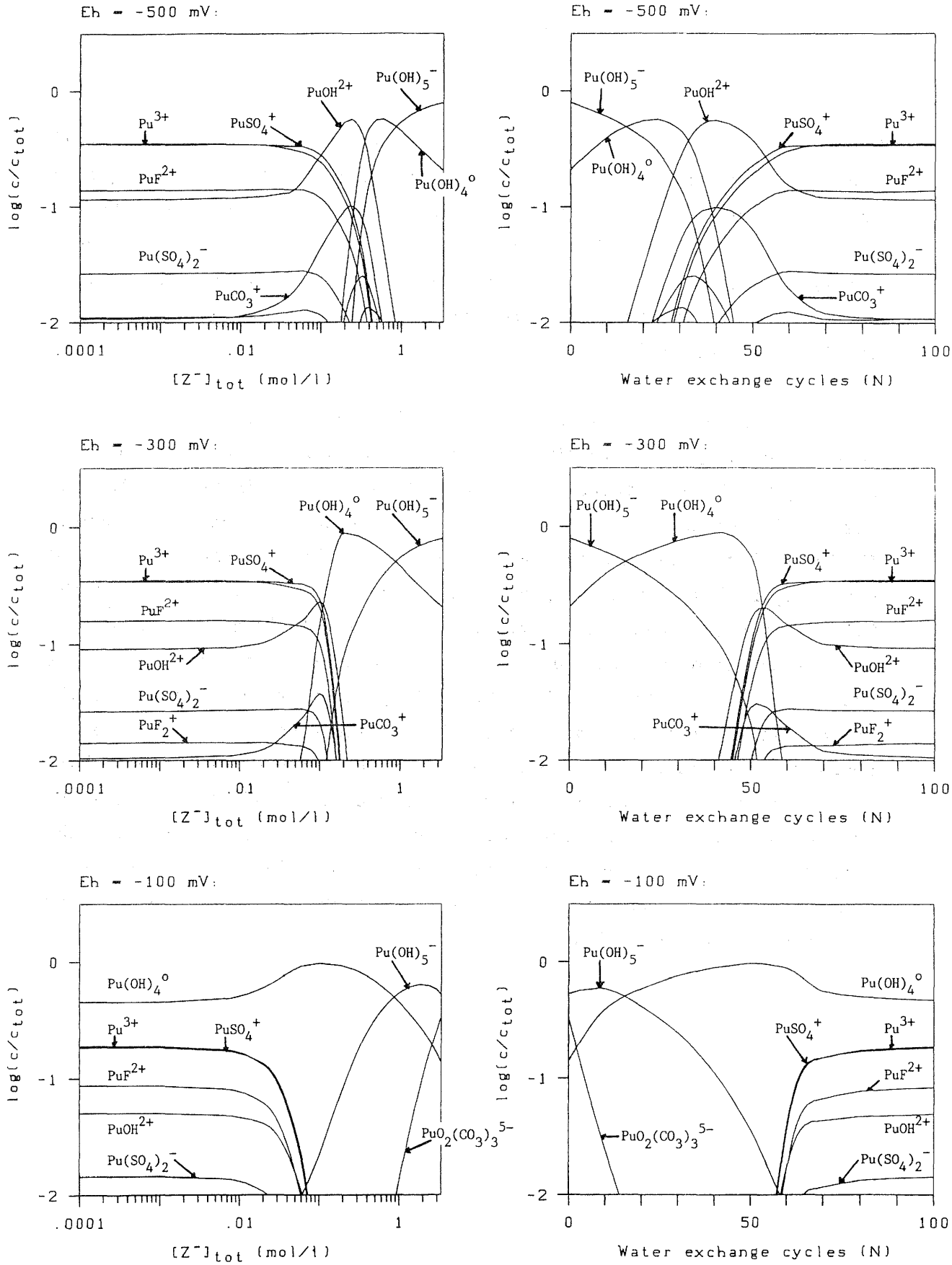

Figure 17: Plutonium speciation plots for selected Eh values (stoichiometric species concentrations divided by total plutonium concentration).

3.5. Thorium

Thorium solubility is completely independent of the redox potential because there is only one stable oxidation state (+IV) in aqueous solution. For a very long time period, the solubility limit of thorium is predicted to be as low as about $2 \cdot 10^{-10}$ M, before a relatively rapid increase to 10^{-8} M takes place (see Figure 18). This will happen after 1.5 million years (N > 50). Subsequently, thorium solubility will not significantly alter further.

Figure 19a shows that the only solid thorium phase will be ThO_2 (s). There are only two thorium complexes which will dominate in solution (see Figure 19b and Figure 20). $Th(OH)_4^o$ is the dominant species at high pH values, whereas the relative stability of the complex $Th(HPO_4)_3^{2-}$ rapidly increases as the pH falls below 8 (compare Figure 20 with Figure 7b) at a total phosphate concentration of $1.9 \cdot 10^{-6}$ M in the Swiss Reference Groundwater (cf. Table 7). It should be mentioned that the dissolution of the waste glass might lead to a higher total phosphate concentration in the near-field pore water, which could result in a higher thorium solubility than calculated with this model. However, the increase cannot be dramatic because the phosphate concentration in natural waters is found to be limited despite the continuous entry of phosphate ions into lakes, possibly due to the formation of hydroxyapatite, $Ca_5(PO_4)_3OH$ (s) [37]. The phosphate content of natural waters is found to be below 10^{-5} M in all cases reported by Grasshoff [38].

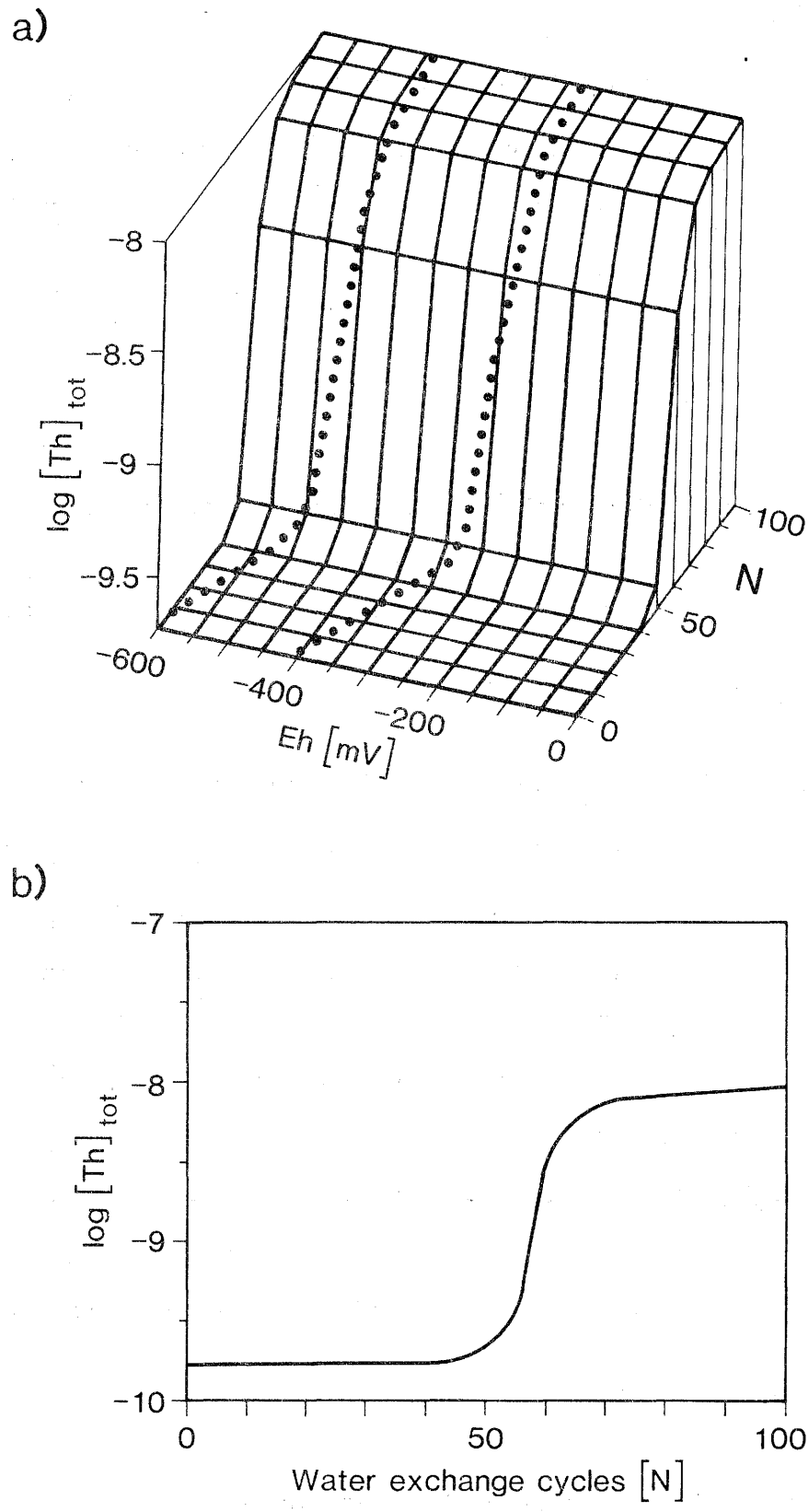

Figure 18: Representation of thorium solubility limits (a) for the entire Eh range considered in the mixing tank model, as well as (b) in the form of cross-sections along the Eh/pH functions (dotted lines in the upper figure) which define the probable Eh range in the near-field.

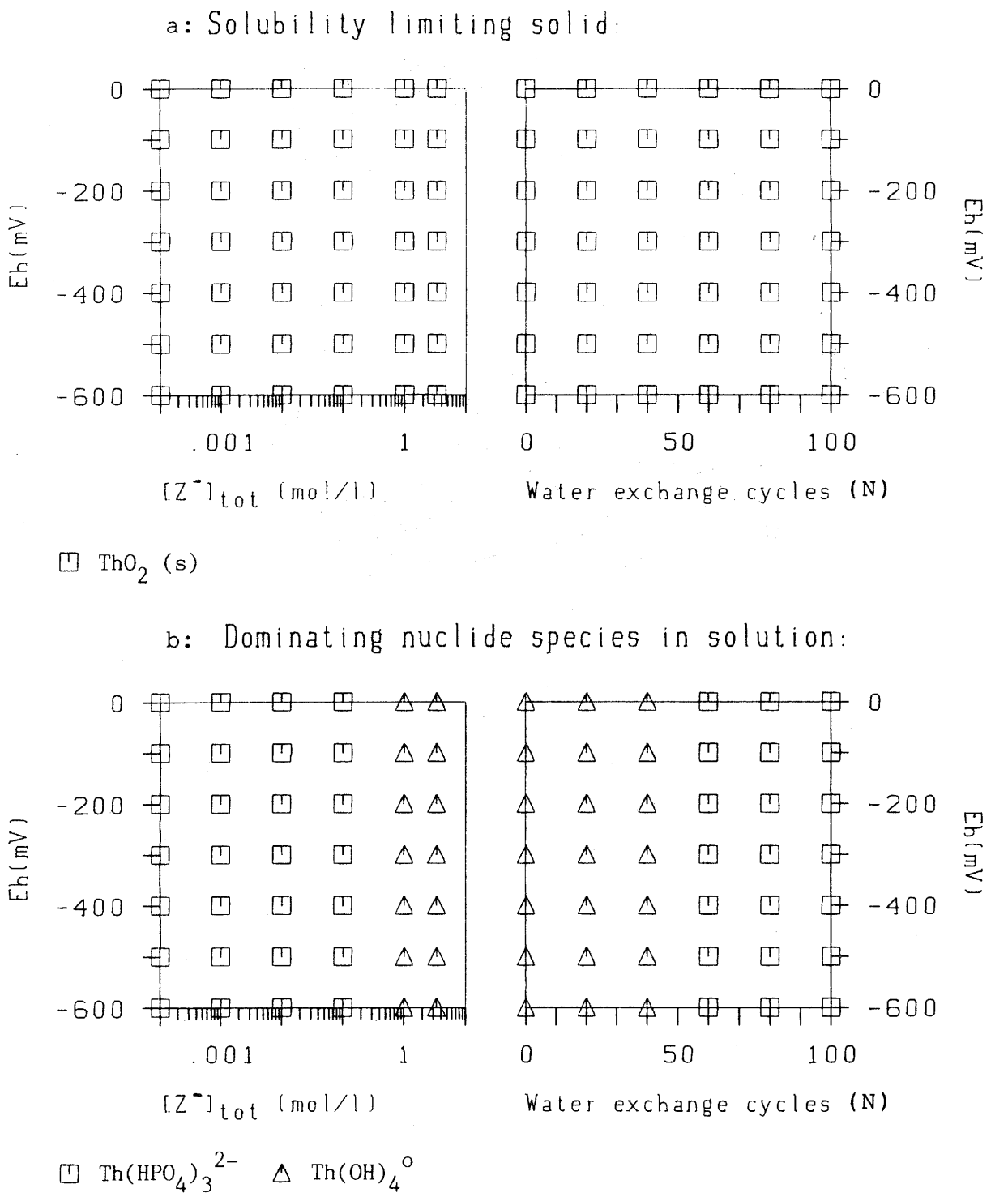

Figure 19: Grid diagram for solubility limiting solids (a) and for the dominant thorium species under the modelled conditions (b). The diagrams on the left hand side refer to the extrapolation model (water speciation depicted in Figure 4) and those on the right hand side to the mixing tank model (water speciation depicted in Figure 7 and listed in Table 8).

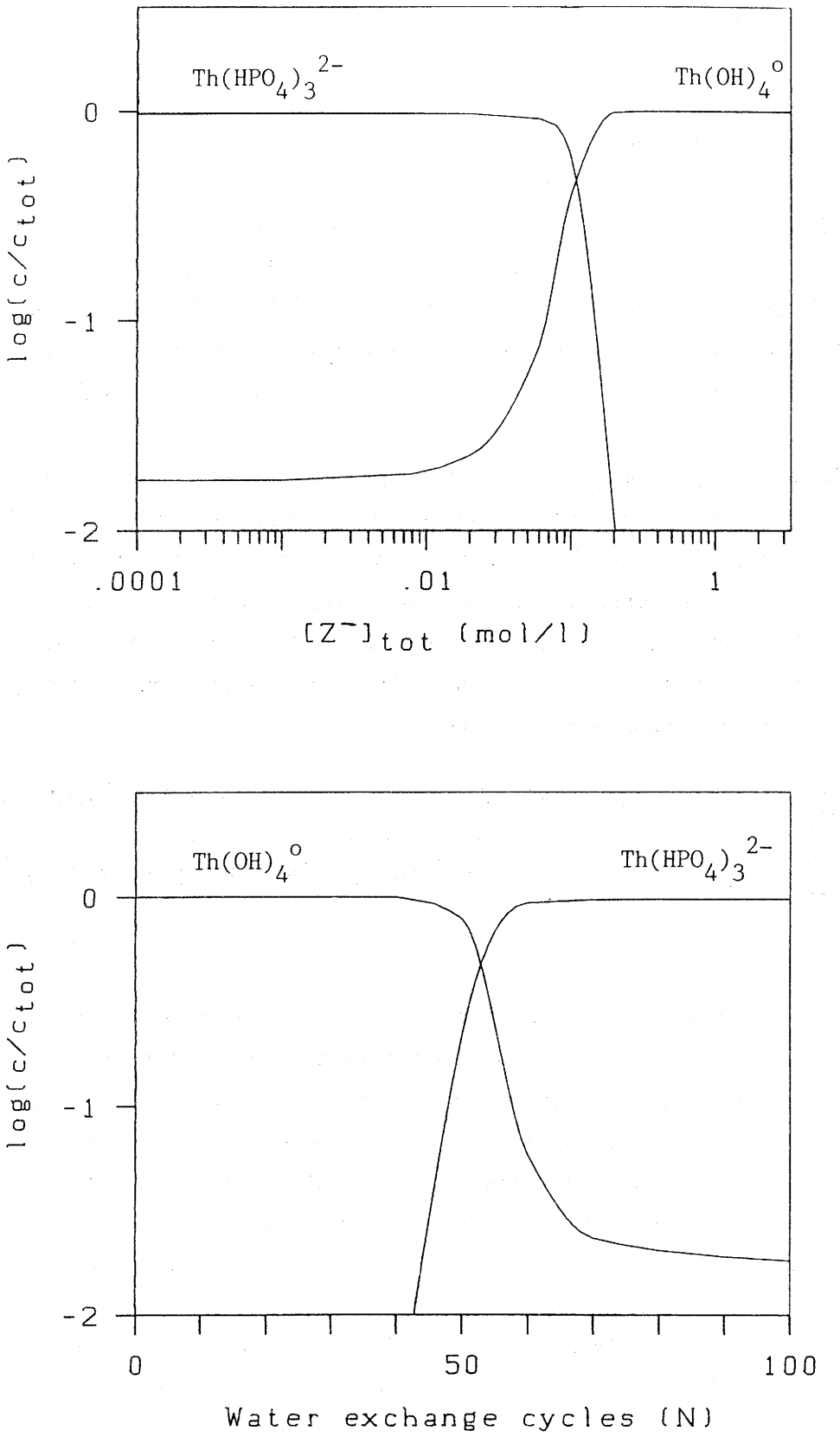

Figure 20: Thorium speciation plots (stoichiometric species concentrations divided by total thorium concentration).

3.6. Americium

Americium is observed to exist in the form of Am(III) species in the absence of powerful oxidising agents, and its solubility limit will therefore not depend on the redox potential under the conditions considered. Figure 21 shows a decrease in the maximum americium solubility from $2 \cdot 10^{-6}$ M initially to $2 \cdot 10^{-7}$ M at N=25, i.e. during the first 700,000 years. After that, the solubility limit increases again to reach a constant value of $5 \cdot 10^{-5}$ M after 1.7 million years (N > 60).

At first sight, it might appear strange that, with increasing N, the solubility limit of americium goes through a minimum rather than altering gradually as the concentrations of the water components do (cf. Figure 7). The explanation for this behaviour can be found in Figures 22 and 23. In the area of interest (N < 50), carbonato complexes of americium dominate in solution. The average complexation degree with respect to the carbonato complexes, $\bar{n}$,

$$\bar{n} = \frac{\sum_{n=o}^{3} n \cdot [Am(CO_3)_n]}{\sum_{n=o}^{3} [Am(CO_3)_n]} = \frac{[AmCO_3] + 2 \cdot [Am(CO_3)_2] + 3 \cdot [Am(CO_3)_3]}{[Am] + [AmCO_3] + [Am(CO_3)_2] + [Am(CO_3)_3]}$$

gradually decreases with increasing N. With the help of the speciation plots in Figure 23, it can be calculated that at N=0, where virtually all dissolved americium is present in the form of $Am(CO_3)_3^{3-}$, the average carbonate complexation degree amounts to $\bar{n}$ = 2.90, whereas at N=100 practically no carbonato complexes of americium exist in solution ($\bar{n}$ = 0.03). Since the carbonate-to-americium ratio of the solubility limiting solid, $Am_2(CO_3)_3$ (s), is 1.5, the americium solubility limit will be minimum if the average carbonate complexation degree, $\bar{n}$, of the dissolved americium is around 1.5 and if carbonato complexes dominate in solution. These conditions are accomplished between N=20 and N=30 and account for the minimum in the solubility curve.

Figure 23 reveals that sulfato and fluoro complexes of americium(III) are significant, although not dominant.

It should be mentioned that there are large uncertainties concerning the americium database used for the calculations. The precipitation of the pure carbonate solid, $Am_2(CO_3)_3$ (s), from aqueous solutions seems to be doubtful because $Am(OH)CO_3$ (s) was found to be the only carbonate solid formed from dilute aqueous bicarbonate solutions [39]. However, Nitsche and Edelstein [40] precipitated americium from J-13 groundwater (pH = 7, alkalinity = 2.34 meq/l) and found by X-ray powder diffraction measurements that the precipitate is a mixture of $Am(OH)CO_3$ and $Am_2(CO_3)_3 \cdot 2H_2O$. A comprehensive set of formation constants for the hydroxo and carbonato complexes of americium(III) are reported by Bernkopf [41], but could be uncertain due to the fact that equilibrium was approached from undersaturation only and the americium solids used for the experiments were not thoroughly characterised. New Am(III) hydrolysis constants have been published by Rai et al. [42], reporting the hydroxo complexes to be less stable plus the solubility of $Am(OH)_3$ (s) to be lower by one order of magnitude.

Finally, a recently published paper reports experimental results on the radiolytic oxidation of Am(III) to Am(V) [43]. In weekly basic carbonate-free 5M NaCl solutions, the authors observed the formation of AmO_2^+. This observation might be worth further investigations because it is not yet known whether this process also occurs at NaCl concentrations of natural groundwaters.

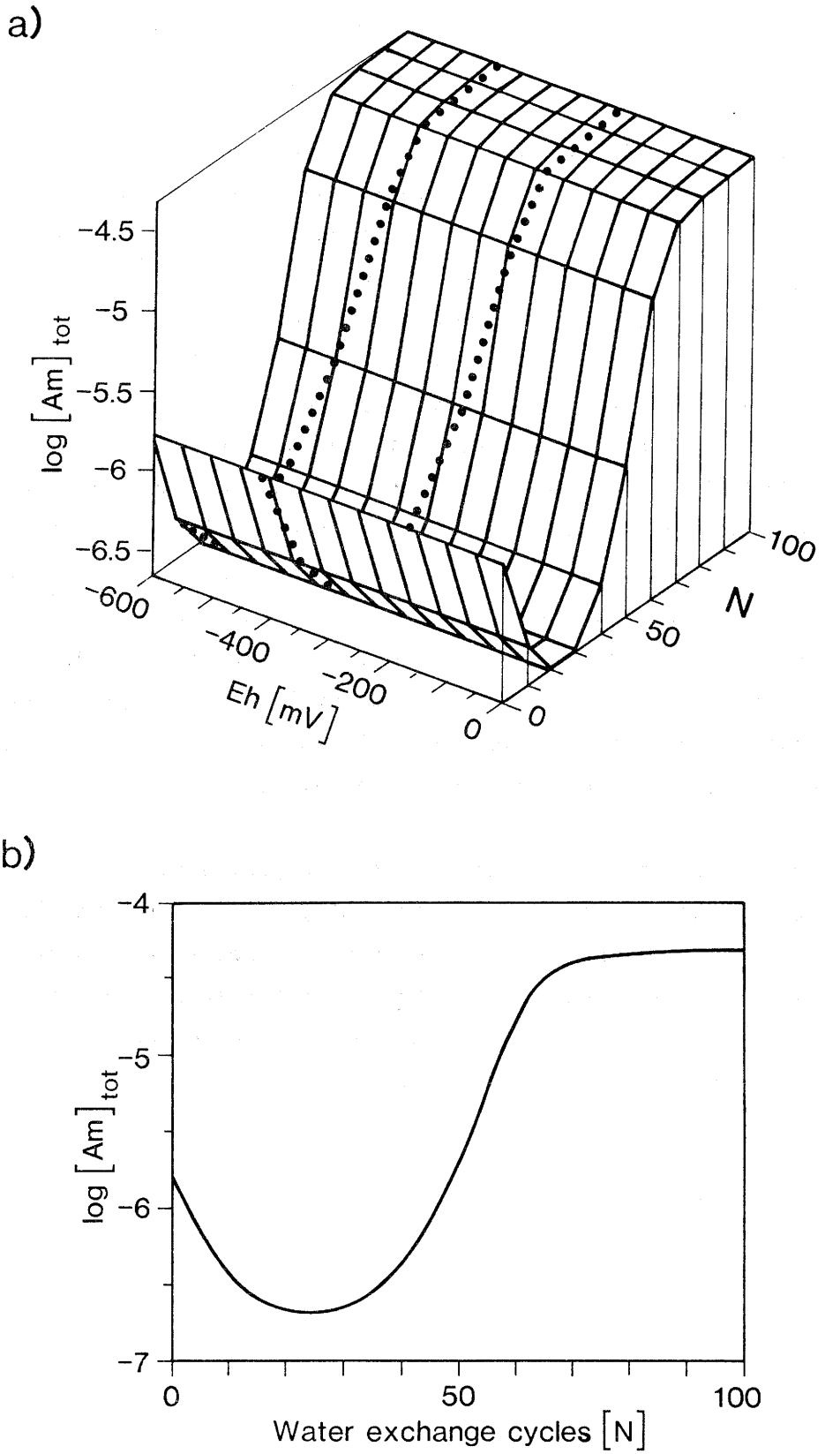

Figure 21: Representation of americium solubility limits (a) for the entire Eh range considered in the mixing tank model, as well as (b) in the form of cross-sections along the Eh/pH functions (dotted lines in the upper figure) which define the probable Eh range in the near-field.

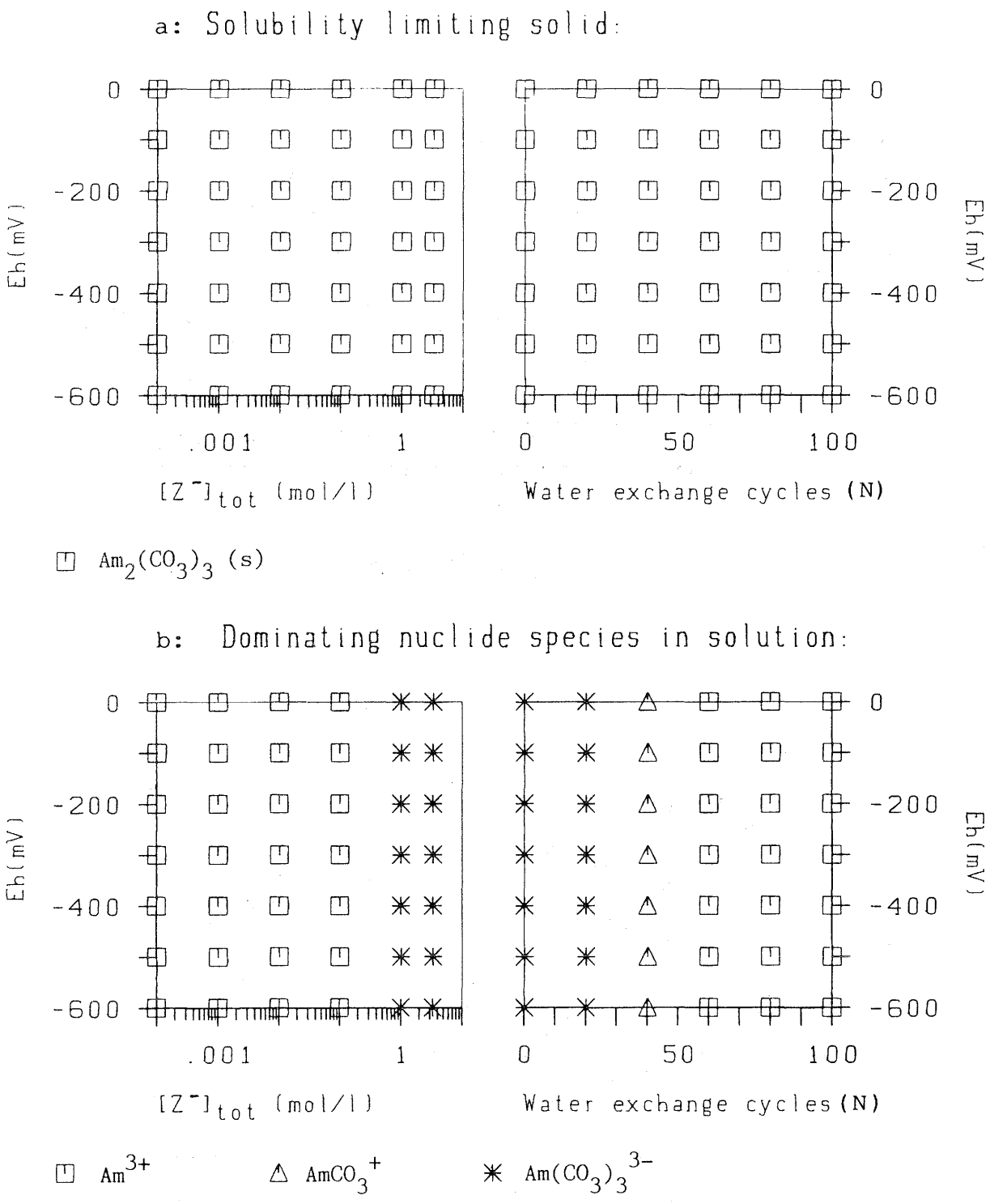

Figure 22: Grid diagram for solubility limiting solids (a) and for the dominant americium species under the modelled conditions (b). The diagrams on the left hand side refer to the extrapolation model (water speciation depicted in Figure 4) and those on the right hand side to the mixing tank model (water speciation depicted in Figure 7 and listed in Table 8).

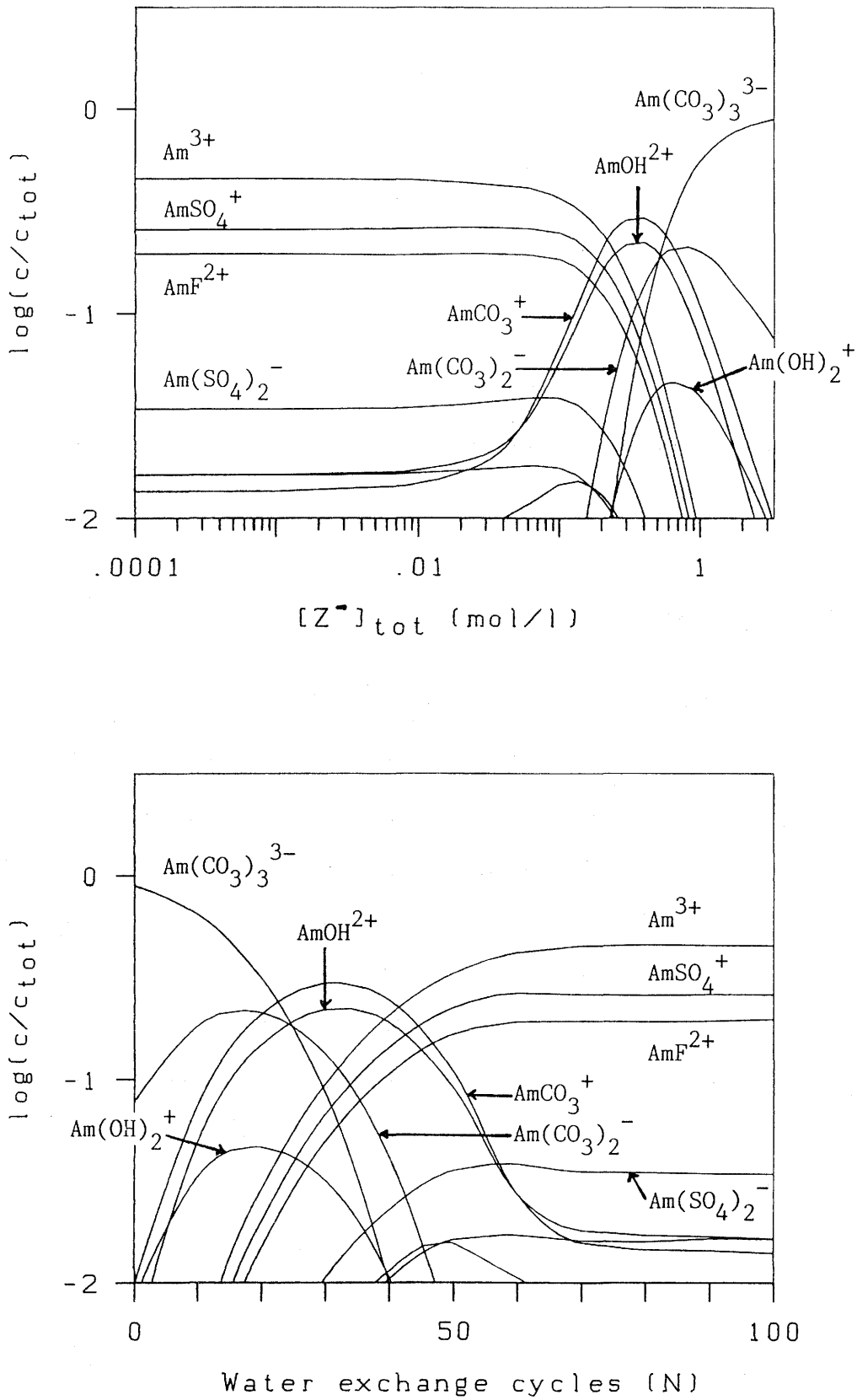

Figure 23: Americium speciation plots (stoichiometric species concentrations divided by total americium concentration).

3.7. Technetium

The maximum technetium solubility will be very low in the near-field of a high-level waste repository: For the entire Eh/pH range expected at any time, the solubility limits of technetium is calculated to be below 10^{-9} M, as Figure 24b shows. In the presence of dihydrogen gas, $H_2(g)$, technetium can even be considered completely insoluble. Figure 24a gives an impression of the extremely strong Eh dependence of technetium solubility.

It can be seen from Figure 25 that metallic technetium, Tc(s), will be the solubility limiting solid under the expected conditions. Tc(III) and Tc(IV) appear to be the predominant oxidation states of technetium in solution, represented by only one species each: TcO^+ and $TcO(OH)_2^o$ (see Figure 26), whereas the highly soluble pertechnetate ion, TcO_4^-, is calculated to be of no importance under these conditions.

The database of technetium appears to be quite small. As can be seen from Table B-8 (Appendix B), only the formation of oxo and hydroxo species of the different technetium oxidation states are considered. An extension of the technetium database would help much in achieving a more realistic prediction of technetium solubility in the bentonite pore water.

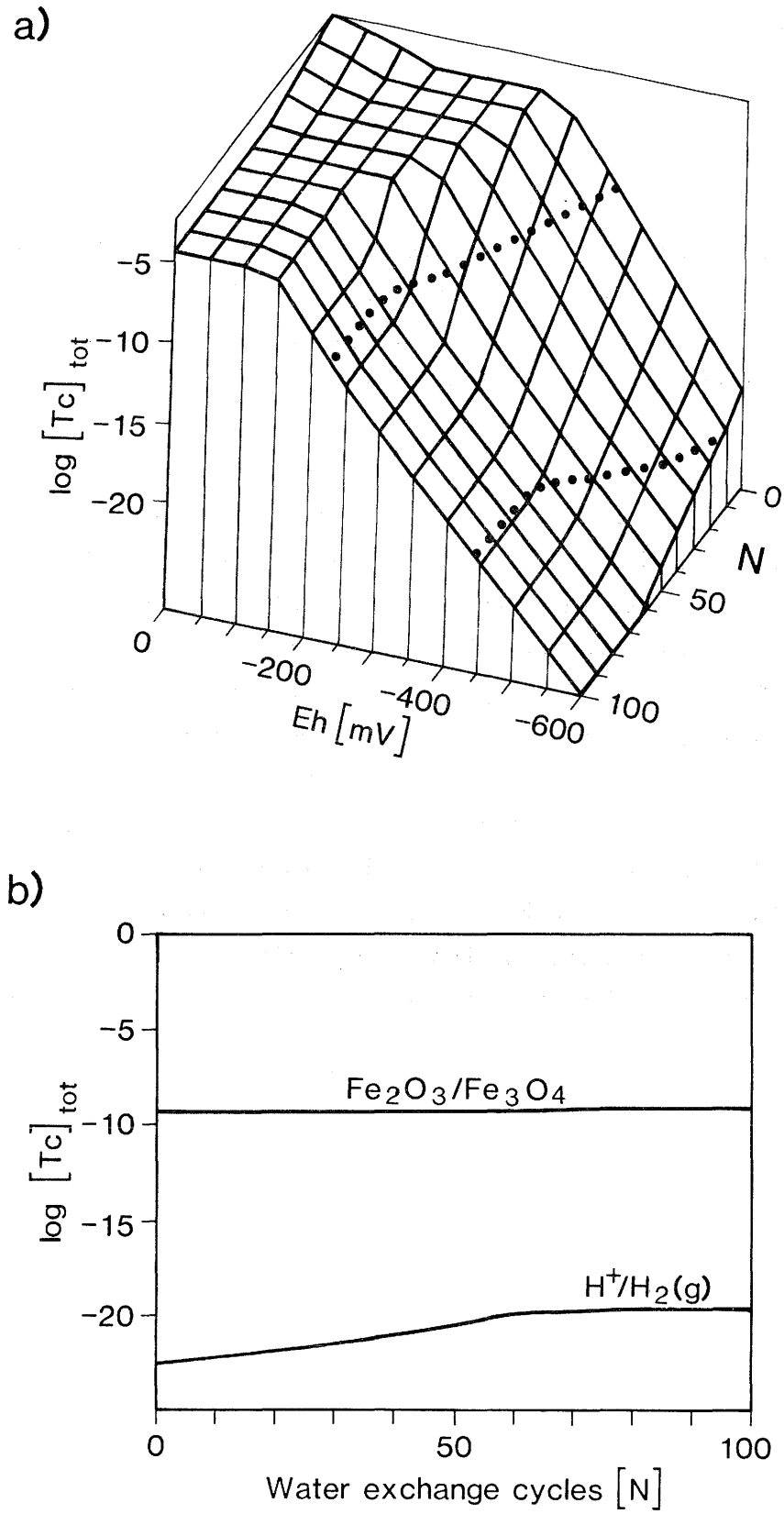

Figure 24: Representation of technetium solubility limits (a) for the entire Eh range considered in the mixing tank model, as well as (b) in the form of cross-sections along the Eh/pH functions (dotted lines in the upper figure) which define the probable Eh range in the near-field.

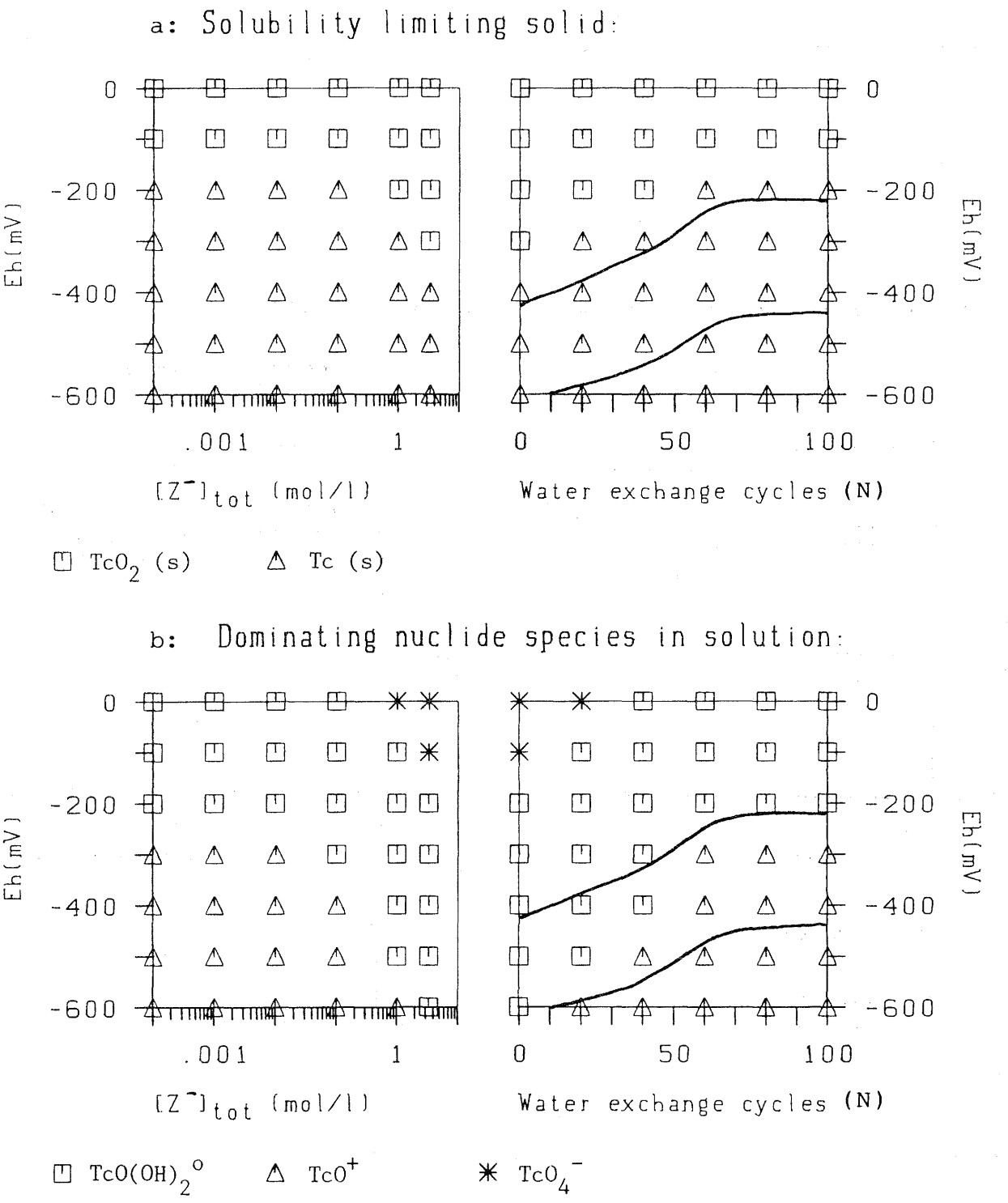

Figure 25: Grid diagram for solubility limiting solids (a) and for the dominant technetium species under the modelled conditions (b). The diagrams on the left hand side refer to the extrapolation model (water speciation depicted in Figure 4) and those on the right hand side to the mixing tank model (water speciation depicted in Figure 7 and listed in Table 8).

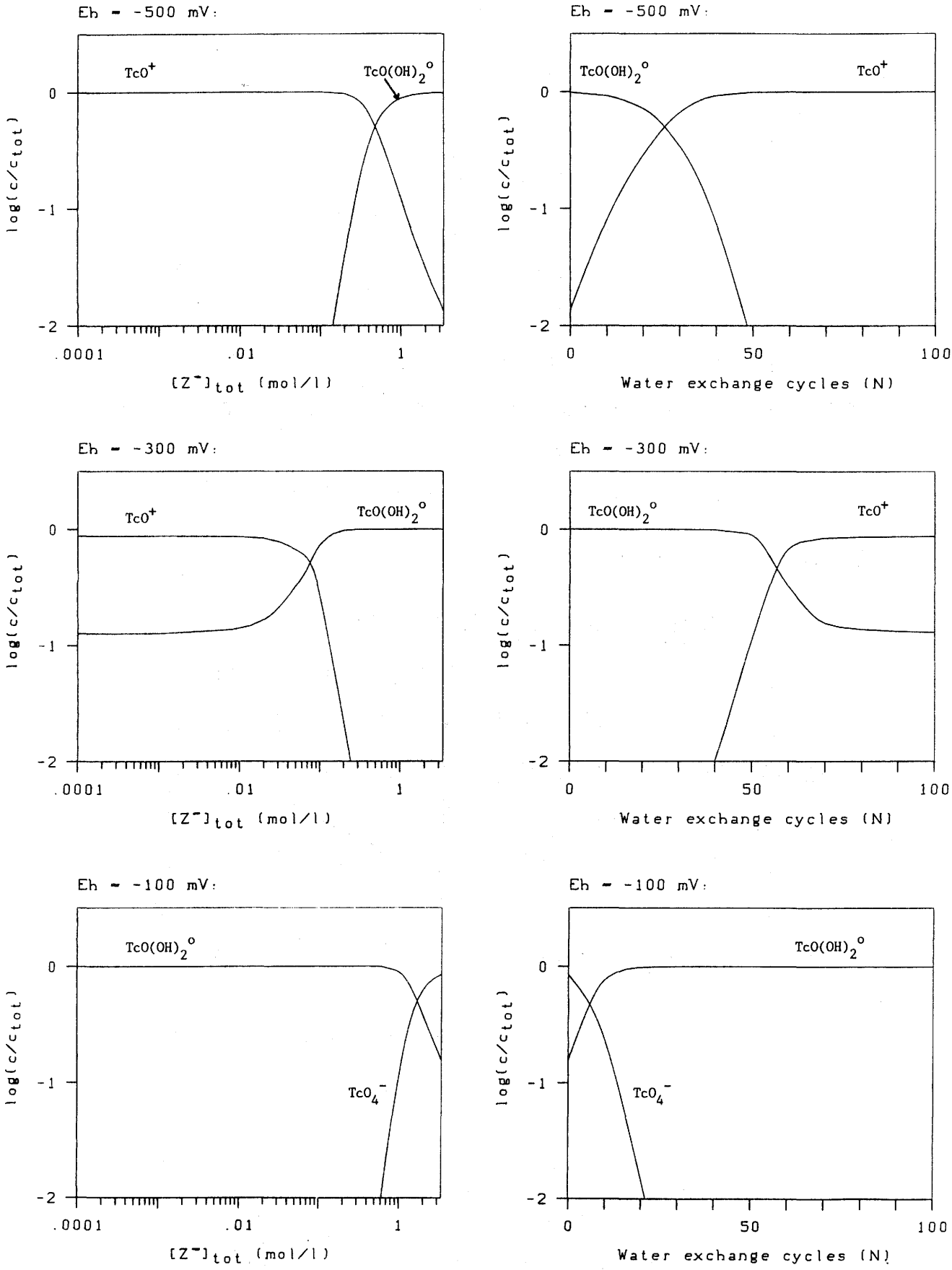

Figure 26: Technetium speciation plots for selected Eh values (stoichiometric species concentrations divided by total technetium concentration).

Conclusions

The model presented here should be considered as a first attempt to quantitatively describe the most important short- and long-term chemical processes expected to take place in the near-field of a high-level radioactive waste repository with sodium bentonite backfill. Although the model is based on the dimensions of a potential Swiss repository, it is applicable to both other repository dimensions and other groundwater compositions. Refinement and extension of the bentonite model described seems sensible only if an extended and consistent experimental dataset on the bentonite-groundwater interaction is available. Although uncertainties in the chosen parameters, such as ion-exchange constants, are estimated to have no principal influence on the model predictions, it would be helpful to know more about the ranges of uncertainty and to reduce them as far as possible. The performance of a number of experiments under completely anaerobic conditions with systematic parameter variations is suggested, e.g. variation of temperature, alteration of the bentonite mass/water volume ratio, and the use of a number of distinctly different groundwaters. The possibility of simultaneously investigating the influence of iron corrosion products should be taken into consideration. Further developments should also try to model the slow effects of clay mineral alteration on the water composition in the near-field. Illite is known to have a considerably smaller ion-exchange capacity than bentonite.

The model calculations show that the solubility limits of uranium and neptunium might be higher by orders of magnitude in the near-field pore water than in the groundwater of the host rock (compare solubility limits calculated in this report with those for the undisturbed far-field [44]). Hence, a comparatively strong downhill concentration gradient could build up at the near-to-far-field boundary. As a possible consequence, the formation of uranium and neptunium colloids cannot be completely excluded. Data on the stability and migration behaviour of such colloids do not exist as yet. A better understanding of the characteristics of colloids could help to solve these problems.

Sodium bentonite is calculated to slowly convert to calcium bentonite in a deep repository. This conclusion is supported by leaching experiments with synthetic groundwater. Obviously, calcium bentonite will be chemically more stable than sodium bentonite in a deep repository. As already concluded by Grauer [18], calcium bentonite would be more suitable as a backfill material than sodium bentonite from the chemical viewpoint, because its effect on the groundwater chemical composition will be considerably less marked, especially with respect to pH and carbonate concentration.

At present the thermodynamic data of many actinide solids and complexes are limited and inconsistent. Discrepancies of many orders of magnitude in different reported values of the stability constants can be encountered in the literature. The stabilitiy constants of some critical species used in this report might be considerably overestimated, as discussed in some subsections of chapter 3. These uncertainties emphasise the urgent need to critically review the existing literature data of the actinides, a project which has been started lately [45] and which is coordinated by the OECD Nuclear Energy Agency. Beside that, there is a fundamental requirement of producing more thermodynamic data which allow a more reliable prediction of the chemical behaviour of the actinides, also at elevated temperatures. The possibility of a specific experimental validation of the predicted actinide and technetium solubility limits in bentonite pore water should be checked, and the theoretical treatment of chemical speciation should be expanded to include sorption processes as well.

Acknowledgements

The author would like to thank M. Schweingruber, J. Hadermann, I. McKinley, R. Grauer, F.J. Pearson Jr., M. Snellman, and L.N. Plummer for valuable discussions, and H.P. Alder, H. Flury, Ch. McCombie, F. van Dorp, and B. Knecht for their interest in this work.

The technical assistance of I. Kusar, as well as the checking of the thermodynamic data tables by U. Berner, are thankfully acknowledged.

C. Bajo kindly translated the summary into french.

References

[1] Projekt Gewaehr 1985, Nuclear Waste Management in Switzerland: Feasibility Studies and Safety Analyses, Nagra NGB 85-09 (Baden, 1985).

[2] I.G. McKinley, The Geochemistry of the Near-Field, Nagra NTB 84-48 (Baden, 1985).

[3] M. Schweingruber, Loeslichkeits- und Speziationsrechnungen fuer U, Pu, Np und Th in natuerlichen Grundwaessern - Theorie, thermodynamische Dateien und erste Anwendungen, EIR-Bericht Nr. 449 (Wuerenlingen, 1981).

[4] M. Schweingruber, User's Guide for Extended MINEQL (EIR version) - Standard Subroutine/Data Library Package, EIR Internal Report TM-45-82-38 (Wuerenlingen, 1982).

[5] M. Schweingruber, Revision 1 of: User's Guide for Extended MINEQL (EIR version) - Standard Subroutine/Data Library Package, EIR Internal Report AN-45-84-39 (Wuerenlingen, 1984).

[6] M. Snellman, Chemical Conditions in a Repository for Spent Fuel, YJT 84-08 (Espoo, 1984).

[7] M. Snellman (private communication, 1985).

[8] F.M.M. Morel, Principles of Aquatic Chemistry, (Wiley Interscience, New York, 1983), p.138.

[9] R.D. Lindberg, D.D. Runnells, Groundwater Redox Reactions: An Analysis of Equilibrium State Applied to Eh Measurements and Geochemical Modeling, Science 225, 925-927 (1984).

[10] W. Stumm, J.J. Morgan, Aquatic Chemistry, Wiley Interscience, 2nd ed. (Wiley Interscience, New York, 1981), pp.273-274.

[11] M. Mueller-Vonmoos, G. Kahr, Mineralogische Untersuchungen von Wyoming Bentonit MX-80 und Montigel, Nagra NTB 83-12 (Baden, 1983), pp.A3-A4.

[12] Ref. [1], p.9-20.

[13] R.A. Couture, Steam Rapidly Reduces the Swelling Capacity of Bentonite, Nature 318, 50-52 (1985).

[14] Final Storage of Spent Fuel - KBS-3, Vol.III (Stockholm, 1983), p.9:3.

[15] J.P. Simpson, Experiments on Container Materials for Swiss High-Level Waste Disposal Projects, Part I, Nagra NTB 83-05 (Baden, 1983), p.5.

[16] R. Grauer, Behaeltermaterialien fuer die Endlagerung hochradioaktiver Abfaelle: Korrosionschemische Aspekte, Nagra NTB 84-19 (Baden, 1984), p.48.

[17] R.M. Johnston, H.G. Miller, Effect of pH on Smectite Stability, KBS TR 84-11, Smectite Alteration, proceedings (Stockholm, 1984), pp.54-56 and 146-161.

[18] R. Grauer, Bentonit als Verfuellmaterial im Endlager fuer hochradioaktiven Abfall: Chemische Aspekte, EIR-Bericht Nr. 576 (Wuerenlingen, 1986).

[19] B. Grambow, H.P. Hermansson, I.K. Bjoerner, L. Werme, Glass/Water Reaction with and without Bentonite Present - Experiment and Model, in: Materials Research Society, Proc. Sci. Basis Nucl. Waste Man. IX (L. Werme, ed.), Stockholm, Sept. 9-11, 1985, North-Holland, New York, in press (1986).

[20] R. Pusch, T. Eriksen, A. Jacobsson, Ion/Water Migration Phenomena in Dense Bentonites, in: Materials Research Society, Vol.11, Proc. Sci. Basis Nucl. Waste Man. V (W. Lutze ed.), North-Holland, New York, pp.649-658 (1982).

[21] M. Schweingruber, On Probable In-Situ pH, pCO_2, and Redox Conditions for Waters Sampled at 400, 600, and 1300 m Depth in Borehole KRISTAL I Boettstein, EIR Internal Report TM-45-84-20 (Wuerenlingen, 1984).

[22] M. Schweingruber, Deep-Crystalline Reference Water for Project "Gewaehr", EIR Internal Report TM-45-84-21 (Wuerenlingen, 1984).

[23] Ref. [1], p.10-12.

[24] Ref. [1], p.5-2.

[25] Ref. [1], p.10-16.

[26] M. Mueller-Vonmoos (private communication).

[27] N.A. Chapman, I.G. McKinley, J.A.T. Smellie, The Potential of Natural Analogues in Assessing Systems for Deep Disposal of High-Level Radioactive Waste, Nagra NTB 84-42 (Baden, 1984).

[28] D.C. Thorstenson, D.W. Fisher, M.G. Croft, The Geochemistry of the Fox Hills-Basal Hell Creek Aquifer in Southwestern North Dakota and Northwestern South Dakota, Wat. Resour. Res. 15, 1479-1498 (1979).

[29] M. Schweingruber, Actinide Solubility in Deep Groundwaters - Estimates for Upper Limits Based on Chemical Equilibrium Calculations, EIR Report No.507 (Wuerenlingen, 1983).

[30] D. Langmuir, Uranium Solution-Mineral Equilibria at Low Temperatures with Applications to Sedimentary Ore Deposits, Geochim. Cosmochim. Acta 42, 547-569 (1978).

[31] J.L. Ryan, D. Rai, The Solubility of Uranium(IV) Hydrous Oxide in Sodium Hydroxide Solutions under Reducing Conditions, Polyhedron 2, 947-952 (1983).

[32] A. Avogadro et al., The MIRAGE Project: Actinide and Fission Product Physico-Chemical Behaviour in Geological Environment, in: Radioactive Waste Management and Disposal, Proc. 2nd European Community Conference (R. Simon, ed.), Luxembourg, April 22-26, 1985, EEC, Brussels, 331-342 (1986).

[33] B. Allard, Actinide Solution Equilibria and Solubilities in Geologic Systems, KBS TR 83-35 (Stockholm, 1983), p.13.

[34] L. Maya, Hydrolysis and Carbonate Complexation of Dioxoneptunium(V) in 1.0 M $NaClO_4$ at 25°C, Inorg. Chem. 22, 2093-2095 (1983).

[35] H. Nitsche, N.M. Edelstein, the paper presented in "12-journees des Actinides, Orsay (1982). (Citation in ref. [32])

[36] D. Rai, J.L. Ryan, Neptunium(IV) Hydrous Oxide Solubility under Reducing and Carbonate Conditions, Inorg. Chem. 24, 247-251 (1985).

[37] G.H. Nancollas, Z. Amjad, P. Koutsoukos, Calcium Phosphates - Speciation, Solubility, and Kinetic Considerations, in: Chemical Modeling in Aqueous Systems, ACS Symp. Ser., Vol. 93 (E.A. Jenne, ed.), Am. Chem. Soc., Washington, D.C., pp.475-497 (1979).

[38] K. Grasshoff, The Hydrochemistry of Landlocked Basins and Fjords, in: Chemical Oceanography, Vol. 2, 2nd Ed. (J.P. Riley, G. Shirrow, ed.), Academic Press, London, pp.455-597 (1975).

[39] R.J. Silva, The Behaviour of Americium in Aqueous Carbonate Systems, in: Materials Research Society, Vol.26, Proc. Sci. Basis Nucl. Waste Man. VII (G.L. McVay, ed.), North-Holland, New York, pp.875-881 (1984).

[40] H. Nitsche, N.M. Edelstein, Determination of the Solubilities and Complexation of Waste Radionuclides Pertinent to Geologic Disposal at the Nevada Tuff Site, LBL-18900 (Berkeley, 1985).

[41] M.F. Bernkopf, Hydrolysereaktionen und Karbonatkomplexierung von dreiwertigem Americium in natuerlichen aquatischen Systemen, Ph.D. dissertation, TU Muenchen (1984).

[42] D. Rai, R.G. Strickert, D.A. Moore, J.L. Ryan, Am(III) Hydrolysis Constants and Solubility of Am(III) Hydroxide, Radiochim. Acta 33, 201-206 (1983).

[43] S. Magirius, W.T. Carnall, J.I. Kim, Radiolytic Oxidation of Am(III) to Am(V) in NaCl Solutions, Radiochim. Acta 38, 29-32 (1985).

[44] Ref. [1], p.10-24.

[45] A.B. Muller, International Chemical Thermodynamic Database for Nuclear Applications, Rad. Waste Manag. Nucl. Fuel Cycle 6(2), 131-141 (1985).

[46] Ref. [8], pp.57-58.

[47] Ref. [10], pp.68-72.

[48] M. Schweingruber, Technetium Solubilities in Deep Groundwaters - Estimates for Upper Limits Based on Chemical Equilibrium Calculations, EIR Internal Report TM-45-84-14 (Wuerenlingen, 1984).

[49] B. Allard, B. Torstenfelt, On the Solubility of Technetium in Geochemical Systems, KBS TR 83-60 (Stockholm, 1983).

Appendix A: The Speciation Model

The term 'speciation' is generally applied to the distribution of an element between the range of possible dissolved forms. An estimation of chemical speciation thus results in concentration or activity values for all the dissolved species considered. A premise for speciation calculations is generally the assumption of thermodynamic equilibrium among the dissolved species.

The term 'solubility limit of an element' is not a well-defined and rigorous scientific expression. Nevertheless, it is so widely used that it may be considered as a new technical term. The solubility limit of an element M, in a specific type of water, is equal to the stoichiometric sum of the concentrations of all M-containing species dissolved, if they are in equilibrium with an M-containing solid phase. Therefore, it is clear that the maximum concentration of an actinide is strongly dependent on the composition and stability of this solid phase. A more theoretical definition of maximum elemental solubility has been given by M. Schweingruber [29].

The basis for the calculation of speciation and solubility limits of the radionuclides considered in this report, is the assumption of overall redox equilibrium among the various oxidation states of these elements. Except for the case of americium, the solubility limiting solids of the waste elements in groundwater are assumed to be pure oxides or hydroxides. Consequently, the aqueous phase will not be oversaturated with respect to any of the radwaste element oxides or hydroxides considered. The least soluble of the potential solubility limiting compounds will control solubility under the conditions given.

The estimation of activity coefficients and the modification of formation constants for temperatures different from 25°C will be briefly presented. The pressure dependence of equilibrium constants is not taken into account due to the lack of the thermodynamic data required.

Estimation of Activity Coefficients

For each species, i, the corresponding activity coefficient, f(i), is derived from Davie's approximation (e.g., [46]):

$$\log f(i) = z(i)^2 \cdot \gamma(T,I)$$

$$\gamma(T,I) = -1.82 \cdot 10^6 \cdot (\varepsilon \cdot T)^{-\frac{3}{2}} \cdot \left\{ \frac{\sqrt{I}}{1 + \sqrt{I}} - 0.2 \cdot I \right\}$$

$$I = 0.5 \cdot \sum_i [A(i)] \cdot z(i)^2$$

where z(i) is the charge of the species i, ε(= 169.1 - 0.301·T) the temperature-dependent dielectric constant of pure water, T the absolute temperature (Kelvin), and I the ionic strength (mol/l). The use of this approximation is found to be limited to the ionic strength interval from I=0 M to I=0.5 M (see Figure A-1). The range of ionic strengths dealt with in the present work lies between I=0.005 M and I=0.25 M.

Temperature Dependence of Equilibrium Constants

The quantitative consideration of the influence of temperature on equilibrium constants is available in the extended version of MINEQL (MINEQL/EIR) [4]. For a given temperature, T (Kelvin), the equilibrium constant is calculated from the value at 25°C using an equation derived from van't Hoff's approach [47]:

$$\log K(T) = \log K(298) + \frac{\Delta H^{o}(298)}{R \cdot \ln 10} \cdot \left\{ \frac{1}{298} - \frac{1}{T} \right\} + \frac{\Delta Cp^{o}(298)}{R \cdot \ln 10} \cdot \left\{ \frac{298}{T} - 1 - \ln \left(\frac{298}{T} \right) \right\}$$

For many species, the heat capacity of formation, ΔCp^{o}, is not known. In these cases, ΔCp^{o} is set equal to zero which means that the enthalpy of formation, ΔH^{o}, is assumed to be independent of temperature.

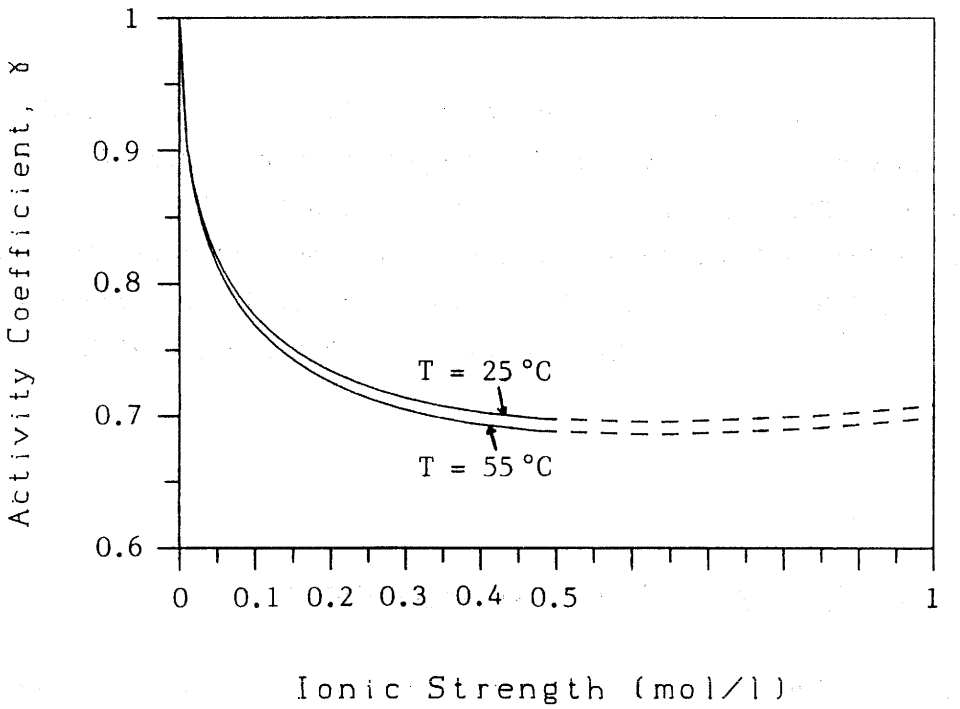

Figure A-1: Activity coefficients for singly charged ions as a function of ionic strength and temperature, calculated with Davie's formula. The approximation is found to be vaild up to I=0.5 M.

Appendix B: Thermodynamic Data

The following tables comprise a comprehensive list of the thermodynamic data used for the MINEQL/EIR calculations reported in the present publication. The sources of the data are various, but the data are the same as those used by Schweingruber [21,29,48] for the speciation calculations in the safety analysis of a potential high-level nuclear waste repository in Switzerland (Project Gewaehr 1985 [1]). In this way, the conservatism of the release rates reported in Project Gewaehr 1985 can be checked. However, it is planned to update the thermodynamic database in the near future.

It should be added that an international chemical thermodynamic database is under development [45] which will comprise internally consistent data critically reviewed by specialist teams of international experts. Selected thermodynamic data for a large number of species are already available from the OECD Nuclear Energy Agency.

The order of the tables is the following:

Table B-1: Ligand protonation (log K, ΔH^o, ΔCp^o)
Table B-2: Formation of groundwater species (log K, ΔH^o, ΔCp^o)
Table B-3: Formation of solid compounds (log K, ΔH^o, ΔCp^o)
Table B-4: Redox data used for the assessment of probable Eh range
Table B-5: Formation of actinide complexes (log K, ΔH^o, ΔCp^o)
Table B-6: Formation of actinide solids (log K, ΔH^o, ΔCp^o)
Table B-7: Actinide redox data (E^o, log K, ΔH^o, ΔCp^o)
Table B-8: Technetium data (E^o, log K)

Table B-1: Ligand protonation (25°C, 1 atm, ionic strength I=0 M)

General reaction: $m\,L + n\,H \rightleftharpoons L_mH_n$

Formation constant: $\log K = \log\{L_mH_n\} - m\cdot\log\{L\} - n\cdot\log\{H\}$

L	m	n	log K	ΔH^o [kcal/mol]	ΔCp^o [cal/(K·mol)]
H2O	0	-1	-14.00	13.34	-55.50
F-	1	1	3.17	3.20	38.50
CO3-2	1	1	10.33	-3.50	66.20
CO3-2	1	2	16.68	-5.50	128.10
SO4-2	1	1	2.00	5.40	81.30
PO4-3	1	1	12.35	-3.50	36.00
PO4-3	1	2	19.55	-4.30	82.60
PO4-3	1	3	21.70	-2.42	116.10
H2SiO4-2	1	1	13.10	-10.00	0.
H2SiO4-2	1	2	22.96	-15.00	0.
H2SiO4-2	4	4	55.90	0.	0.
H2SiO4-2	4	6	78.20	0.	0.
NH3	1	1	9.24	-12.45	0.

Table B-2: Complex formation (25 °C, 1 atm, ionic strength I=0 M)

General reaction: $m\,M + a\,A + b\,B \rightleftharpoons M_mA_aB_b$

Formation constant: $\log K = \log\{M_mA_aB_b\} - m\cdot\log\{M\} - a\cdot\log\{A\} - b\cdot\log\{B\}$

M	m	A	a	B	b	log K	ΔH^o [kcal/mol]	ΔCp^o [cal/(K·mol)]
Na+	1	CO3-2	1			1.20	0.	0.
Na+	1	SO4-2	1			0.70	1.10	0.
K+	1	SO4-2	1			0.85	3.00	0.
Mg+2	1	H+	-1			-11.42	0.	0.
Mg+2	1	F-	1			1.80	3.20	0.
Mg+2	1	CO3-2	1			2.88	3.00	0.
Mg+2	1	CO3-2	1	H+	1	11.30	0.	0.
Mg+2	1	SO4-2	1			2.23	1.40	0.
Mg+2	1	PO4-3	1	H+	1	15.26	-0.50	0.
Mg+2	1	NH3	1			0.10	0.	0.
Mg+2	1	NH3	2			0.00	0.	0.
Mg+2	1	NH3	3			-0.30	0.	0.
Mg+2	1	NH3	4			-1.00	0.	0.
Ca+2	1	H+	-1			-12.70	15.30	0.
Ca+2	1	F-	1			1.10	3.50	0.
Ca+2	1	CO3-2	1			3.15	4.00	0.
Ca+2	1	CO3-2	1	H+	1	11.35	0.	0.
Ca+2	1	SO4-2	1			2.30	1.60	0.
Ca+2	1	PO4-3	1			6.46	3.00	0.
Ca+2	1	PO4-3	1	H+	1	15.10	-0.50	0.
Ca+2	1	PO4-3	1	H+	2	20.95	-1.30	0.
Ca+2	1	NH3	1			-0.10	0.	0.
Ca+2	1	NH3	2			-0.70	0.	0.
Ca+2	1	NH3	3			-1.50	0.	0.
Ca+2	1	NH3	4			-2.60	0.	0.
Sr+2	1	H+	-1			-13.20	14.50	0.
Sr+2	1	Cl-	2			0.00	0.	0.
Sr+2	1	CO3-2	1			2.80	0.	0.
Sr+2	1	SO4-2	1			2.55	0.	0.
Sr+2	1	PO4-3	1			6.00	0.	0.
Sr+2	1	PO4-3	1	H+	1	14.10	0.	0.

Table B-2: Complex formation (continued)

General reaction: $m\,M + a\,A + b\,B \rightleftharpoons M_mA_aB_b$

Formation constant: $\log K = \log\{M_mA_aB_b\} - m\cdot\log\{M\} - a\cdot\log\{A\} - b\cdot\log\{B\}$

M	m	A	a	B	b	log K	ΔH^o [kcal/mol]	ΔCp^o [cal/(K·mol)]
Fe+2	1	H+	-1			-9.50	0.	0.
Fe+2	1	Cl-	1			0.90	0.	0.
Fe+2	1	SO4-2	1			2.20	1.60	0.
Fe+2	1	PO4-3	1	H+	1	15.95	0.	0.
Fe+2	1	PO4-3	1	H+	2	22.55	0.	0.
Fe+2	1	NH3	1			1.30	0.	0.
Fe+2	1	NH3	2			2.10	0.	0.
Fe+2	1	NH3	4			3.60	0.	0.
Mn+2	1	H+	-1			-10.60	13.34	0.
Mn+2	1	H+	-3			-34.20	0.	0.
Mn+2	1	Cl-	1			1.10	0.	0.
Mn+2	1	Cl-	2			1.10	0.	0.
Mn+2	1	Cl-	3			0.60	0.	0.
Mn+2	1	CO3-2	1	H+	1	12.10	0.	0.
Mn+2	1	SO4-2	1			2.26	2.10	0.
Mn+2	1	PO4-3	1	H+	1	16.20	0.	0.
Mn+2	1	NH3	1			0.70	0.	0.
Mn+2	1	NH3	2			1.20	0.	0.

Table B-3: Potential solids (25°C, 1 atm, ionic strength I=0 M)

General reaction: $a\ A + b\ B + c\ C \rightleftharpoons A_aB_bC_c\ (s)$

Formation constant: $\log K = -a \cdot \log\{A\} - b \cdot \log\{B\} - c \cdot \log\{C\}$

A	a	B	b	C	c	log K	ΔH° [kcal/mol]	ΔCp° [cal/(K·mol)]
Mg+2	1	H+	-2			-16.85	26.00	0.
Mg+2	1	F-	2			8.18	2.00	0.
Mg+2	1	CO3-2	1			8.04	6.20	98.00
Mg+2	3	PO4-3	2			28.40	0.	0.
Ca+2	1	H+	-2			-22.80	31.00	0.
Ca+2	1	F-	2			10.41	-3.80	74.40
Ca+2	1	CO3-2	1			8.36	3.15	107.70
Ca+2	1	SO4-2	1	[gypsum]		4.86	-0.22	57.20
Ca+2	1	SO4-2	1	[anhydrite]		4.65	3.75	74.40
Ca+2	1	PO4-3	1	H+	1	18.93	-4.50	0.
Ca+2	4	PO4-3	3	H+	1	46.90	0.	0.
Ca+2	2	H2SiO4-2	1	H+	-2	-15.80	41.20	-11.00
Ca+2	1	Mg+2	1	CO3-2	2	17.00	8.36	200.00
Sr+2	1	F-	-2			8.54	-1.00	0.
Sr+2	1	CO3-2	1			9.03	0.10	0.
Sr+2	1	SO4-2	1			6.50	-0.50	0.
Sr+2	1	H2SiO4-2	1			2.40	0.	0.
Fe+2	1	H+	-2			-12.90	21.80	0.
Fe+2	1	CO3-2	1			10.69	5.05	100.00
Fe+2	3	PO4-3	2			36.00	0.	0.
Fe+2	2	H2SiO4-2	1	H+	-2	5.74	21.70	-34.00
Mn+2	1	H+	-2			-15.20	0.	0.
Mn+2	1	CO3-2	1			10.52	2.07	102.00
Mn+2	1	H2SiO4-2	1			10.70	0.	0.
H+	2	H2SiO4-2	1	[Quartz]		26.94	-21.00	0.
H+	2	H2SiO4-2	1	[SiO2 am]		25.98	-19.40	0.
H+	2	H2SiO4-2	1	[Chalcedony]		26.50	-19.70	0.
Gaseous carbon dioxide:								
H+	2	CO3-2	1			18.14	-0.51	90.70

Table B-4: Redox data used for the evaluation of probable Eh range ($25^{o}C$, 1 atm, ionic strength I=0 M)

Reaction			E^{o} [mV]	log K	ΔH^{o} [kcal/mol]	ΔCp^{o} [cal/(K·mol)]
2 H+ + 2 e-	$\rightleftharpoons$	H2 (g)	0.	0.00	0.00	0.
Fe203 (s, hematite) + 2 e- + 2 H+	$\rightleftharpoons$	Fe304 (s, magnetite) + 2 H20	215.	7.47	-12.38	0.

Table B-5: Actinide complexes (25°C, 1 atm, ionic strength I=0 M)

General reaction: $m\,M + a\,A + b\,B \rightleftharpoons M_mA_aB_b$

Formation constant: $\log K = \log\{M_mA_aB_b\} - m\cdot\log\{M\} - a\cdot\log\{A\} - b\cdot\log\{B\}$

M	m	A	a	B	b	log K	ΔH^o [kcal/mol]	ΔCp^o [cal/(K·mol)]
Np+3	1	H+	-1			-7.00	0.	0.
Np+3	1	H+	-2			-15.00	0.	0.
Np+3	1	H+	-3			-25.00	0.	0.
Np+3	1	H+	-4			-35.00	0.	0.
Np+3	2	H+	-2			-14.00	0.	0.
Np+3	3	H+	-5			-32.00	0.	0.
Pu+3	1	H+	-1			-7.50	12.80	0.
Pu+3	1	H+	-2			-16.50	0.	0.
Pu+3	1	H+	-3			-26.50	0.	0.
Pu+3	1	H+	-4			-37.00	0.	0.
Pu+3	2	H+	-2			-14.00	0.	0.
Pu+3	3	H+	-5			-33.00	0.	0.
Am+3	1	H+	-1			-7.50	0.	0.
Am+3	1	H+	-2			-16.50	0.	0.
Am+3	1	H+	-3			-26.50	0.	0.
Am+3	1	H+	-4			-37.00	0.	0.
Am+3	2	H+	-2			-14.00	0.	0.
Am+3	3	H+	-5			-33.00	0.	0.
Pu+3	1	F-	1			4.30	0.	0.
Pu+3	1	F-	2			7.60	0.	0.
Pu+3	1	F-	3			10.80	0.	0.
Am+3	1	F-	1			4.30	0.	0.
Am+3	1	F-	2			7.60	0.	0.
Am+3	1	F-	3			10.80	0.	0.
Np+3	1	CO3-2	1			9.60	0.	0.
Np+3	1	CO3-2	2			12.90	0.	0.
Np+3	1	CO3-2	3			16.20	0.	0.
Pu+3	1	CO3-2	1			6.00	0.	0.
Pu+3	1	CO3-2	2			10.00	0.	0.
Pu+3	1	CO3-2	3			13.00	0.	0.
Am+3	1	CO3-2	1			6.00	0.	0.
Am+3	1	CO3-2	2			10.00	0.	0.
Am+3	1	CO3-2	3			13.00	0.	0.

Table B-5: Actinide complexes (continued)

General reaction: $m\,M + a\,A + b\,B \rightleftharpoons M_mA_aB_b$

Formation constant: $\log K = \log\{M_mA_aB_b\} - m\cdot\log\{M\} - a\cdot\log\{A\} - b\cdot\log\{B\}$

M	m	A	a	B	b	log K	ΔH^o [kcal/mol]	ΔCp^o [cal/(K·mol)]
Pu+3	1	SO4-2	1			3.50	3.50	0.
Pu+3	1	SO4-2	2			5.20	0.	0.
Am+3	1	SO4-2	1			3.50	0.	0.
Am+3	1	SO4-2	2			5.20	0.	0.
Pu+3	1	PO4-3	1	H+	1	18.30	0.	0.
Pu+3	1	PO4-3	1	H+	2	22.00	3.50	0.
Am+3	1	PO4-3	1	H+	1	18.40	0.	0.
U+4	1	H+	-1			-0.65	11.81	-19.40
U+4	1	H+	-2			-2.25	17.78	-24.70
U+4	1	H+	-3			-4.90	22.64	-24.80
U+4	1	H+	-4			-8.50	24.77	-60.50
U+4	1	H+	-5			-13.15	27.58	-118.90
U+4	6	H+	-15			-17.20	0.	0.
Np+4	1	H+	-1			-1.50	11.60	0.
Np+4	1	H+	-2			-3.00	17.80	0.
Np+4	1	H+	-3			-6.00	23.00	0.
Np+4	1	H+	-4			-10.00	25.50	0.
Np+4	1	H+	-5			-20.00	29.00	0.
Np+4	2	H+	-2			-2.00	0.	0.
Pu+4	1	H+	-1			-0.50	11.50	0.
Pu+4	1	H+	-2			-2.50	17.80	0.
Pu+4	1	H+	-3			-5.50	23.10	0.
Pu+4	1	H+	-4			-9.50	26.10	0.
Pu+4	1	H+	-5			-19.00	30.10	0.
Pu+4	2	H+	-2			-1.00	0.	0.
Th+4	1	H+	-1			-3.20	5.95	0.
Th+4	1	H+	-2			-6.95	13.80	0.
Th+4	1	H+	-3			-11.70	20.40	0.
Th+4	1	H+	-4			-15.90	24.70	0.
Th+4	2	H+	-2			-6.10	14.80	0.
Th+4	4	H+	-8			-21.10	57.80	0.
Th+4	6	H+	-15			-36.70	108.40	0.

Table B-5: Actinide complexes (continued)

General reaction: $m\,M + a\,A + b\,B \rightleftharpoons M_mA_aB_b$

Formation constant: $\log K = \log\{M_mA_aB_b\} - m\cdot\log\{M\} - a\cdot\log\{A\} - b\cdot\log\{B\}$

M	m	A	a	B	b	log K	ΔH^o [kcal/mol]	ΔCp^o [cal/(K·mol)]
U+4	1	F-	1			8.60	4.97	27.80
U+4	1	F-	2			14.50	7.15	68.90
U+4	1	F-	3			19.10	7.22	117.70
U+4	1	F-	4			23.50	4.54	128.30
U+4	1	F-	5			25.20	4.70	127.60
U+4	1	F-	6			27.70	3.39	190.00
Np+4	1	F-	1			8.60	5.50	0.
Np+4	1	F-	2			14.50	7.20	0.
Np+4	1	F-	3			19.10	7.20	0.
Np+4	1	F-	4			23.60	4.50	0.
Np+4	1	F-	5			25.30	4.70	0.
Pu+4	1	F-	1			8.60	5.90	0.
Pu+4	1	F-	2			14.50	7.00	0.
Pu+4	1	F-	3			19.10	7.00	0.
Pu+4	1	F-	4			23.60	5.00	0.
Pu+4	1	F-	5			25.30	5.00	0.
Th+4	1	F-	1			8.00	-1.40	0.
Th+4	1	F-	2			14.20	-2.10	0.
Th+4	1	F-	3			18.90	-3.00	0.
Th+4	1	F-	4			22.30	-3.80	0.
U+4	1	Cl-	1			3.00	1.77	109.40
Th+4	1	Cl-	1			1.10	-0.20	0.
Th+4	1	Cl-	2			0.80	20.90	0.
Th+4	1	Cl-	3			1.65	15.75	0.
Th+4	1	Cl-	4			1.26	12.30	0.
U+4	1	CO3-2	1	H+	-3	-1.00	0.	0.
Np+4	1	CO3-2	5			36.50	0.	0.
Np+4	1	CO3-2	1	H+	-3	0.00	0.	0.
Pu+4	1	CO3-2	5			36.50	0.	0.
Pu+4	1	CO3-2	1	H+	-3	0.00	0.	0.
Th+4	1	CO3-2	1			11.00	0.	0.

Table B-5: Actinide complexes (continued)

General reaction: $m\,M + a\,A + b\,B \rightleftharpoons M_mA_aB_b$

Formation constant: $\log K = \log\{M_mA_aB_b\} - m\cdot\log\{M\} - a\cdot\log\{A\} - b\cdot\log\{B\}$

M	m	A	a	B	b	log K	ΔH^o [kcal/mol]	ΔCp^o [cal/(K·mol)]
U+4	1	SO4-2	1			4.70	1.20	82.70
U+4	1	SO4-2	2			8.00	5.52	96.10
Np+4	1	SO4-2	1			5.60	2.00	0.
Np+4	1	SO4-2	2			10.30	7.50	0.
Pu+4	1	SO4-2	1			5.60	3.00	0.
Pu+4	1	SO4-2	2			10.30	10.00	0.
Th+4	1	SO4-2	1			5.45	3.70	0.
Th+4	1	SO4-2	2			9.75	7.50	0.
Th+4	1	SO4-2	3			10.50	11.70	0.
Th+4	1	SO4-2	4			8.50	13.10	0.
U+4	1	PO4-3	1	H+	1	24.30	7.49	117.50
U+4	1	PO4-3	2	H+	2	46.70	1.89	225.50
U+4	1	PO4-3	3	H+	3	67.60	-8.02	378.90
U+4	1	PO4-3	4	H+	4	88.00	-26.01	511.70
Np+4	1	PO4-3	1	H+	1	25.40	7.00	0.
Np+4	1	PO4-3	1	H+	2	24.10	0.00	0.
Np+4	1	PO4-3	2	H+	2	48.50	0.50	0.
Np+4	1	PO4-3	2	H+	4	48.00	0.00	0.
Np+4	1	PO4-3	3	H+	3	70.50	-10.00	0.
Pu+4	1	PO4-3	1	H+	1	25.40	6.20	0.
Pu+4	1	PO4-3	1	H+	2	24.10	0.	0.
Pu+4	1	PO4-3	2	H+	2	48.50	-0.60	0.
Pu+4	1	PO4-3	2	H+	4	48.00	0.	0.
Pu+4	1	PO4-3	3	H+	3	70.50	-11.70	0.
Th+4	1	PO4-3	1	H+	1	25.55	-3.60	0.
Th+4	1	PO4-3	1	H+	2	24.10	12.90	0.
Th+4	1	PO4-3	1	H+	3	23.60	13.70	0.
Th+4	1	PO4-3	2	H+	2	51.10	-10.25	0.
Th+4	1	PO4-3	2	H+	4	48.00	-3.80	0.
Th+4	1	PO4-3	3	H+	3	72.00	-15.70	0.

Table B-5: Actinide complexes (continued)

General reaction: $m\,M + a\,A + b\,B \rightleftharpoons M_mA_aB_b$

Formation constant: $\log K = \log\{M_mA_aB_b\} - m\cdot\log\{M\} - a\cdot\log\{A\} - b\cdot\log\{B\}$

M	m	A	a	B	b	log K	ΔH^o [kcal/mol]	ΔCp^o [cal/(K·mol)]
UO2+	1	H+	-1			-9.40	0.	0.
NpO2+	1	H+	-1			-8.90	16.00	0.
PuO2+	1	H+	-1			-9.70	16.60	0.
NpO2+	1	F-	1			3.70	0.	0.
PuO2+	1	F-	1			3.70	0.	0.
NpO2+	1	CO3-2	1			5.90	0.	0.
NpO2+	1	CO3-2	2			11.10	0.	0.
NpO2+	1	CO3-2	3			16.30	0.	0.
PuO2+	1	CO3-2	1			5.00	0.	0.
PuO2+	1	CO3-2	2			10.00	0.	0.
PuO2+	1	CO3-2	3			15.30	0.	0.
NpO2+	1	SO4-2	1			2.00	0.	0.
PuO2+	1	SO4-2	1			2.00	0.	0.
UO2+2	1	H+	-1			-5.80	10.96	-3.90
UO2+2	1	H+	-2			-12.00	17.43	-37.20
UO2+2	1	H+	-3			-23.60	0.	0.
UO2+2	1	H+	-4			-37.80	0.	0.
UO2+2	2	H+	-1			-4.40	0.	0.
UO2+2	2	H+	-2			-5.60	10.09	-48.40
UO2+2	3	H+	-4			-12.20	0.	0.
UO2+2	3	H+	-5			-15.50	24.98	-91.90
UO2+2	3	H+	-7			-31.00	49.10	71.20
NpO2+2	1	H+	-1			-5.10	11.00	0.
NpO2+2	1	H+	-2			-10.40	17.00	0.
NpO2+2	1	H+	-3			-19.00	0.	0.
NpO2+2	2	H+	-2			-6.40	12.00	0.
NpO2+2	3	H+	-5			-17.00	29.00	0.
PuO2+2	1	H+	-1			-5.60	10.80	0.
PuO2+2	1	H+	-2			-10.20	17.00	0.
PuO2+2	1	H+	-3			-20.00	0.	0.
PuO2+2	2	H+	-2			-8.30	0.	0.
PuO2+2	3	H+	-5			-21.60	33.40	0.

Table B-5: Actinide complexes (continued)

General reaction: $m\,M + a\,A + b\,B \rightleftharpoons M_mA_aB_b$

Formation constant: $\log K = \log\{M_mA_aB_b\} - m\cdot\log\{M\} - a\cdot\log\{A\} - b\cdot\log\{B\}$

M	m	A	a	B	b	log K	ΔH^o [kcal/mol]	ΔCp^o [cal/(K·mol)]
UO2+2	1	F-	1			5.00	-0.56	48.30
UO2+2	1	F-	2			8.90	-0.84	57.20
UO2+2	1	F-	3			11.50	-0.96	25.50
UO2+2	1	F-	4			12.60	-0.98	102.20
NpO2+2	1	F-	1			5.70	-1.00	0.
NpO2+2	1	F-	2			11.10	-2.00	0.
NpO2+2	1	F-	3			15.90	-4.00	0.
NpO2+2	1	F-	4			18.80	-5.00	0.
PuO2+2	1	F-	1			5.70	-1.30	0.
PuO2+2	1	F-	2			11.10	-3.70	0.
PuO2+2	1	F-	3			15.90	-7.00	0.
PuO2+2	1	F-	4			18.80	-9.60	0.
UO2+2	1	Cl-	1			0.20	0.04	130.70
UO2+2	1	CO3-2	1			10.05	-2.76	181.10
UO2+2	1	CO3-2	2			17.00	3.60	33.90
UO2+2	1	CO3-2	3			21.40	-9.70	260.50
NpO2+2	1	CO3-2	1			10.10	-3.00	0.
NpO2+2	1	CO3-2	2			16.70	5.00	0.
NpO2+2	1	CO3-2	3			23.80	-9.00	0.
NpO2+2	3	CO3-2	6			60.10	0.	0.
NpO2+2	2	CO3-2	1	H+	-3	-1.00	0.	0.
NpO2+2	3	CO3-2	1	H+	-3	1.00	0.	0.
PuO2+2	1	CO3-2	1			9.00	-3.00	0.
PuO2+2	1	CO3-2	2			15.00	4.00	0.
PuO2+2	1	CO3-2	3			22.00	-10.00	0.
PuO2+2	3	CO3-2	6			60.10	0.	0.
PuO2+2	2	CO3-2	1	H+	-3	-1.00	0.	0.
PuO2+2	3	CO3-2	1	H+	-3	1.00	0.	0.

Table B-5: Actinide complexes (continued)

General reaction: $m\,M + a\,A + b\,B \rightleftharpoons M_mA_aB_b$

Formation constant: $\log K = \log\{M_mA_aB_b\} - m\cdot\log\{M\} - a\cdot\log\{A\} - b\cdot\log\{B\}$

M	m	A	a	B	b	log K	ΔH^o [kcal/mol]	ΔCp^o [cal/(K·mol)]
UO2+2	1	SO4-2	1			3.00	5.20	125.70
UO2+2	1	SO4-2	2			4.00	0.	0.
UO2+2	1	SO4-2	3			3.70	0.	0.
NpO2+2	1	SO4-2	1			3.00	5.00	0.
NpO2+2	1	SO4-2	2			4.30	0.	0.
PuO2+2	1	SO4-2	1			3.00	4.80	0.
PuO2+2	1	SO4-2	2			4.30	0.	0.
UO2+2	1	PO4-3	1	H+	1	20.50	-2.02	105.80
UO2+2	1	PO4-3	1	H+	2	22.60	-3.51	114.40
UO2+2	1	PO4-3	2	H+	2	43.20	-11.50	297.60
UO2+2	1	PO4-3	2	H+	4	44.50	-16.39	212.80
UO2+2	1	PO4-3	3	H+	6	65.80	-27.99	330.10
NpO2+2	1	PO4-3	1	H+	1	20.80	-2.00	0.
NpO2+2	1	PO4-3	1	H+	2	22.50	-4.00	0.
NpO2+2	1	PO4-3	2	H+	2	43.20	-11.50	0.
PuO2+2	1	PO4-3	1	H+	1	20.80	-2.00	0.
PuO2+2	1	PO4-3	1	H+	2	22.50	-5.00	0.
PuO2+2	1	PO4-3	2	H+	2	43.20	-11.50	0.
UO2+2	1	H2SiO4-2	1	H+	1	20.80	0.	0.

Table B-6: Potential actinide solids (25°C, 1 atm, I=0 M)

General reaction: $a\,A + b\,B + c\,C + d\,D \rightleftharpoons A_aB_bC_cD_d\ (s)$

Formation constant: $\log K = -a\cdot\log\{A\} - b\cdot\log\{B\} - c\cdot\log\{C\} - d\cdot\log\{D\}$

A	a	B	b	C c D d	log K	ΔH^o [kcal/mol]	ΔCp^o [cal/(K·mol)]
Pu+3	1	H+	-3		-18.50	35.50	0.
Pu+3	1	F-	3		10.20	11.10	0.
Pu+3	2	C03-2	3		31.00	0.	0.
Pu+3	1	P04-3	1		23.00	0.	0.
Am+3	1	H+	-3		-18.50	0.	0.
Am+3	1	F-	3		10.20	0.	0.
Am+3	2	C03-2	3		31.00	0.	0.
Am+3	1	P04-3	1		23.00	0.	0.
U+4	1	H+	-4	[U02]	4.60	18.69	-9.20
U+4	1	H+	-4	[U(OH)4]	-9.80	0.	0.
U+4	1	F-	4		18.50	11.97	156.10
U+4	1	F-	4	[2.5 H20]	27.55	4.30	146.30
U+4	1	S04-2	1	H+ -2	3.20	0.	0.
U+4	1	P04-3	2	H+ 2	51.50	-3.82	263.50
U+4	1	P04-3	2	Ca+2 1	54.10	0.	0.
U+4	1	H2Si04-2	1	H+ -2	32.10	0.	0.
U+4	2	U02+	2	H+ -10	16.30	39.81	-41.80
Np+4	1	H+	-4		0.00	15.00	0.
Np+4	1	F-	4		24.00	18.00	0.
Np+4	1	P04-3	2	H+ 2	51.70	-1.00	0.
Pu+4	1	H+	-4		1.00	13.00	0.
Pu+4	1	F-	4		24.00	0.	0.
Pu+4	1	P04-3	2	H+ 2	51.70	1.30	0.
Th+4	1	H+	-4	[Th02]	-6.30	27.20	0.
Th+4	1	H+	-4	[Th(OH)4]	-13.80	7.50	0.
Th+4	1	F-	4		30.10	2.80	0.
Th+4	1	F-	4	[2.5 H20]	33.10	-7.15	0.
Th+4	1	P04-3	2	H+ 2	51.50	-2.00	0.
U02+	1	H+	-1		-5.00	0.	0.
U02+	1	H+	-2	Na+ 1	-9.90	14.98	0.
U02+	1	H+	-4	Na+ 3	-57.90	72.11	0.
Np02+	1	H+	-1		-4.90	10.00	0.
Pu02+	1	H+	-1		-5.00	10.20	0.

Table B-6: Potential actinide solids (continued)

General reaction: $a\,A + b\,B + c\,C + d\,D \rightleftharpoons A_aB_bC_cD_d\ (s)$

Formation constant: $\log K = -a\cdot\log\{A\} - b\cdot\log\{B\} - c\cdot\log\{C\} - d\cdot\log\{D\}$

A	a	B	b	C D	c d	log K	ΔH^o [kcal/mol]	ΔCp^o [cal/(K·mol)]
UO2+2	1	H+	-2	[Gamma]		-7.70	19.27	0.70
UO2+2	1	H+	-2	[Beta]		-5.70	13.59	-3.50
UO2+2	1	H+	-2	[Schoepite]		-5.60	13.60	-7.30
UO2+2	1	H+	-4	Na+	2	-31.55	43.25	0.
UO2+2	1	H+	-4	Mg+2	1	-23.20	47.87	0.
UO2+2	1	H+	-4	Ca+2	1	-15.00	31.50	0.
UO2+2	1	CO3-2	1			14.45	5.57	93.30
UO2+2	1	CO3-2	3	Na+	4	21.10	0.	0.
UO2+2	1	SO4-2	1			-2.00	19.93	75.70
UO2+2	3	PO4-3	2			49.00	14.38	295.70
UO2+2	2	PO4-3	2	H+	2	48.10	3.42	282.80
UO2+2	2	PO4-3	2	Na+	2	47.20	0.	0.
UO2+2	2	PO4-3	2	K+	2	48.00	0.	0.
UO2+2	2	PO4-3	2	Mg+2	1	43.90	0.	0.
UO2+2	2	PO4-3	2	Ca+2	1	44.20	0.	0.
UO2+2	2	PO4-3	2	Sr+2	1	44.60	0.	0.
UO2+2	2	PO4-3	2	Fe+2	1	44.50	0.	0.
UO2+2	2	PO4-3	2	H+	2			
				NH3	2	70.20	0.	0.
UO2+2	2	H2SiO4-2	2	H+	-2			
				Ca+2	1	28.30	0.	0.
UO2+2	1	UO2+	2	H	-4	1.00	19.24	-27.25
NpO2+2	1	H+	-2			-5.30	11.00	0.
NpO2+2	1	CO3-2	1			13.80	6.00	0.
NpO2+2	3	PO4-3	2			48.20	14.00	0.
NpO2+2	1	PO4-3	1	H+	1	25.00	0.	0.
PuO2+2	1	H+	-2			-5.00	8.60	0.
PuO2+2	1	CO3-2	1			13.80	6.00	0.
PuO2+2	3	PO4-3	2			48.20	14.00	0.
PuO2+2	1	PO4-3	1	H+	1	25.00	-1.00	0.

Table B-7: Actinide redox data (25°C, 1 atm, ionic strength I=0 M)

Reaction	E° [mV]	log K	ΔH° [kcal/mol]	ΔCp° [cal/(K·mol)]
$UO_2^+ + e^- + 4\,H^+ \rightleftharpoons U^{+4} + 2\,H_2O$	379.	6.40	-31.16	-2.33
$UO_2^{+2} + e^- \rightleftharpoons UO_2^+$	166.	2.80	-3.32	18.77
$Np^{+4} + e^- \rightleftharpoons Np^{+3}$	154.	2.60	0.	0.
$NpO_2^+ + e^- + 4\,H^+ \rightleftharpoons Np^{+4} + 2\,H_2O$	651.	11.00	-40.00	0.
$NpO_2^{+2} + e^- \rightleftharpoons NpO_2^+$	1231.	20.80	-12.00	0.
$Pu^{+4} + e^- \rightleftharpoons Pu^{+3}$	1009.	17.05	-13.30	0.
$PuO_2^+ + e^- + 4\,H^+ \rightleftharpoons Pu^{+4} + 2\,H_2O$	1100.	18.60	-46.20	0.
$PuO_2^{+2} + e^- \rightleftharpoons PuO_2^+$	958.	16.20	-22.20	0.

Table B-8: Technetium data (25°C, 1 atm, ionic strength I=0 M)

The data listed below are taken from an internal note by Schweingruber [48]. The main source to this compilation has been a review by Allard and Torstenfelt [49].

Reaction			E° [mV]	log K
Complex formation:				
$TcO^{+2} + H_2O$	$\rightleftharpoons$	$TcOOH^{+} + H^{+}$		-1.40
$TcO^{+2} + 2\ H_2O$	$\rightleftharpoons$	$TcO(OH)_2 + 2\ H^{+}$		-3.40
Solid formation				
$TcO^{+2} + 2\ H_2O$	$\rightleftharpoons$	$TcO_2\ (s) + 2\ H^{+}$		0.90
Redox equilibria				
$Tc^{+2} + 2\ e^-$	$\rightleftharpoons$	$Tc\ (s)$	400.	13.52
$TcO^{+} + e^- + 2\ H^{+}$	$\rightleftharpoons$	$Tc^{+2} + H_2O$	31.	-0.52
$TcO^{+2} + e^-$	$\rightleftharpoons$	TcO^{+}	370.	6.25
$TcO_4^- + 6\ H^{+} + 3\ e^-$	$\rightleftharpoons$	$TcO^{+2} + 3\ H_2O$	720.	36.50